Progress in Particle and Nuclear Physics 129 (2023) 104006

Contents lists available at ScienceDirect

Progress in Particle and Nuclear Physics

journal homepage: www.elsevier.com/locate/ppnp

Review

Theoretical studies of Pygmy Resonances

E.G. Lanza [a,b,*], L. Pellegri [c,d], A. Vitturi [e,f], M.V. Andrés [g]

[a] INFN, Sezione di Catania, Italy
[b] Dipartimento di Fisica e Astronomia "Ettore Majorana", Università di Catania, Italy
[c] School of Physics, University of the Witwatersrand, Johannesburg 2050, South Africa
[d] iThemba LABS, Old Faure Road, Faure 7131, South Africa
[e] Dipartimento di Fisica e Astronomia "Galileo Galilei", Università di Padova, Italy
[f] INFN, Sezione di Padova, Italy
[g] Departamento de FAMN, Facultad de Física, Sevilla, Spain

ARTICLE INFO

Article history:
Available online 21 November 2022

Keywords:
Pygmy Dipole Resonances
Isoscalar dipole excitations
Collective modes
Semiclassical Coupled Channel equations

ABSTRACT

This review aims at giving a critical description of the theoretical researches conducted on the low-lying dipole states traditionally denoted as Pygmy Dipole Resonances (PDR). A brief survey of the experimental techniques and recent experimental findings is presented as an introduction to the main part of the paper. The presence of the PDR on stable and unstable nuclei with neutron excess is well established in theoretical and experimental studies. The theoretical approaches are reviewed starting from the macroscopic collective models to the microscopic mean-field theories. The isospin mixed nature of the PDR – reproduced by all the microscopic approaches – allows to study the excitation with isovector and isoscalar probes. To draw a better picture on the structure of this mode is therefore important to complement the theoretical studies with detailed investigation on the reaction mechanism. To this mean, this paper gives specific focus to the description of the cross section calculations. The semiclassical Coupled Channel equations are shortly reviewed with particular attention to the construction of the nuclear potential and radial form factors with the microscopic transition densities. The interplay of Coulomb and nuclear contributions, their dependence on mass, charge and incident energy are analysed with the help of few selected examples. Most of the features of the PDR are well described by the theoretical approaches even though few open question remain to be clarified. Among them a discussion on the collectivity of the mode, isospin splitting and role of deformation is presented. Most of the theoretical works and the new experimental findings on the collective properties of the PDR jeopardise the common picture of this excitation mode as related to the oscillation of the neutron skin against an inert core The question on the influence of the neutron excess on other multipolarities is also reviewed.

Contents

* Corresponding author at: INFN, Sezione di Catania, Italy.
E-mail address: lanza@ct.infn.it (E.G. Lanza).

https://doi.org/10.1016/j.ppnp.2022.104006
0146-6410/

1. Introduction

The analysis of the neutron capture results in the sixties was well established for neutron energies below 1 MeV and above 8 MeV, while some difficulties were encountered in the investigation of the intermediate energy regime. In fact, for neutron-reach nuclei with mass number (A) between 130 and 200, the theoretically predicted cross section and the γ-ray spectrum, calculated on the basis of a level density formulae, were found to underestimate the experimental data. Although a better agreement was reached by including in the model the E1 Giant Resonance (GR), the data could only be reproduced by Stadfelt [1] by introducing in the calculation also the experimental evidence of an excess of strength around 6 MeV in photo-nuclear reactions. The same method was applied by Brzosko et al. [2] for the calculation of the cross section for the (n, γ) reaction obtaining a much better agreement with the experimental data. It was then the first time where this low-energy peak was referred to as Pygmy Resonance.

In developing a theory to correlate nuclear reaction data, Lane [3] was performing detailed calculation on ^{208}Pb using an R-matrix approach with zero range particle–hole interaction. As by-product he found an interpretation of the Pygmy Dipole Resonance (PDR) as a concentration of few percent of the dipole strength generated by few one-particle one-hole configurations which did not participate to the construction of the Isovector Giant Dipole Resonance (IVGDR). The distribution of dipole strength in heavy nuclei was also studied within a schematic model [4] where these states were found to have a strong collective nature [5] in contrast with Lane's findings. This is still a debating point nowadays even though a large amount of work on the PDR has been performed since then and a section of this review is dedicate to help in addressing this controversy.

Nowadays some of the properties of the PDR are well established, by both theoretical and experimental sides [6–10]. The low-lying dipole states are found to be a common feature of all the measured stable and unstable nuclei with neutron excess. They appear with a strength of a few per cent of the Energy Weighted Sum Rule (EWSR) and are located at an energy lower than the GDR peak, at around the neutron emission energy threshold. The theoretical studies are found in agreement in defining the strong isospin mixing, associated with the transition densities shape at the nuclear surface, the common evidence for these states. This characteristic opened the possibility to investigate these low-lying dipole states with isovector and isoscalar probes. A great selection of experimental methods were therefore conducted and they are

briefly discussed in Section 2. They varies from pure electromagnetic probe like the (γ, γ') or the pioneering works on relativistic Coulomb excitation in unstable nuclei, to the use of hadronic probes like protons, α particle or ^{17}O. Both type of probes have been used to study the properties of the PDR in spherical and deformed light and heavy ions. A large varieties of theories are needed to investigate this assortment of nuclear reactions. The kind of theoretical approaches used span from macroscopic models – where the nucleus is seen as a liquid drop composed by protons and neutrons – to very sophisticated microscopic mean-field theories. The excitation are then described, in the first case, as oscillation of the nuclear surface or as compression of the entire nuclear body. In the latter, the excitations are formed by a cooperative behaviour of many particle–hole configurations governed by the residual interaction. These theories and models often have been adapted and modified to reach a good description of the PDR mode. The interest in studying this new excitation mode relies also in the implications on other physics fields. The presence of the PDR in nuclei with neutron excess could be related to the symmetry energy parameters. In particular, the electric dipole response of nuclei should depend on the neutron-to-proton asymmetry and therefore possibly determined by the symmetry energy. Several attempts were made to use the PDR data to constrain the symmetry energy and to extract a relation with the neutron skin thickness of neutron-rich nuclei [11–15]. The neutron skin is defined as the difference between the root mean square of the neutrons and protons radii $r_{skin} = r^n_{rms} - r^p_{rms}$. The correlation between this quantity and the symmetry energy and other quantities related to the equation of states has been investigated within a statistical analysis based on the covariance method [16]. This was done within a self-consistent mean field theory with a nuclear energy density functional SV-min [17] of Skyrme type. In Ref. [16] a strong correlation was found between the neutron skin and the dipole polarisability (α_D) rather than with the dipole strength. The dipole polarisability can be defined as

$$\alpha_D = \frac{8\pi e^2}{9} \int_0^\infty F(\omega; E1)\omega^{-1} d\omega = \frac{8\pi e^2}{9} m_{-1}(E1) \tag{1}$$

where the electric dipole strength $F(\omega; E1)$ is integrated over the whole energy range and $m_{-1}(E1)$ is the sum of the inverse energy weighted strength. Some of the conclusions extracted from the statistical analysis may depend on the model and the set of observables chosen. In fact, guided by a classical droplet model, the authors of Ref. [18] have found that it is the product $\alpha_D J$ of the electric dipole polarisability and the symmetry energy at saturation density J that has a stronger correlation with the r_{skin} and with the slope of the symmetry energy at saturation density L. Therefore, a precise measurement of the α_D would allow to establish a tight relation between L and J improving the knowledge on the symmetry energy.

The knowledge of the electromagnetic transition strength from nuclear states around the neutron emission threshold is of paramount importance for the calculation of the neutron capture rates in the r-process (rapid neutron-capture process). This is thought to be the main astrophysical process producing about half of the heavy elements (heavier than iron) in the universe. The process follow a path across nuclei with neutron excess by increasing their atomic number through a competition of neutron captures and β-decays. The neutron capture rates are commonly evaluated within the framework of the statistical model of Hauser and Feshbach [19] whose main assumption is that this process occur via an intermediary formation of a compound nucleus in thermodynamic equilibrium. The independent decay of the (n, γ) reaction is regulated by the electromagnetic transition strengths which conventionally are described with parametrised functions and are used to estimate the photon de-excitation probability. Variation in the E1 strength, as due to the presence of the PDR close to the neutron emission threshold, may affect the neutron capture cross sections as was first noted by Goriely [20]. The dipole states of PDR, having very short lifetimes close to the typical neutron evaporation times, may favour a fast depopulation of the capture levels to lower-lying bound states. This competition may stabilise the newly formed nucleus against subsequent neutron emissions. It is then important to have a very good description of the electromagnetic strength distribution. Almost all the microscopic mean-field theories – presented in Section 4 – have been employed in order to give a detailed and precise description of the contribution of the PDR to the dipole distribution strength [20–26].

This paper reviews the various theoretical approaches that attempted to give a reasonable interpretation of the experimental data trying to highlight some characteristics of these excitation which are still under experimental verification. All these calculations have succeeded in the interpretation of the experimental data and in the understanding of the main feature of the PDR. Most of the theoretical effort concentrated in the calculation of the PDR structure while paying less attention to the cross section calculations that are crucial for proper comparison with the measurements, especially the ones in which the nuclear interaction became relevant such as for the isoscalar probes. The use of these probes has become more frequent in the last years in connection with the importance of the isospin in the excitation process of the PDR. The interplay between isoscalar and isovector properties revealed to be one of the most fascinating aspect of this mew mode. In the calculation of the cross section one has to pay attention to the dynamic of the excitation process taking at the same time in consideration the characteristic structure of the excited states. In this review particular attention was placed on this aspect. We have described the different information that one can extract from Coulomb and nuclear interaction and the importance of the detailed structure of the excited state for a good description of the radial form factor, main ingredient in the calculation of the inelastic cross section.

The paper is organised as follows. In Section 2 a short review on the main experimental techniques are illustrated underlining the difference between photo-reactions and particle-induced reactions. Some highlights on recent experimental result are presented in Section 3 with particular emphasis on open problems treated also – from the theoretical point of view – in Section 6. The theoretical models are presented in Section 4 and are separately reviewed starting from the

macroscopic approaches to the semiclassical ones, passing to the many microscopic theories based on the mean-field approaches and their extensions. Section 5 is dedicated to the derivation of the cross section using semiclassical models. Two subsections are present focusing on the calculation of the radial form factors and on the different aspects of the Coulomb and nuclear excitations. The controversy regarding the collectivity of the PDR and the interplay between the isovector and isoscalar contribution to the cross section are addressed in Section 6. To conclude, the possibility of the existence of new excitation modes induced by the neutron excess for other multipolarities is investigated in Section 7 where the quadrupole case is presented.

2. Experimental techniques

Several experimental studies have been conducted in the past 20 years to measured the low-lying electric dipole strength in nuclei and a clear evolution in the techniques used can be delineated. The use of multiple probes to excite the pygmy states and the focus on its decay mechanism proved to be very useful to unveil important characteristics of this strength. With the present section we want to highlight the main findings on the PDR by briefly describing the experimental methods used to extract these quantities in order to allow a more comprehensive comparison with the theoretical results on which this review is based on. The experimental methods are divided into photonuclear and particle-induced reactions and for each techniques remarks on the specific characteristics and main facilities are given. The most recent results are then explicitly illustrated in the next section. The reader can also find a more complete presentation on the experimental studies in previous reviews [7–10].

2.1. Photonuclear reactions

Real photons have been extensively used to study the low-lying E1 strength due to their high selectivity in exciting dipole transitions. Since the reaction is dominated by the well known electromagnetic interaction, the electromagnetic response of the nuclei (i.e. EM transition probability) can be extracted from the experimental observables in a model independent way. For the purpose of this review we will concentrate only on the photoreactions that allow the excitations of states around particle separation threshold (for more details see the review [27]). This excitation mechanism is often identified as Nuclear Resonance Fluorescence (NRF) or photon scattering and is refereed to with the symbol (γ, γ') [28]. In these reactions, the photon beam impinging on the target nucleus is absorbed in correspondence of an excited state forming a resonance state that decays by γ-rays emission. A setup composed by High Purity Germanium (HPGe) and Lanthanum Bromide ($LaBr_3$:Ce) detectors is used to detect the de-excitation γ rays. Two techniques are used to produce the photon beam resulting in different accuracy on the measured quantities.

The photon beams produced by bremsstrahlung are generated from the interaction of an electron beam with a radiator material (such as silver, gold, copper etc.). The photon flux and energy end point depend on the atomic number of the radiator material and the energy of the incident electrons. A partial polarisation of the photon beam could also be achieved. The photon beam obtained with this method is characterised by a continuous energy spectrum with an intensity that decreases exponentially with increasing photon energy. Although the continues nature of the beam spectrum allows the extraction of absolute cross sections using a well known calibration source (typically ^{11}B) to deduce the photon flux, the energy of the individual incoming photons is not known. This implies that assumptions on the branching ratios and feeding from high-lying states on the measured γ-ray transitions need to be made in order to deduce the incoming photon energy, the corresponding integrated scattering cross section, and the ground state decaying width Γ_0 of the populated excited states. Ratios of the integrated cross sections obtained at different electron beam energies could be used to filter out the feeding contributions [29]. The γELBE facility at the Helmholtz-Zentrum Dresden-Rossendorf [30] and the Darmstadt High Intensity Photon Setup (DHIPS) at TU Darmstadt [31] in Germany are among the bremsstrahlung-beam facilities that extensively contributed in the study of the PDR below particle emission threshold. A considerable improvement to this NRF technique is the possibility to estimate the energy of the incident photons event by event. This allows to constrain the energy of the excited levels and to determine with more accuracy the scattering cross section. For the bremsstrahlung beams this condition can be achieved by measuring the energy of the scattered electrons in coincidence with the decaying γ rays. The resulting photon energy will be therefore given by the difference between the electron beam energy and the "tagged-electron" energy (the recoil energy of the target nucleus is a small correction and within the obtained energy resolution). The energy calculated as such is a good approximation of the real photon energy for thin radiator materials where only one interaction per electron is expected.

The second NRF method is based on the possibility to obtain quasi-monoenergetic photon beams with relative high intensities. This condition is achieved by exploiting the Compton scattering of low-energy laser photons off electrons accelerated to ultra-relativistic energies using storage rings. In fact, in head-on collision, the energy of the scattered photons depends on the scattering angle reaching a maximum boost for backscattering angles ($\theta_\gamma = \pi$). At this angle the energy of the scattered photon can be approximated to $E_\gamma^{max} \approx 4\gamma^2 E_{laser}$ (where γ indicates the relativistic Lorentz factor of the electrons and E_{laser} the energy of the primary optical photons). With this method, refer to as Laser Compton Backscattering (LCB), it is possible to select monoenergetic photons by using specific collimator systems and producing fully polarised beams (the polarisation of the initial laser photons is maintained by the Compton scattering mechanism). The energy of the produced photon beam depends on the energies of the electron and the laser-photon beams. For laser

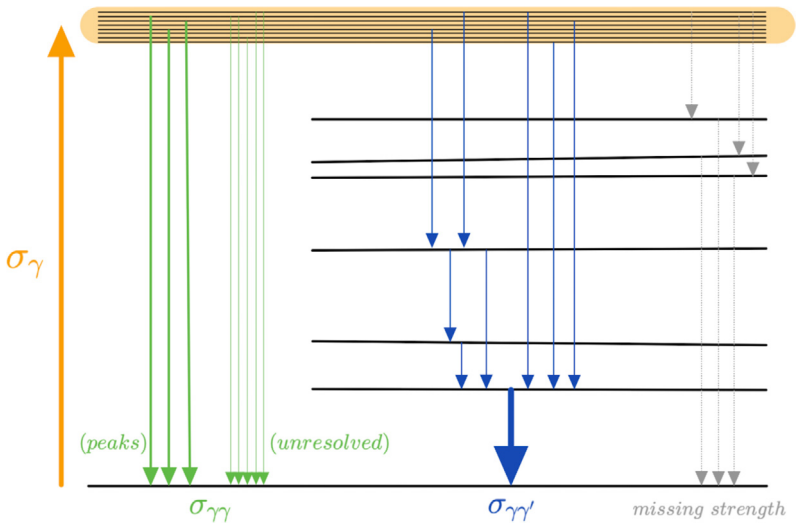

Fig. 1. A schematic representation of the decay of the PDR excited using LCS beams.

in the optical range and electrons of several hundreds MeV, photons of few MeV can be produced with an energy spread $\Delta E_\gamma/E_\gamma$ (FWHM) of about 3%–5%. Few of LCB facilities are available in the world and among them the High Intensity γ-ray Source (HIγS) at the Duke Free Electron Laser Laboratory at Duke University [32,33] in the United States is currently the most used facility to study the low-lying dipole strength. One of its advantages is the coupling of the quasi monoenergetic HIγS beam to the high-resolution and high-efficiency γ^3 setup [34] that allows a more detailed understanding of the PDR decay via the use of γ–γ coincidence detection. A schematic representation of the decay of the PDR is depicted in Fig. 1. The photoabsorption cross section σ_γ (orange arrow) is indirectly measured via the γ decay of the excited strength: $\sigma_\gamma = \sigma_{\gamma\gamma} + \sigma_{\gamma\gamma'}$. The quantity $\sigma_{\gamma\gamma}$ represent the total elastic cross section derived from the contribution of all the transitions (in peaks and unresolved) depopulating the excited region (green arrows). The mixed composition of the γ^3 array (HPGe + $LaBr_3$:Ce crystals) permits the detection with high-resolution of the strength in peaks and also an efficient measurement of the unresolved strength cause by the weak ground-state transitions. The second contribution to the total cross section comes from the inelastic component of the decay (blue arrows). Those transitions predominately decay via the first low-lying states (mainly the first 2_1^+ as shown via statistical model calculations [35]). Therefore the intensity of the low-lying level decays is proportional to this contribution. A small percentage of the decay could go via higher excited states (grey arrows) and will not be detected with the method described. This missing strength will produce an underestimation of the $\sigma_{\gamma\gamma'}$; although according to statistical calculations it account for few percentage of the total strength. The discrimination between the cascade decay and the direct decay of the pygmy states can also be extracted via $\gamma - \gamma$ coincidence matrix. In Section 3 results obtained with this method are shown.

A higher sensitivity in the discrimination between multipolarities is also achieved using the complete polarisation capabilities of the LCB beams as demonstrated in recent experiments [28,36,37]. Among the future LCB facilities, it is worth to mention the Extreme Light Infrastructure-Nuclear Physics (ELI-NP) in construction at Magurele, Romania [38] which will provide extremely intense monoenergetic photon beams ($N_\gamma \sim 10^{11}$ γ/s, E_γ = 1–19.5 MeV) with very high resolution (<0.5%). The superb characteristics of this beam will allow an accurate screening of the E1 strength below and, above particle emission threshold and together with the detection system ELIGANT-GN (ELI Gamma Above Neutron Threshold-Gamma Neutron) [39–41], a measurement of the γ-ray and neutron decay could be studied with high efficiency.

2.2. Particle-induced reactions

For these probes, the reaction mechanism is governed by the electromagnetic and nuclear interactions inducing excitations of different spin/parity states that could have comparable probabilities. Even though this fact would affect the selectivity in exciting the electric dipole strength, different experimental techniques are used to overcome this issue. In particular, the interplay of the two interactions can be tuned by adjusting the characteristics of the projectile, such as mass, charge, energy and scattering angle.

2.2.1. Inclusive measurements

The use of relativistic-proton beams detected at scattering angles around 0° by high-resolution magnetic spectrometers proved to be a powerful method to identify the electric dipole contribution around particle emission threshold [42]. In this experimental conditions, in fact, the Coulomb excitation dominates the total cross section together with the strong spin–isospin part of the effective proton–nucleus interactions implying a greater selectivity to dipole transitions. To disentangle

E1, M1 and other multipolarity contributions, two independent processes are used: the multipole decomposition analysis (MDA) of the cross section angular distributions and the polarisation transfer coefficients analysis [43] making use of a polarisation proton beam. The Research Center for Nuclear Physics (RCNP) [44] in Japan, and iThemba LABS [45] in South Africa, are the two facilities capable of performing such experiments. The beam energy available can reach up to 300–400 MeV at RCNP and 200 MeV at iThemba LABS. Their magnetic spectrometers Gran Raiden and K600, respectively, are used in dispersion matched mode to detect the scattered particles with very high resolution. The energy resolution achieved is around 25–30 keV (FWHM) for thin target (~ 0.5 mg/cm^2). The measured energy range explore simultaneously the region below and above particle emission threshold allowing the investigation of the total E1 strength in one single experiment. Additionally, since in this method the E1 excitation is dominated by the Coulomb interaction it is possible to convert the measured (p,p') cross section in terms of photoabsorption cross section or B(E1) strength by using the virtual photon method described in [46].

Driven by the question around the collectivity of the PDR [14,15,47–54], transfer reactions, such as (d,p) or (p,d), have been recently used to investigate the neutron single-particle character of these low-lying states [55]. To select the direct component of these reactions, the scattered particles can be detected by high-resolution magnetic spectrometers at forward angles. In general, the assignment of the multipolarity of the states excited with this method is not unique and therefore comparison with other experiments and theoretical calculations is crucial to draw conclusions on the pygmy states. The measurement of the cross section at different scattering angles allows the identification of the angular-moment transferred, by means of DWBA calculations based on theoretical models describing the PDR. It is also possible to extract the spectroscopic factors which quantify, in a model dependent way, the p–h configurations contributing to the wave function of the excited states studied. The first results obtained with this technique are discussed in Section 3.

2.2.2. Exclusive measurements

The inelastic scattering of particles and light-nuclei at intermediate energies (20–30 MeV/A and for protons up to 80 MeV) was used in recent years to investigate the nature of the pygmy dipole states by mean of the nuclear interaction. Theoretical calculations showed that at these beam energies the excitation of the PDR is enhanced in comparison to the IVGDR contribution [56]. Moreover these probes explore mainly the superficial part of the transition densities of the PDR in the target nuclei showing different aspects of the strength when compared with photons or relativistic protons. The isospin character of the excited transition can also be studied by using different type of probes. In particular, experiments conducted using α-particles, ^{17}O and protons show an interesting characteristic of the pygmy states compare to what was known previously. These experiments were based on the detection of the scattered beam at forward angles using magnetic spectrometers (BIGBITE at KVI [57–62] and Gran Raiden at RCNP [63]) or silicon-detector arrays (TRACE at INFN-LNL [8,64–68]). The γ-decay from the PDR was measured in coincidence with γ-ray spectrometers (HPGe detectors at KVI, CAGRA at RCNP and AGATA at INFN-LNL). The particle(recoil)-γ coincidence allows the selection of the E1 strength via the angular correlation $W(\theta_\gamma)$ of the outgoing products. Theoretical calculations using the experimental setup conditions predicts a very distinct behaviour of the $W(\theta_\gamma)$ for dipole, quadrupole and octupole transitions. By comparing these expected functions with the values extracted from the experiment and combining the known information from NRF measurements, it is possible to assign the corresponding multipolarity to the observed transitions. The advantage of using the γ spectrometers of new generation, such as AGATA [69,70], allows the determination of the measured angular distribution in an almost continues way. The results of these experiments were compared with the one from (γ, γ') and a clear distinction in the population of what was associated to the pygmy strength in previous experiments was observed. The probes with a dominant isoscalar character and with a tendency to excite the peripheral part of the nucleus (i.e. α, ^{17}O and protons at low/intermediate energies) excite exclusively the lower-energy region of the PDR while the photons, that probe the entire nuclear volume, populate also the high-energy part of the strength. It should be stressed that this comparison is conducted by imposing a selection of the states that decay directly to the ground state (i.e. $E_x \approx E_\gamma$) in all the experiments considered. Therefore, since the same quantity is compared, one expect that the discrepancy seen between the probes is not associated with missing branching ratios to low-lying states or cascade decays. This behaviour seems to be a characteristic of the PDR in medium-heavy nuclei and it is commonly refereed to as isospin-splitting or PDR splitting, more details in Section 3. To extract the total cross section, the measurement of all the possible decay branches to excited states should be taken into account in addition to the ground state decay. In these experiments, the approximation of $\Gamma_0/\Gamma \sim 1$ was used to deduce the excitation cross sections but it seems that, especially for the higher-energy states, additional contributions become relevant, see Section 3. Particular note should be given to the (^{17}O, ^{17}O$'\gamma$) experiments where the TRACE + AGATA setup allowed the measurement of the elastic cross section distribution, used to deduce the optical model parameters for the DWBA calculations of the PDR states. The measured cross sections were well reproduced by DWBA calculations with microscopic form factors based on Random Phase Approximation (RPA) Relativistic Quasiparticle RPA (RQRPA) and Relativistic Quasiparticle Time-Blocking Approximation (RQTBA) transition densities in which clear contribution of the neutrons at the surface was found [56,71,72].

The use of the particle-γ coincidence technique with low-energy beam (10 MeV/A) was also exploited by measuring the scattered particles at backward angles with silicon arrays such as SONIC at the Tandem accelerator of the University of Cologne [73,74] and SiRi at the Oslo Cyclotron Laboratory [75]. In these experimental conditions the nucleus as a whole would be predominantly investigated. A specific analysis method is used to extract the photon strength function (PSF) from which the PDR could be identified, the so called Oslo-method [76–79]. The method is based on the extraction of the

first-generation γ-rays spectra from the particle-γ coincidences through an iterative subtraction technique. Information on the level density and the γ-ray strength function can then be extracted from the distribution of these primary γ rays. This method relies on the validity of the generalised Brink-Axel hypothesis. These results on medium-heavy nuclei show a presence of small deviations from the expected tail of the Lorentzian shape in the region below the neutron separation energy. This excess of strength has been assigned to the PDR, although a direct measurement of the multipolarity of this strength is not possible with this method.

The γ rays following β decays to high-lying states was recently considered as a possible method to investigate the pygmy dipole states, highlighting the advantage of being able to detect weak branching ratios [80]. The total absorption gamma-ray spectroscopy (TAGS) is the technique used in these experiments to detect the decaying cascades from the excited levels rather than only the individual γ rays by making use of large 4π scintillation detectors. The region up to the q-value for beta decay (Q_β) can be explored and by choosing nuclei with $J^\pi = 1^-$ ground state or, more generally, low ground-state spin and negative parity, a subset of pygmy dipole states can be excited since the β decay favours levels with similar spin/parity. The powerful characteristic of the β decay technique is that allows the measurement of small branching ratios to low-lying states since the background conditions are much reduced compared to photon scattering experiments where the background from atomic scattering can become an issue. The results obtained with this method populate a substantial number of pygmy dipole states that have also been identified in (γ, γ') reactions. The measurements of their branching ratios was also obtained. The comparison of population probabilities of β decay and (γ, γ') experiments guided by the corresponding theoretical calculations can give an alternative insight into the microscopic structure of the wave functions of the pygmy states. One limitation of this method is the reduced number of nuclei that can be investigated due to the restriction on possible Q-values to access the PDR region and on the β-decay selection rules to populated specific final states.

2.2.3. Inverse kinematic method with radioactive beam

The methods discussed so far have shown to be very effective to extract informations on the electric dipole strength mainly in stable neutron-rich nuclei. Since the PDR is predicted to be related to the neutron excess, different attempts to investigate more exotic nuclei were made in the past years [81–91]. To explore these nuclei experiments in inverse kinematics were performed. This technique comprise the use of radioactive beams generated by the in-flight fragmentation of a primary beam on light targets (like beryllium). The isotopes of interest are then selected from the secondary beams using fragment separators. The main facilities used to study the PDR are the RIBF@RIKEN in Japan, FAIR@GSI in Germany, FRIB@MSU in US and FRIBs@LNS-INFN in Italy. The experimental setups can be divided into two groups according to which decay, neutron or γ, is used to extract the PDR strength. In the first case, to reconstruct the excitation energy of the projectile a kinematically complete measurement needs to be performed by detecting the residual nuclei and the emitted neutrons and γ rays. For these setups a high detection efficiency of the emitted neutrons is essential and it is usually performed with plastic scintillators walls placed at a large distance from the target position. The outgoing charged fragments are analysed by combining a dipole magnet located right after the target position to a silicon telescope array or drift chambers + plastic scintillators placed few metres downstream of the target. The de-excitation γ rays produced after neutron emission are detected at target position by using a high-efficiency γ-ray spectrometer made of scintillator detectors. Since this decay might consist of several photons, a high efficiency array is crucial for a proper reconstruction of the excitation energy. The momentum vectors of the beam, the outgoing fragments and the neutrons together with the sum of the γ rays are measured and used to extract the excitation energy of the projectile of interest via the invariant mass method. Setups with this characteristic are present at RIKEN, MSU and GSI. The dipole strength can be also characterised by measuring its corresponding γ decay. The experimental setups in this case will comprise of high-efficiency and high-resolution γ spectrometers couple to charge-particle detector arrays as described above. By selecting the outgoing fragment to be the same as the projectile is possible to measure γ decay spectrum of the excited nucleus. The dipole response was studied above and below threshold by enhancing either the Coulomb excitation and/or the nuclear inelastic scattering to resemble the isospin investigation performed in stable nuclei. To this mean accurate selections of the beam energy, experimental targets and scattering angles were made. The majority of experiments focused on extracting the isovector response by using high-Z targets (like Pb or Au) and measuring at scattering angles smaller than the grazing angle to enhance the virtual photon excitation. The isoscalar component was studied in only two nuclei so far ^{20}O [81] and ^{68}Ni [89] where a liquid helium and a ^{12}C targets were used respectively. The future goal for these studies will be to expand the nuclear region of investigation to heavy neutron-rich nuclei up to the lead region. This will be possible with FAIR in the next years. A full energy range of the dipole response measured with higher precision will also be achieved with the next-generation of experimental instruments providing important information to characterise this strength.

3. Experimental results highlights

This section focuses mainly on the results obtained in the last few years. To help the reader, a summary on the major features found over the past decades is also briefly presented, while a more detailed description can be found in previous dedicated reviews [7–10]. The experimental findings are here grouped into the main points of discussion around the PDR.

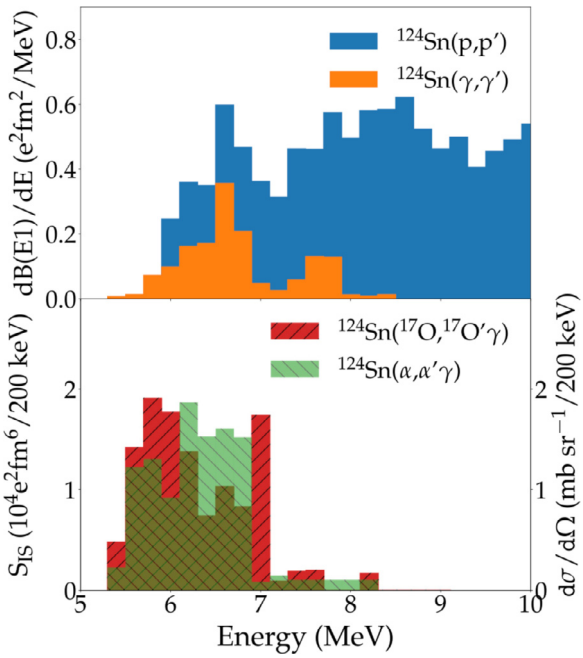

Fig. 2. Electric dipole strength distributions measured in ^{124}Sn using with different probes: relativistic protons, photons, α particles and ^{17}O. *Source:* Figure taken from [92].

3.1. Strength below particle emission threshold

As expressed in Section 2, there is not a unique technique that could highlight all the characteristics of the low-lying dipole response in neutron-rich nuclei. Although by combining the results of complementary probes a clearer picture was drawn over the years. A recent example of this investigation was reported in [92] where the PDR populated using relativistic protons, photons, α particles and ^{17}O was compared, see Fig. 2.

Two aspects are evident while observing this plot: the results from (p, p′) shows a much stronger population of the E1 strength above 7 MeV than in the case of a similar probe like photons and secondly the isoscalar component of the PDR investigated using α and ^{17}O is basically concentrated between 5 and 7 MeV. These differences were found also in other nuclei such as ^{112,116,120}Sn [92,93], ^{140}Ce [62], ^{90,94}Zr [63] etc. identifying them as general characteristics of the PDR. Possible justifications for the discrepancies between (p, p') and (γ, γ') results can be attributed to the lack of sensitivity of the NRF measurements to the unresolved ground-state transitions (see Fig. 1) originating from the high-level density of the investigated nuclei [29,94,95] and/or to the contribution of the γ decay to excited states that it is usually assumed to be negligible [35,96,97]. Banking on the high efficiency of the new γ^3 setup at HIγS it was possible to investigate forward these two points. From the high efficiency of the $LaBr_3$:Ce detectors and the $\gamma - \gamma$ coincidences the contributions from the unresolved strength and the inelastic cross section were extracted as explained in Section 2.1. Fig. 3 shows the results for ^{128,130}Te [36]. The two top panels show the extent of the contribution to the total elastic cross section derived from the unresolved transitions. This fraction is related to the fragmentation of the E1 strength and therefore could be in percentage different for each isotope. In general, an increasing trend with the excitation energy is found reaching up to 70% at 8.9 MeV for the case of ^{128}Te. This is where the coupling to complex configurations becomes more relevant. In these regions also the inelastic cross section contribution (coming from the combination of cascade and direct decays) becomes important as it can be seen in the bottom panels of Fig. 3, especially for the case of ^{128}Te. In this work an estimation of the direct decay of the PDR to the first excited states (2_1^+) was also studied and the results are in line with the one extracted for ^{140}Ce where the fraction of primary transitions to the 2_1^+ relative to the ground-state decay was found to be not-negligible giving important information on the PDR build on excited states. Similar analyses were conducted on other nuclei [35,37,95,97–99] supporting the importance of including the quasicontinuum and inelastic decay channels in NRF experiments to obtain a meaningful conclusion when compared with complementary reactions such as inelastic proton scattering.

The localised enhancement of the isoscalar response deduced by probing the strength with α particles and ^{17}O nuclei (shown as an example for ^{124}Sn in Fig. 2) was found to be a general characteristic of the low-lying E1 strength [7,8,10]. These findings, when compared with the theoretical interpretation of these states, could trigger a point of discussion on what can actually be identified as PDR. If we described the PDR as a collection of states characterised by a strong neutron contributions at the surface, the lower part (below roughly 7 MeV for heavy stable nuclei) would be more appropriately

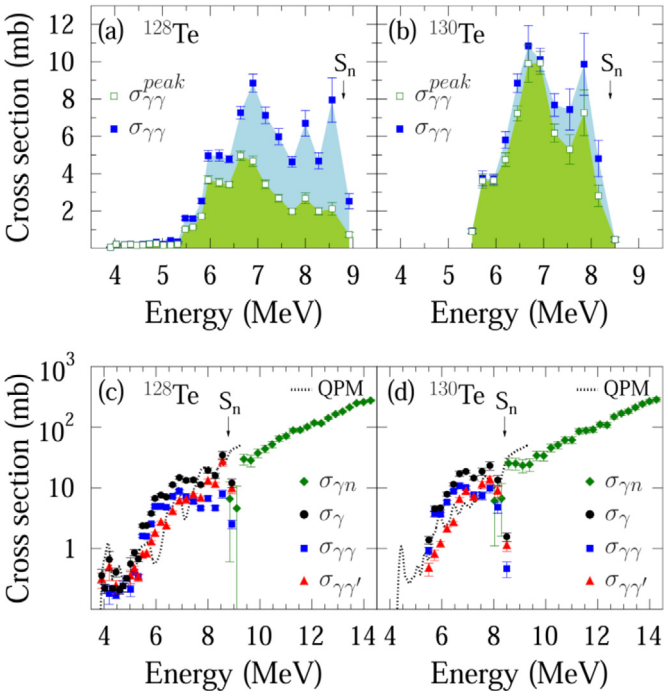

Fig. 3. Average cross sections measured in ^{128}Te and ^{130}Te with quasi-monochromatic photons. Panels (a) and (b) depict the total elastic cross section (blue squares) highlighting the contribution of the strength in peaks with green open squares. Panels (c) and (d) shows the photoabsorption cross sections dividing the contributions into total elastic (blue squares), inelastic (red triangles) component. The total cross section below particle emission threshold is shown with black circles and the one obtained from (γ, n) measurement is drawn with green diamonds.
Source: Figure taken from [36].

defined as such. In fact, the high-energy part shows a more prominent isovector character with a complex decay pattern being more likely to belong to the tail of the IVGDR distribution.

3.2. Strength above particle emission threshold

Theoretical calculations have pointed to the PDR as a low-lying dipole strength located around the particle emission threshold and related to the neutrons contribution. Most of the experimental work performed focused on stable nuclei where a signature of this strength was clearly identified below particle emission threshold as a concentration of 1^- states in even–even nuclei. These states show a progressively more complex signature with increasing excitation energy reaching a transition character when located on the tail of the IVGDR. The natural evolution of these studies was to explore the electric dipole strength above threshold. The presence of the predicted response was found in several exotic neutron-rich nuclei using virtual photon excitation. The first results found at GSI for unstable neutron-rich nuclei ^{130,132}Sn [88,100] and ^{68}Ni [82,86] with relativistic Coulomb excitation have been extensively discussed in previous reviews [7,10]. A clear excess of E1 strength on the tail of the GDR was observed in ^{20,22}O, ^{26}Ne, ^{68,70}Ni, ^{130,132}Sn. In most neutron-rich nuclei the percentage of EWSR exhausted is around 2%–5% and shows an increasing trend for higher values of the N/Z ratio and the location of centroid is found to be between 9 and 11 MeV. An interesting study was conducted to explore if the character of PDR above threshold shows the same isospin characteristic of the response below threshold. The experiment in question was performed using CHIMERA + FARGO arrays at INFN-LNS in Italy [89]. The secondary beam of ^{68}Ni was delivered via the FRIBs@LNS fragment separator. The isoscalar response was studied using ^{12}C target. After considering the contribution from statistical decays of ^{68}Ni, the γ-ray energy spectrum showed an enhancement around 10 MeV proved to be of E1 character after the analysis of the γ-rays angular distribution. The results of the isovector response are however in disagreement on the location of the centroid of the PDR. In fact in [82] a value of 11.0(5) MeV ($\sigma < 1$ MeV) is reported while in [86] the centroid is given at 9.55(17) MeV ($\sigma = 0.51(13)$ MeV). However from the comparison of the two isovector and the isoscalar excitation results, see Fig. 4, the isospin splitting of the PDR is not evident for the present nucleus. If this phenomenon is related specifically to the strength above neutron emission threshold or to ^{68}Ni cannot be concluded from the available data. To draw a clearer picture of the PDR above S_n is therefore critical to perform more experiments with improved experimental conditions, such as better energy resolution and statistics, using a combination of isovector and isoscalar probes.

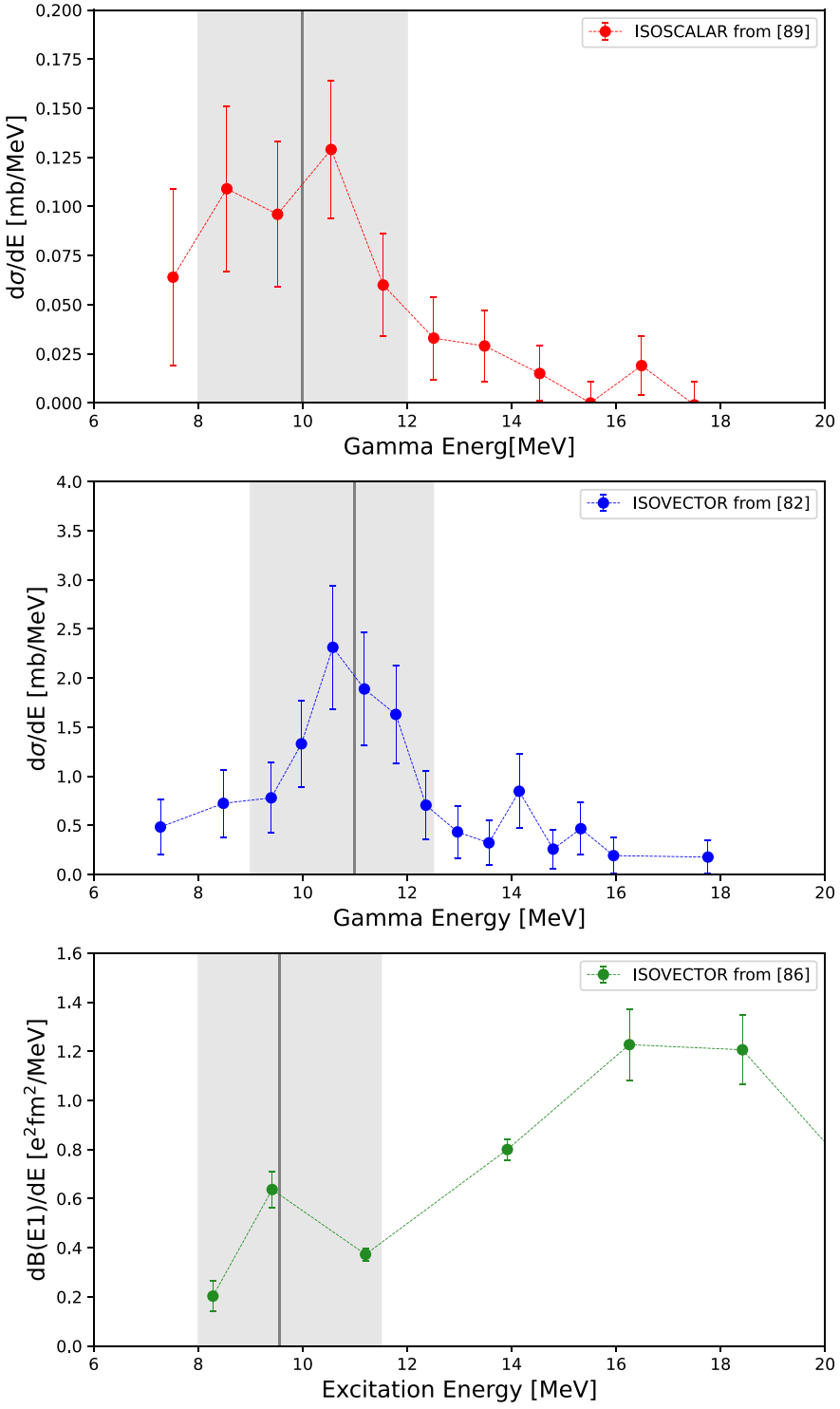

Fig. 4. Comparison of the γ-ray differential cross sections and the E1 strength distribution for ^{68}Ni obtained in [82,86,89], respectively.

3.3. Collectivity

A (d,p) transfer reaction was recently used to investigate the neutron single-particle character of ^{208}Pb [55]. The experiment was performed at the Q3D spectrograph of the Maier-Leibnitz Laboratory, Germany [101]. The deuterons

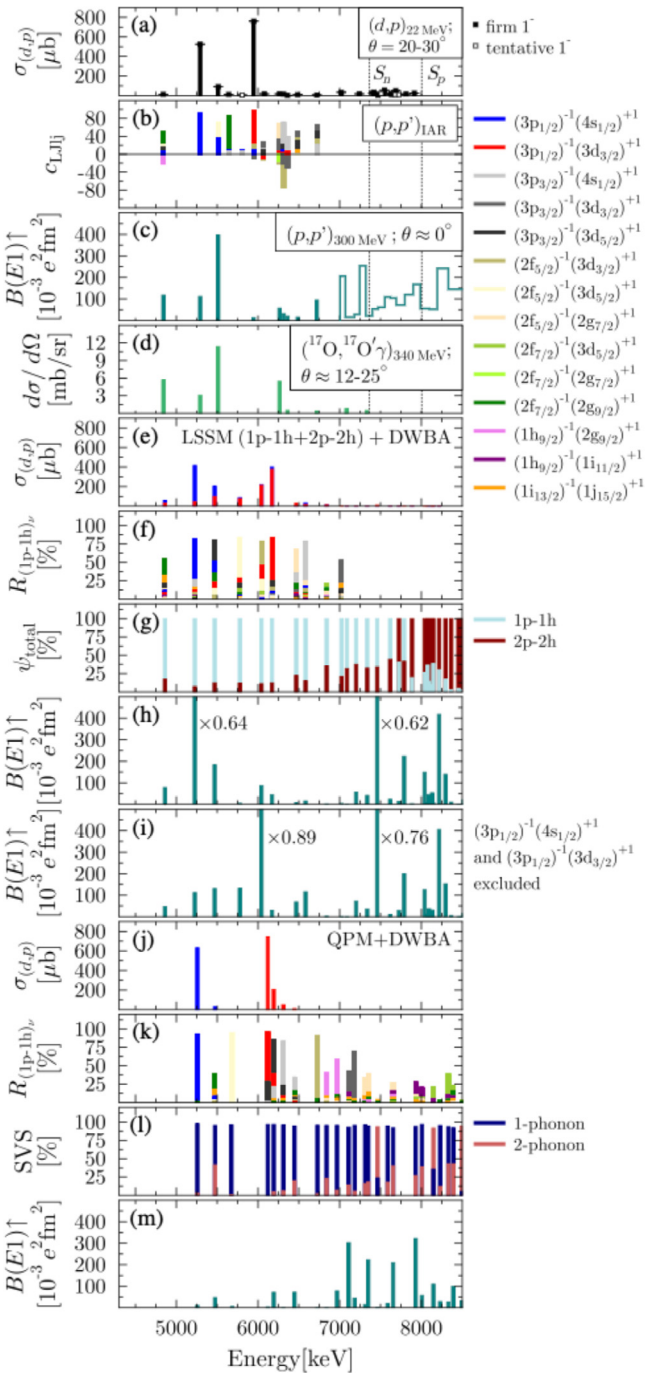

Fig. 5. Experimental results obtained for ^{208}Pb in (d,p) reaction in comparison to a selection of other experimental data on the PDR and with theoretical calculations.
Source: Figure taken from [55].

were accelerated to 22 MeV and a 99% enriched ^{207}Pb target on a Carbon backing (thickness 0.11 mg/cm^2) was used. The angular distribution of the scattered particles was measured at three different scattering angles (20°, 25°, 30°). A resolution of 6 keV (FWHM) was achieved, allowing the identification of several known 1^- states in the PDR region. The data were compared with Large Scale Shell Model (LSSM) [102] and Energy-Density Functional plus Quasiparticle Phonon Model (EDF + QPM) [103] calculations. Two 1^- states at 5292 and 5947 keV were strongly excited via the (d,p) reaction (panel (a) of Fig. 5) and their angular distributions showed a dominant contribution of the two distinct neutron

1p–1h configurations (namely $(3p_{1/2})^{-1}(4s_{1/2})^{+1}[S = 0.77(4)]$ and $(3p_{1/2})^{-1}(3d_{3/2})^{+1}[S = 0.66(4)]$ respectively). These results are in good agreement with the LSSM (from panel (e) to panel (i) of Fig. 5) and EDF + QPM (from panel (j) to panel (m) of Fig. 5) where both calculations predicts the strength coming from the $(3p_{1/2})^{-1}(4s_{1/2})^{+1}$ concentrated in one state while the $(3p_{1/2})^{-1}(3d_{3/2})^{+1}$ is more fragmented in the case of LSSM calculations. Consistency in the total strength predicted by the two models and the experiment was found. However, the two theoretical models do not generate enough spectroscopic strengths above the neutron separation energy. The summed transition densities of the first 1^- states show characteristics which are in agreement with the oscillation of the neutron skin and completely different from the IVGDR. A distinction is observed above 7.5 MeV, where, as predicted by both LSSM and EDF + QPM models, 2p–2h configurations contribute substantially to the wave function.

The question on the collectivity was studied also in ^{120}Sn [104] where a (d, p′ γ) reaction was used to investigate the single particle nature of the pygmy states. A deuteron beam ($E_d = 8.5$ MeV) was provided by the 10 MV FN-Tandem accelerator laboratory at the University of Cologne, Germany. The SONIC@HORUS allowed combined detection of the outgoing protons and the de-excitation γ rays. The multipolarity of the excited states was determined using proton-γ correlations. The experimental results were compared with EDF + QPM calculations. Also in this case two dominant configurations were identify to contribute mainly to the states between 6 and 7 MeV while for the high-energy part is predicted to have more complicated 2ph + 3ph configurations. It will be important to expand these measurements to mass regions with different proton and neutron number where other underlying single-particle structures can be investigated.

3.4. Role of deformation

If we associate the PDR with the picture of a neutron skin oscillating against an isospin saturated core one could expect a splitting of the dipole response in deformed nuclei similar to the one observed for the IVGDR where a double-humped structure is visible for the most deformed nuclei. This structure is commonly associated with different frequencies of the longitudinal (K = 0) and transversal (K = 1) vibrations respect to the symmetry axis. Experimental information on the PDR in strongly deformed nuclei is currently limited to few measurements recently performed [105–108]. The response of ^{76}Se ($\beta_2 = 0.309(4)$) above 4 MeV was studied using quasi-monochromatic gamma beam at the HIγS facility [108]. The E1 strength obtained did not show any clear evidence of a splitting distribution in this nucleus. From the theoretical interpretations obtained using a Time Dependent Hartree Fock (TDHF), the picture of the PDR – as the isospin saturated core vibrating against the neutron skin – was not validated probably in connection to the low excess of neutrons in this specific nucleus. A strong remark was made on the importance to account for the contribution of the branching to excited states in the estimation of the total dipole strength as previously commented in Section 2.1. In [107] the authors compare the summed B(E1) measured between 6 and 8 MeV for the Xe and Mo isotopic chains by trying to correlate the strength with the neutron excess ratios and the quadrupole deformation parameter β_2. The general trend observed is an increase of the strength with N/Z ratio for both Mo and Xe isotopes while a decrease with deformation is seen in the Xe chain. Overall in this study it seems that the deformation does not induce a considerable effect on the total strength found in these neutron-rich nuclei. Even though some attempts were made to gain information on deformation in the PDR, the results extracted in these experiments are unfortunately inconclusive to give any final answer to this question.

To have a better indication of the connection of the PDR structure with the K-quantum number its γ decay has to be measured. In fact, the K-quantum numbers of the excited states can be determined by comparing their decay branching ratios to the ground state band with the predictions of the Alaga rules [109,110]. According to the rule for quadrupole deformed nuclei, a 1^- state of pure K-number is expected to have the following ratio:

$$R = \frac{B(E1;\, 1^- \longrightarrow 2_1^+)}{B(E1;\, 1^- \longrightarrow 0_1^+)} = \begin{cases} 2.0 & \text{for K} = 0 \\ 0.5 & \text{for K} = 1 \end{cases} \tag{2}$$

The task of measuring this ratio for the pygmy states is non-trivial especially due to the fact that, for the strongly deformed nuclei, the first 2^+ state is energetically very close to the ground state making very difficult to distinguish this decay to the ground state one. An example of this is discussed in [37] where the PDR in ^{164}Dy ($\beta = 0.3486(21)$) was studied via (γ, γ') reaction at HIγS. Even if a good beam resolution (FWHM), around 3% of the beam centroid energy, was achieved it was not sufficient to clearly separate the contributions of the PDR decay to 2_1^+ state ($E(2_1^+) = 73.393(5)$ keV) from the one to the ground state, see top panel of Fig. 6. Therefore, a complementary estimation of the branching ratio was extracted by using the mean azimuthal asymmetries $\langle\epsilon\rangle$ of the transitions. Ground-state decays are characterised by $\langle\epsilon\rangle \approx \pm 1$ according to the E1 or M1 multipolarity of the transition as depicted in Fig. 6 (bottom panel). The decay via the 2_1^+ gives an almost isotropic distribution inducing a deviation of $\langle\epsilon\rangle$ from the ground state values. By observing the experimental $\langle\epsilon\rangle$ values in the PDR region a reduction from the E1 expected value was found and associated with the presence of a mixing between the decays to the 2_1^+ state and to the ground state. The authors concluded, from the results extracted, that no evidence for a splitting of the PDR built on the ground-state band was visible in ^{164}Dy. This conclusion was also reached for another rare-earth nucleus, ^{156}Gd, in [99]. These works underline the need of a much small energy spread of the photon beam to provide significant advantages for a clean separation of the decays to the ground state and the first excited state. This will be possible with the LCB beam at ELI-NP where a spread of less than 1% could be achieved.

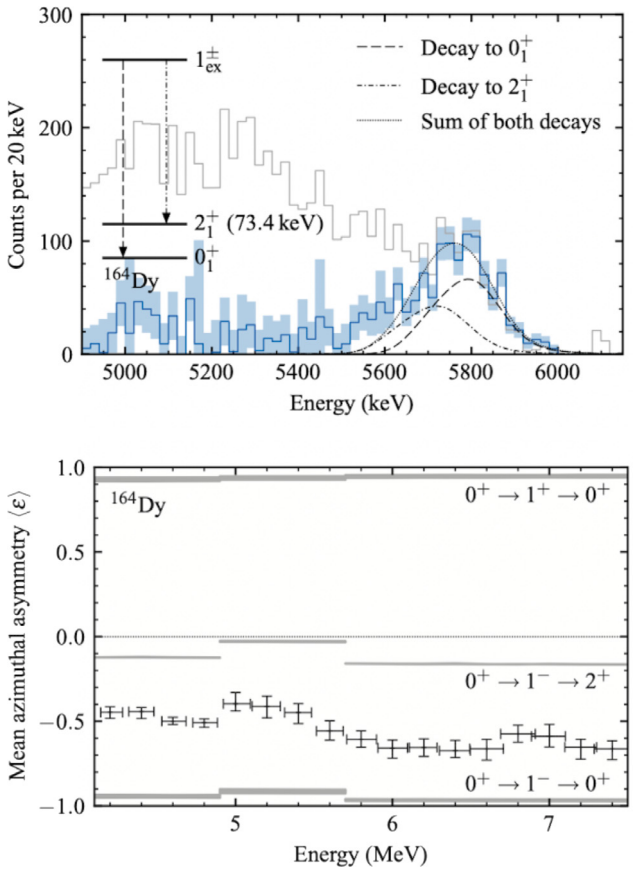

Fig. 6. Top panel: Determination of mean branching ratios to the ground state and first 2_1^+ state for a beam energy of $E_beam = 5.8$ MeV. Gamma ray spectrum of ^{164}Dy excited with LCB beam of 5.8 MeV. The grey spectrum is the original one while the blue is deconvoluted and background-corrected. The decay to the ground state and the first excited state are also depicted. Bottom panel: Mean azimuthal asymmetries for PDR region measured in ^{164}Dy.
Source: Figures taken from [37].

3.5. The neutron excess and the other multipolarities

After the extensive work on the PDR in neutron-rich nuclei, a natural question was raised from theoretical works, see Section 7, on the possibility that the neutron skin could affect other multipolarities. The experimental methods described in Section 2 could be used to address this concern and results on the quadrupole component were extracted [65,111,112]. Learning from the features found for the dipole case, the experiments were set to look for specific characteristics in the quadrupole response: presence of a group of 2^+ states in a energy region between 2.5–5 MeV, presence of isospin mixing in their structure, and strong decay to the ground state. The difficult part for this multipolarity is that similar characteristics could be found for multi-phonon excitations making conclusive statements even more complicated than for the E1 case. The first experimental evidence of a concentration of 2^+ states was extracted from the experiment conducted with a ^{17}O beam on ^{124}Sn using a particle-γ coincidence setup (TRACE + AGATA) as described in Section 2.2.2. A group of new transitions decaying to the ground state with energies between 3 and 5 MeV was found and identified to be of E2 origin via the angular distribution analysis. The measured energy and intensity distributions of these 2^+ states were found to be very similar to QPM calculations providing a reasonable ground to infer the evidence of PDR-like mode in the quadruple channel, referred to as Pygmy Quadrupole Resonance (PQR). An attempt to critically disentangle the one-phonon response from the multi-phonon one expected in the same energy region was performed when a comparison between the results from a $(\alpha, \alpha'\gamma)$ and a (γ, γ') experiments on ^{124}Sn was done in Ref. [111]. The ground state γ-decay branching ratio $b_0 = \Gamma_0/\Gamma$, with Γ_0 being the ground state width and Γ the total width, was obtained. A predominant grounds-state decay, identified in the value of b_0 being greater than 0.5, was consider a signature for one-phonon type excitations. Several transitions with this characteristics were observed in the region 2–5 MeV. The authors therefore conclude about the presence of the PQR in this nucleus. The experimental and theoretical investigations of the PQR were then extended to two other Sn isotopes (i.e. ^{112,114}Sn) to describe the evolution of this strength with charge asymmetry [113]. The experimental technique used in this case was based on $(p, p'\gamma)$ Doppler-shift attenuation (DSA) coincidence measurements

performed at the SONIC@HORUS setup. The B(E2) strengths, the ground-state and 2_1^+-state γ-decay branching ratios could be extracted from the measurement and critical comparison with QPM calculation was conducted. The outcome was also in this case supporting towards the existence of a new quadrupole mode in nuclei with neutron skin. In fact, in addition to the features found in previous experiments, the EDF + QPM calculations of neutron-skin thickness and B(E2) transition probabilities indicate an increase of the total PQR strength with the neutron excess. Multi-phonon excitations were also present in the PQR region. However, this contribution was found to be less important in the decay of the PQR preserving the relationship between the total PQR ground state transition strength and the neutron-skin thickness. An extended discussion on this topic is presented in Section 7.

4. Theoretical approaches

4.1. Macroscopic models

The gross features of collective excitations are fairly well described by macroscopic models which are based on classical or semiclassical theories. These approaches rely on the fact that the nucleus can be thought as a liquid drop composed of protons and neutrons fluids that are allowed to undergo small collective oscillations around the equilibrium. They may show up as neutrons and protons in-phase motion (isoscalar mode) or in a out-of-phase displacement (isovector mode). These are also usually classified into two different kind of motion, one related to the surface oscillation and another to the compression mode. In the first case the surface is expanded in terms of spherical harmonics to describe the small harmonic oscillations. Their coefficients obey a harmonic Hamiltonian which describes the surface oscillation via the restoring force and the inertial mass of the liquid. This approach is valid for modes whose angular momentum λ is larger or equal to two. The compressional modes are better described by a density oscillation around its equilibrium density and the equations of motion of the fluids are governed by the hydrodynamic equations. For more details see Ref. [114,115] and references therein.

Just after the discovery of the GDR [116] few attempts were made to describe this resonance and among them the theory formulated by Goldhaber and Teller [117] (GT) was the first one. They interpreted the GDR as a different resonance from the one generated by the nuclear levels such as caused by the collective motion of all the proton of the nucleus in one direction and the motion of the all neutrons in the opposite direction. This gives rise to a dipole vibration whose frequency was calculated and compared to the available experimental data. The model assumes that the protons and neutrons are incompressible fluids, have a spherical shape and during the displacement the surface of the two fluids do not overlap. In the liquid drop model, the part of the energy that changes when the protons moves with respect to the neutrons is the symmetry energy. Under the assumption that the potential varies quadratically with small displacement values, the frequency of the mode depends on the nuclei mass number as $A^{-1/6}$. This trend was in good agreement with the data known at that time.

Few years later Steinwedel and Jensen [118] (SJ) build up another macroscopic model for the GDR which was already considered as an other possible model in Ref. [117]. Within a hydrodynamical approach, it is assumed that both fluids are compressible and irrotational however the total fluid must be incompressible. Therefore in this model there is no separation between protons and neutrons at the surface but only a variation of their densities. The GDR is obtained as a density oscillation of the protons against the neutrons and the resonance energy is related to the restoring force of the vibration. The latter can be deduced from the symmetry energy

$$E_s = a_s \int \frac{(\rho_n(\vec{r},t) - \rho_p(\vec{r},t))^2}{\rho_0}\, d\vec{r} \tag{3}$$

with ρ_n and ρ_p the neutron and proton densities and ρ_0 the total nuclear density, $\rho_0 = \rho_n + \rho_p$. The symmetry energy parameter a_s, in the Bethe–Weizsäcker mass formula, has a value of about 20 MeV. The A dependence of the GDR centroid goes as $A^{-1/3}$ which seems more appropriate for heavy nuclei than the A dependence of the GT model ($A^{-1/6}$) that works better for light nuclei. Apart from the different energy prediction, the important distinction between the two models reside in the different radial form factors associated to them, as we will see in Section 5.1.

The classical hydrodynamic model of SJ was extended to a three fluid model [119] in order to account for the nuclei with neutron excess. In this version the three fluids arise from the protons and the neutrons, occupying the same orbitals in the core, and the excess neutrons. The oscillatory motion of the three fluids was taken into account with the condition that the density should remain constant inside the nuclear radius R

$$\rho_p + \rho_{nb} + \rho_{ne} = \rho_0 = \text{constant for } r \leq R \tag{4}$$

where the subscript p, nb and ne refers to protons, neutrons bounded at same orbital of the protons and neutrons in excess, respectively. Furthermore, there are no surface vibrations allowed and the three fluids are supposed to be compressible

$$\rho_i + \mathrm{div}\rho_i\vec{v}_i = 0, \qquad i = p, nb, ne \tag{5}$$

the $\vec{v}_i$ are the local flow velocity of the fluids. Considering all the possible vibration modes, a Lagrangian can be written taking into account the damping due to friction and interaction with the electromagnetic field. Then, neglecting all second and higher order terms in the velocities (an usual approximation in hydrodynamics), the equation of motion can be

obtained. Differently from the two-fluid model, where there is only one allowed dipole mode, in this three-fluid model two independent dipole modes exist. In fact, taking ^{208}Pb as a explanatory example two dipole resonances are found at 13.3 and 4.4 MeV. The resonance at higher energy is in agreement with the experimental GDR peak while the low-lying one, showing a much smaller strength, has an energy very close to the one found by Lane [3].

A disadvantage of this model is that there are three parameters needed for the restoring forces of the three fluids. This can be partially avoided by assuming that the protons and neutrons that occupy the same nuclear levels, move simultaneously forming a unique core fluid, $\rho_c = \rho_p + \rho_{nb}$, with a displacement in the opposite direction of the remaining excess neutron ρ_{ne} as discussed in Ref. [120]. This classical hydrodynamic model is conceived to study the PDR mode considered as produced by an out of phase oscillation of the core against the neutron excess forming a kind of skin. A fair agreement with the available experimental data was achieved [120].

The picture of the PDR as generated by an oscillation of the core against the neutron skin is common in most of the literature although does not coincide, in many details, with the outcomes of microscopic theories, as we will see in the following sections. Nevertheless, if one wants to stay attached to a macroscopic view of the mode this is the most logical way to picture it. As stated in Ref. [121], "The presence of such a mantle of dominantly neutron matter" should affect some properties of the collective modes or give rise to new ones. The authors of Ref. [121] allowed the displacement of the core in opposite direction of the one of the skin, using the GT model. In this approach the restoring force is not obtained via the symmetry energy but rather evaluating the potential energy as function of the linear displacement. In the case of the GDR, the change in the neutron–proton interaction, responsible for the oscillations is

$$\Delta V_{GDR}(z, R_n, R_p) = V_{GDR}(z, R_n, R_p) - V_{GDR}(z = 0, R_n, R_p) \tag{6}$$

with

$$V_{GDR}(z, R_n, R_p) = K \int \rho_n(\mathbf{r} + z_n, R_n)\rho_p(\mathbf{r} - z_p, R_p)d\mathbf{r} \tag{7}$$

where $z = z_n + z_p$ is the relative displacement of the neutron and proton densities and the strength K can be obtained by the volume integral of the nucleon–nucleon interaction. The presence of the neutron skin does not have a prominent effect on the deduced GDR energy because the percentage of the neutron of the skin is small compared to the bulk motion of all neutrons. The effect is greater in the case of the PDR, its energy is evaluated relative to the GDR and the classical sum rule is satisfied, a result similar to the one obtained in Ref. [120].

Along a somewhat similar approach Bastrukov et al. [122] have considered the macroscopic excitation mechanism of the PDR as related to an elastodynamic excitation in which the nucleus is considered as a spherical piece of elastic continuous medium – a core – with a normal nuclear and electric charge densities uniformly distributed surrounded by a layer. The excitation mode in this case is therefore generated by the oscillation of the layer against the core induced by the elastic restoring force. The total dipole strength of the electromagnetic response was computed as squared dipole moment of the charge-current density showing a reasonable agreement with the experimental data. A fair agreement was also found for the energy of the low dipole mode where it is predicted to decrease with the mass number of the nuclei as $E_{PDR} \approx 31A^{-1/3}$ MeV. Describing the PDR as an elastodynamic excitation mechanism implies the isoscalar nature of this soft mode.

Within the macroscopic models one can derive expressions for the transition densities and/or radial form factors. We will deal with these approaches in Section 5.1.

4.2. Microscopic models

The most detailed description of the structure of medium- and heavy-mass nuclei relies on the microscopic self-consistent mean field models based on effective interactions. These theories have been applied successfully to describe the ground state properties of the nuclei as well as the their excited states including the Giant Resonances (GRs). This description of the nuclear structure includes an accurate explanation of the damping mechanism of the collective states related to the width of these states. All these mean-field approaches have been extensively applied in the studies of the low-lying dipole states where even the most simple one, such as Hartree–Fock (HF) plus Random Phase Approximation (RPA), reproduce very well the main properties of the PDR. In this section, the main mean-field approaches are presented starting from the HF + RPA, and their extension to treat open-shell nuclei as the Quasiparticle RPA (QRPA) and its Relativistic version (RQRPA). Following with the more sophisticated ones where the coupling of the elementary one-particle one-hole (1p–1h) excitations with more complex configurations are taken into account. The approaches that include the coupling with multiphonon states are presented in the last subsections.

4.2.1. HF plus RPA

The Hartree–Fock method consists in constructing a self consistent mean field [123], describing the interaction generated by all the nucleons of a nucleus, from an effective two-body interaction. Starting from a trial wave-functions, the Schödinger equation is solved iteratively until self consistency is obtained. The method relies on the use of effective nucleon–nucleon interactions which are derived from a bare nucleon–nucleon one. They contains several parameters which are fitted to reproduce the ground state properties of nuclei. The most used is the zero-range Skyrme interaction [124] where the three-body term is expanded at low order. With this force the nuclear binding energy and the

nuclear radii for many nuclei along the periodic table were reproduced with the same set of parameters [125]. Another largely used force is the Gogny interaction [126] which is a finite range force obtained by replacing parts of the expression of the Skyrme force with Gaussians. That was necessary to overcome the difficulty of the Skyrme interaction to correctly describe the pairing correlation in nuclei. Many parameterisations of both forces are available but only few of them are currently used, because able to describe with equal accuracy the ground state properties of stable nuclei. For closed-shell nuclei the average nuclear interaction obtained with the Hartree–Fock method is not only able to predict the ground state properties but also to reproduce the correct order of the single-particle levels. The most elementary excitation are the one-particle one-hole (1p–1h) excitations which are generated by the promotion of a particle above the Fermi level leaving a hole in the level below it. These 1p–1h excitations can be mixed by the residual interaction, namely the difference between the two-body interaction and the mean field obtained by the H–F method. Each p–h configuration has a definite angular momentum which is given by the coupling of the spin and angular momentum of the corresponding states. The residual interaction allow the coherent mixing of p–h configurations with the same angular momentum giving rise to a collective state. The Tamm–Dancoff Approximation (TDA) consists in diagonalising the residual interaction in the 1p–1h space without taking into consideration the ground state correlations [123]. The energies of the states depends on the matrix element of the p–h configurations that are different from the unperturbed ones. In particular, for the states of isovector nature (with isospin T = 1) the two-body matrix elements result to be positive in contrast to the isoscalar (T = 0) ones that are negative. This induce the collective isovector and isoscalar states to be pushed up and down in comparison to the corresponding unperturbed levels. In general the TDA works very well however some experimental feature are not well predicted. This is due to the fact that in this approximation the excited states are constructed upon an uncorrelated ground state, i.e. an HF Slater determinant. This correlations can be implemented by recurring to the Random Phase Approximation (RPA) they allow that the nucleus can be excited through the creation of a particle–hole or the annihilation of the p–h pair present in the ground state. The RPA equation can be deduced by the equation of motion method [123,127] where an excited state $|\Psi_\nu\rangle$ is described as superpositions of p–h and h–p configurations with respect to the correlated ground state $|\Psi_0\rangle$

$$|\Psi_\nu\rangle = q_\nu^\dagger |\Psi_0\rangle \,. \tag{8}$$

The ground state is defined as the vacuum of the q_ν operator

$$q_\nu |\Psi_0\rangle = 0 \,. \tag{9}$$

The explicit expression of the $q_\nu^\dagger$ operator is

$$q_\nu^\dagger = \sum_{ph} \left[X_{ph}^\nu a_p^\dagger a_h - Y_{ph}^\nu a_h^\dagger a_p \right] . \tag{10}$$

where the amplitude X and Y are solutions of the RPA secular equation. Since these p–h amplitudes can be written as

$$X_{ph}^\nu = \langle \nu | a_p^\dagger a_h | 0 \rangle \tag{11}$$

$$Y_{ph}^\nu = \langle \nu | a_h^\dagger a_p | 0 \rangle, \tag{12}$$

their absolute square gives the probability to find the configuration $a_p^\dagger a_h|0\rangle$ and $a_h^\dagger a_p|0\rangle$ in the excited state ν. The term Y describes the correlation in the ground state. When the Y amplitudes are zero the equations reduce to be the TDA ones.

The RPA equation are written in compact form as

$$\begin{pmatrix} A & B \\ B^* & A^* \end{pmatrix} \begin{pmatrix} X^\nu \\ Y^\nu \end{pmatrix} = \hbar E_\nu \begin{pmatrix} X^\nu \\ -Y^\nu \end{pmatrix} \tag{13}$$

where the matrix A and B are

$$A_{php'h'} = \langle HF | a_h^\dagger a_p [H, a_{p'}^\dagger a_{h'}] | HF \rangle \tag{14}$$

$$B_{php'h'} = -\langle HF | a_h^\dagger a_p [H, a_{h'}^\dagger a_{p'}] | HF \rangle \tag{15}$$

where it has been assumed that the correlated ground state is not much different from the Hartree–Fock ground state $|HF\rangle$ and therefore the expectation values can be calculated using the $|HF\rangle$. This is known as the quasi-boson approximation. More details, including explicit expressions which take care of the coupling to total angular momentum and isotopic spin, can be found in Ref. [123,127]. The RPA solutions are composed by superposition of many p–h configurations, that when they sum up coherently they correspond to collective states. The RPA is the most fundamental approach in describing the nuclear collective motion. It provides a very good description of the vibrational collective states both low-lying and the giant resonances. The excitation of these states are calculated using operators which describe the action of electromagnetic (isovector) or hadronic (isoscalar) external fields. They are usually expressed in terms of Bessel functions and in the case of dipole states their explicit expressions, in the long wavelength limit, are given by

$$O_{1M}^{(IV)} = \frac{eN}{A} \sum_{p=1}^{Z} r_p Y_{1M}(\hat{r}_p) - \frac{eZ}{A} \sum_{n=1}^{N} r_n Y_{1M}(\hat{r}_n). \tag{16}$$

where the effective charge for protons ($\frac{eN}{A}$) and neutrons ($\frac{eZ}{A}$) have been introduced to remove the centre of mass motion which is a spurious translational mode. For the dipole isoscalar operator the lowest term of the expansion correspond to a spurious translational motion and therefore the next-order term which correspond to a $3\hbar\omega$ dipole nuclear transition is considered and the leading-order dipole transition operator can be written as

$$O^{(IS)}_{1M} = \sum_{i=1}^{A}(r_i^3 - \frac{5}{3}\langle r^2\rangle r_i)Y_{1M}(\hat{r}_i) \tag{17}$$

where the term ($\frac{5}{3}\langle r^2\rangle$) has been introduced to eliminate the spurious contribution of the centre of mass. The reduced transition probability from the ground state to the excited state ν can be written as

$$B(E\lambda, 0 \rightarrow \nu) = \left| \sum_{ph}(X^{\nu}_{ph} - Y^{\nu}_{ph})\langle p\|O_\lambda\|h\rangle \right|^2 = \left| \sum_{ph} b_{ph}(E\lambda) \right|^2 \tag{18}$$

where $\langle p\|O_\lambda\|h\rangle$ are the reduced multipole transition amplitudes associated with the elementary p–h configurations. The $b_{ph}(E\lambda)$ can be considered as the partial contribution of a p–h configuration to the reduced transition probability for the given state. Another very important quantity that can be calculated within the RPA is the transition density which describes the characteristic of the excited state. In particular, information on the type of excitation (volume or surface) or whether neutrons and protons are in- or out-of-phase can be deduced establishing, in this way, their isoscalar or isovector nature. It is important to stress that the transition density can be directly related to the radial form factors and consequentially to the inelastic cross sections. Although they are not a measurable quantity per se their features are of paramount importance for a good description of the experimental data. The radial part of an RPA transition density for a state ν with an angular momentum λ can be written as

$$\delta\rho^{\nu} = \frac{1}{\sqrt{4\pi}}\sum_{ph}\frac{\hat{j}_p\hat{j}_h}{\hat{\lambda}}(-)^{j_p+j_h-\frac{1}{2}}\langle j_h\frac{1}{2}j_p - \frac{1}{2}|\lambda 0\rangle\delta(\lambda + l_p + l_h, even)[X^{\nu}_{ph} - Y^{\nu}_{ph}]\,R_{l_pj_p}(r)R_{l_hj_h}(r) \tag{19}$$

where the X and Y are the RPA amplitudes, $\hat{\lambda} = 2\lambda + 1$, l and j are the angular and the total momentum of the single-particle states and the R's their radial wavefunction which are solution of the HF equations. The transition densities for protons and neutrons can be calculated by running the summation separately over the number of p–h configurations of protons and neutrons respectively and the isoscalar and isovector transition densities can be constructed as

$$\delta\rho^{\nu}_{IV}(r) = \delta\rho^{\nu}_{n}(r) - \delta\rho^{\nu}_{p}(r) \tag{20}$$

$$\delta\rho^{\nu}_{IS}(r) = \delta\rho^{\nu}_{n}(r) + \delta\rho^{\nu}_{p}(r) \tag{21}$$

The first studies of the effect of the neutron excess on collective states in nuclei far from the stability valley were carried out within the HF plus RPA approach [128–132]. It turns out that while the effect on the monopole and quadrupole states is moderate, the one on the dipole states is stronger. As an example, the first calculation performed on a set of calcium and oxygen isotopes is here presented. The calculations were done employing a SGII Skyrme interaction [133,134] in a discrete RPA, where the system is confined in a large box so the continuum is discretised. As it is shown in Fig. 7, the effect of the neutron excess is the spreading of the isovector dipole strength. The increase in the neutrons number reflects in a shift of the strength towards lower energy resulting in a peak at around 10 MeV. Also the centroid of the strength, corresponding to the IVGDR, is moving downwards with a displacement larger than the $A^{-1/6}$ dependence predicted by the Goldhaber–Teller model [114] and more in line with the trend of $A^{-1/3}$ expected by the of the hydrodynamical Steinwedel–Jensen model [114]. The isoscalar response, obtained by using the operator of Eq. (17), is shown in Fig. 8 for the same Ca isotopes of Fig. 7. The continuous curves have been obtained by folding the discrete spectrum with Lorentzian functions with a width $\Gamma = 3$ MeV. We note that the strength is split in two main components whose centroids do not change consistently with the increasing neutron number. While the isoscalar GDR (ISGDR) peak around 30 MeV maintains its magnitude, the lower one, which is evidently related to the neutrons excess, does increase with the neutrons number.

The presence of a peak in the dipole strength distribution at low energy is also found in stable nuclei with neutron excess. Fig. 9 shows the strength function for the isovector (a) and isoscalar (b) response for the ^{208}Pb [14] as example. The calculation have been performed with a self consistent mean field approach based on HF plus RPA [135] with three different Skyrme effective interactions, namely SGII [133,134], SLy5 [136] and SkI3 [137]. The continuous curves have been obtained by convoluting the discrete B(E1) values with Lorentzian of 1 MeV width. The three interactions produce very similar results for the IVGDR and compatible with the experimental findings. A clear difference is found for the low-lying peak corresponding to the PDR excitation whose details can be appreciate in the inset of panel (a) of Fig. 9. In panel (b) the shaded area highlights the PDR region where a very strong isoscalar response is obtained.

Already with this not sophisticate HF + RPA approach one can obtained some of the characteristic features of the low-lying dipole states. In fact an isovector strength appears in the low-energy region for nuclei with N > Z while the isoscalar one, present also for nuclei with N = Z, does considerably increase with the neutron excess. These main features are maintained also when more sophisticated theories are used to describe the structure of the low-lying dipole states as presented in the next sections.

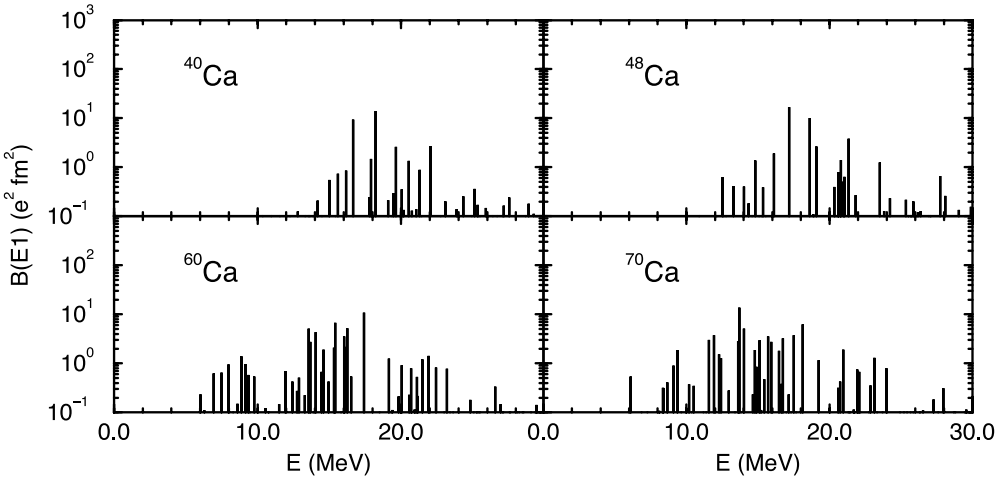

Fig. 7. Isovector dipole response obtained in a HF + RPA calculation for four Ca isotopes.
Source: Adapted from Ref. [131].

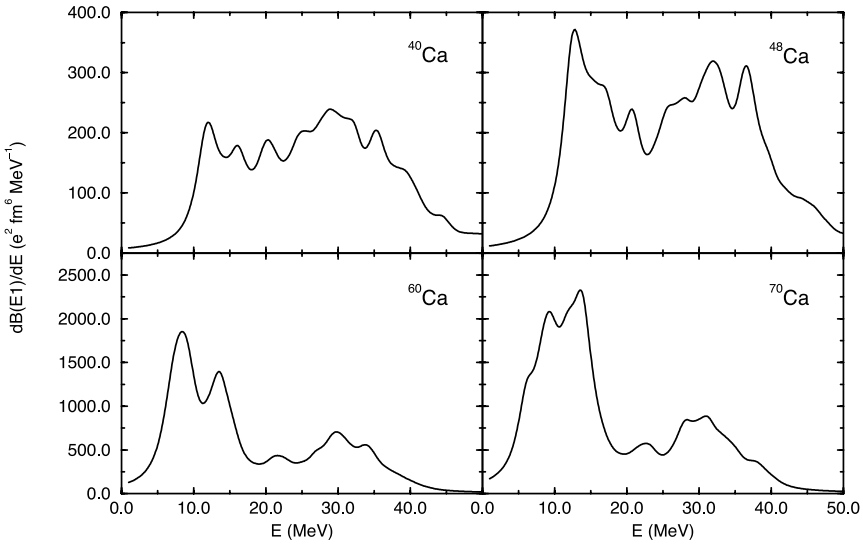

Fig. 8. Isoscalar dipole response obtained in a HF + RPA calculation for four Ca isotopes. The curves are obtained by averaging the discrete spectra with a Lorentzian with a width $\Gamma = 3$ MeV.
Source: Taken from Ref. [131].

As pointed out before, the transition densities are the fundamental quantities that describe the excitation process of the considered states. In fact, from their shapes and relative displacement of the proton and neutron transition density one can infer some of the properties of the state. As an example we show in Fig. 11 the transition densities for the ^{68}Ni calculated with an HF + RPA with a SGII Skyrme interaction [133,134]. The calculations have been done for three states belonging to the three highlighted regions of the strength functions, shown in Fig. 10, corresponding to the PDR, IVGDR and ISGDR modes. Since several states contribute to the three peaks in Fig. 11, an equivalent single state was constructed with an energy given by the average value obtained by weighting the energy of each single state by their corresponding $B(E\lambda)$ values. Their components are obtained with the constrain that the fraction of the EWSR exhausted is given by the sum of the EWSR of the considered states. (See also Section 5).

The transition densities for the three states obtained as explained above are shown in Fig. 11. In the upper panels the neutron (solid red line) and proton (dashed black line) are plotted as function of the radial distance of the nucleus while the isovector (solid black line) and isoscalar (dot-dashed blue line) ones are separately plotted in the lower panels. In panel (b) of Fig. 11 the proton and neutron transition densities have opposite sign in all the radial region of the nucleus and they are in agreement with the macroscopic picture of the IVGDR excitation as due to the out-of-phase oscillation of the neutrons against the protons of the nucleus. On the other hand the proton and neutron transition densities for the

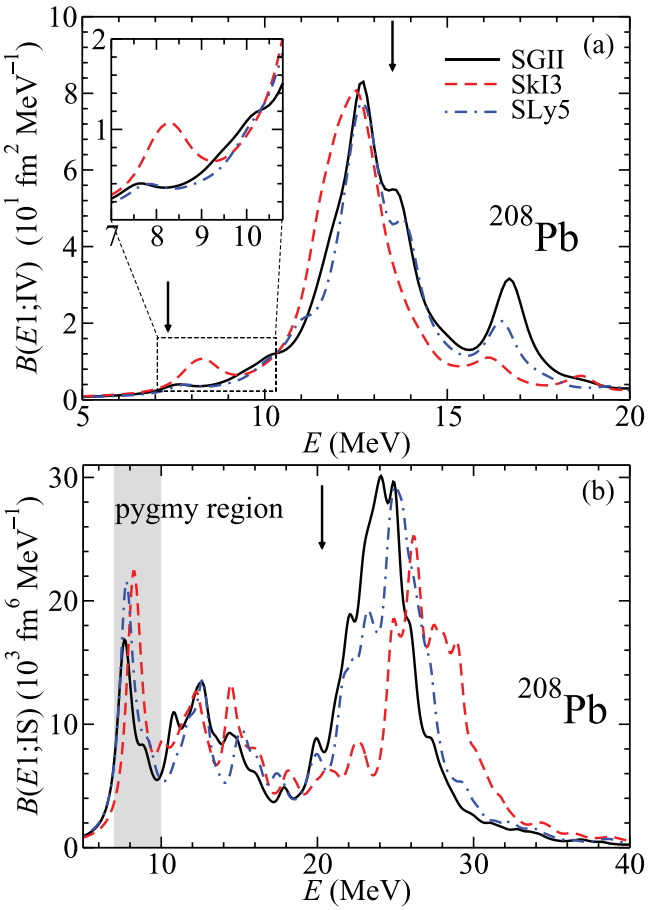

Fig. 9. Isovector (upper frame) and isoscalar (lower frame) dipole response obtained in a self-consistent HF + RPA calculation for ^{208}Pb. The strength function were calculated by convoluting the corresponding reduced transition probability with a Lorenzian of 1 MeV width.
Source: Taken from Ref. [14].

ISGDR, in panel (c) of Fig. 11, are in phase in the bulk and on the surface of the nucleus showing an almost pure isoscalar mode. This isoscalar dipole mode is a $3\hbar\omega$ excitation [114]. A different behaviour is found for the transition densities in panel (a), where the neutron and proton are in phase in the interior of the nucleus while at the surface only the neutron transition density is different from zero. These behaviour have a consequence on the shape of the isoscalar and isovector transition densities. The IVGDR has a definite isovector character as can be appreciated in panel (e) while the ISGDR is clearly an almost pure isoscalar state having the transition density the typical shape of a compressional mode (panel (f)). On the other hand, the isospin nature of the PDR state is not well definite because both isoscalar and isovector transition densities contribute. In particular, at the nuclear surface, a similar strength for the isovector and isoscalar component is predicted due to fact that the contribution come almost entirely from the neutrons. As a consequence, the excitation of this low-lying dipole mode can also be generated by an isoscalar probe, which in most of the case induce a peripheral reaction where the contribution of the nuclear surface is predominant. Similar results have been obtained with HF + RPA calculation with different Skyrme interactions [14,138]

4.2.2. QRPA

The RPA starts from the H–F ground-state wave function where it is assumed a sharp separation between the occupied and unoccupied levels below and above the Fermi level. This assumption is not satisfied in open-shell nuclei where the pairing correlation is important and it must be included in the description of the ground-state wave function. This can be achieved within the Bardeen, Cooper and Schrieffer (BCS) model [123], constructed to determine the ground-state of a superconductor, where it is assumed that the Fermi surface is diffused meaning that the levels around the Fermi energy are not completely full or completely empty. Such description is realised using the Bogoliubov transformation

$$\alpha_k^\dagger = u_k a_k^\dagger - v_k a_{-k} \tag{22}$$

$$\alpha_{-k}^\dagger = u_k a_{-k}^\dagger + v_k a_k \tag{23}$$

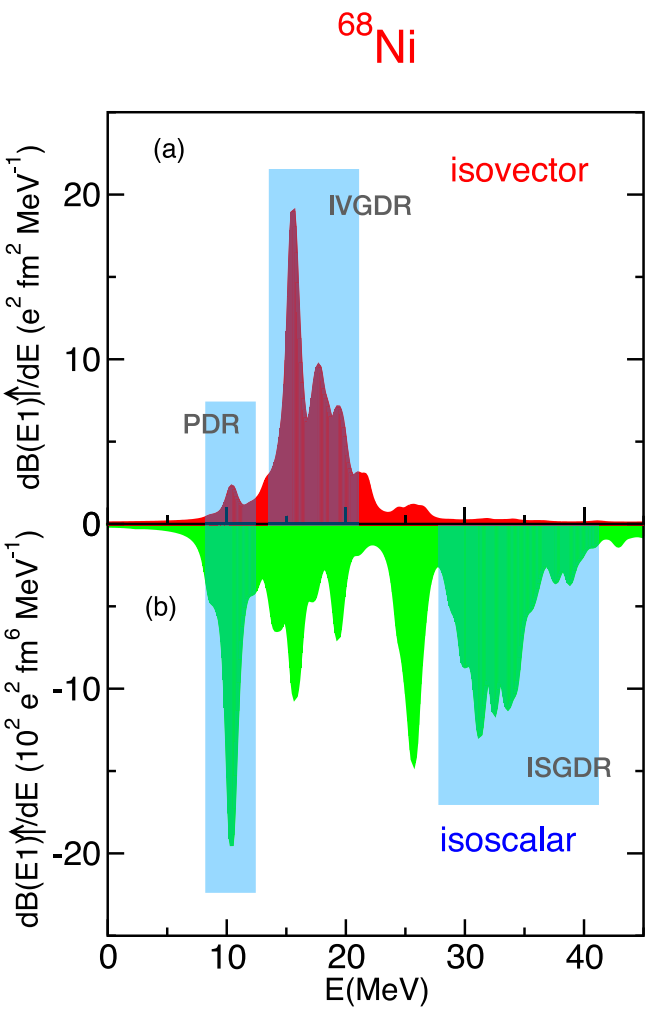

Fig. 10. Isovector (upper frame) and isoscalar (lower frame) (multiplied by −1) dipole response obtained in a HF + RPA calculation with a SGII interaction for ^{68}Ni. The strength function were calculated by convoluting the corresponding reduced transition probability with a Lorenzian of 1 MeV width. The shaded areas underline the energy regions corresponding to the three excitation modes of interest, as indicated in the figure.

where $|-k\rangle$ is the time reversal state of $|k\rangle$ and $u_k^2 + v_k^2 = 1$. The parameters u_k and v_k are determined by the conditions that the corresponding energy has a minimum and the expectation value of the particle number operator is conserved. The self-consistent version of the BCS theory is the Hartree–Fock–Bogoliubov (HFB) theory which is the basis space for the quasiparticle RPA where the operator responsible for the excitation, in analogy with Eq. (10), is

$$Q_\nu^\dagger = \sum_{kk'} \left[X_{kk'}^\nu \alpha_k^\dagger \alpha_{k'}^\dagger - Y_{k'k}^\nu \alpha_{k'} \alpha_k \right]. \tag{24}$$

with $Q_\nu|0\rangle = 0$ for all ν. Where the ground-state wave function (BCS ground state) has the following form

$$|0\rangle = \prod_{k>0} (u_k + v_k \alpha_k^\dagger \alpha_{k'}^\dagger)|\rangle, \tag{25}$$

where $|\rangle$ is the bare vacuum. It is interesting to observe that in the QRPA particle–particle (p–p) matrix elements are present in addition to the p–h configurations already appearing in the RPA model. As a consequence now the residual interaction, responsible of the inelastic excitation, is formed by a p–h interaction and a p–p interaction.

The QRPA allows to perform calculations to describe the structure of the excited states of open-shell nuclei, stable and far from the stability line, for which many of experimental studies of the PDR region have been made (see Sections 2, 3, and [7,8,10]). This approach is suited non only for the open-shell nuclei but also for deformed nuclei. In Section 4.3 we will discuss the theoretical studies of the PDR in deformed nuclei.

A detailed investigation using QRPA with few different Skyrme effective interactions has been performed for even Ca, Ni and Sn isotopes spanning from the proton to the neutron drip line [139]. A spherical symmetry is assumed for

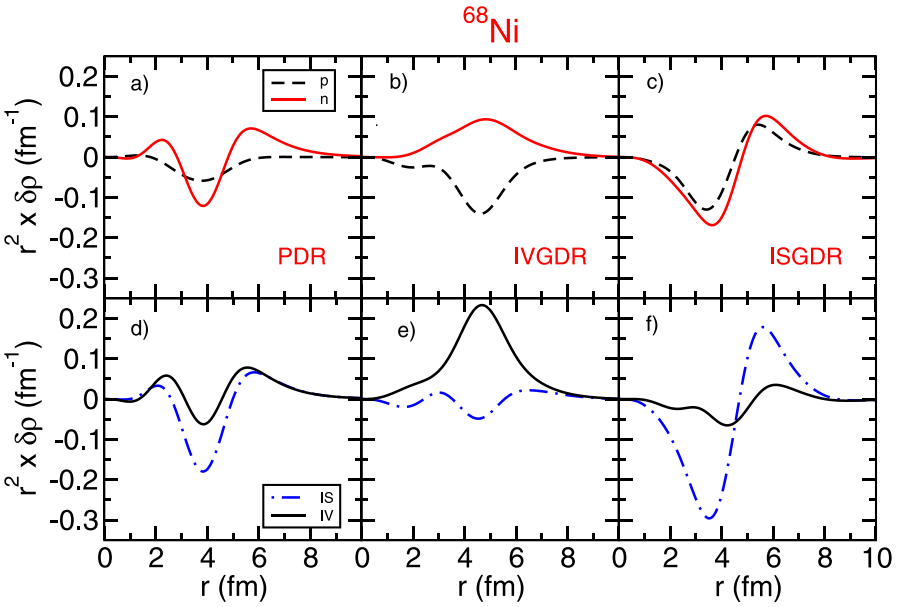

Fig. 11. RPA proton and neutron transition densities (upper frames) and isoscalar and isovector transition densities (lower frames) for the dipole states for ^{68}Ni nucleus. The three states have been obtained with the "bunching" procedure explained in the text. Their energies are 10.8, 15.6 and 31.6 MeV for the PDR, IVGDR and ISGDR, correspondingly.

these nuclei and a coordinate-space HFB calculation is performed to build a two quasiparticle QRPA hamiltonian. This hamiltonian is diagonalised to obtain isoscalar and isovector strength functions and transition densities. The calculations were performed for 0^+, 1^- an 2^+ states and the results show an enhancement of the low-energy strength as the neutron excess increases. This behaviour is common for all the analysed multipoles and is most pronounced for the dipole case. The transition densities for the nuclei with neutron excess have the same properties that have been discussed above. According to these results, the enhancement of the low-lying dipole strength near the drip line has to be ascribed to the long neutron tail in the transition density.

Another systematic study on even Ca, Sn and Ni isotopes based on a self consistent QRPA has been carried out [140,141] with a finite range interaction Gogny DS1 [142] and a quasi-realistic interaction, namely Argonne V18 plus phenomenological three body contact term [143]. Assuming spherical symmetry, the QRPA is constructed in the canonical basis of HFB model which is used to describe the ground states, the p–h and p–p channels. Significant strength at low energy was found for the isoscalar response of nuclei with N = Z; the peak is shifting towards low energy with increasing neutrons number. These results are similar to the one described in the previous quoted studies. For the Sn isotopes, the summed isoscalar strength below the particle emission threshold has been found to be some order of magnitude for the isotopes with N between 50 and 82. For the same group of isotope also the summed isovector strength shows a constant value. The calculated transition densities are pure isoscalar for N = Z; the proton and neutron transition densities are in phase inside and at the nuclear surface (they almost coincide). It is evident from the calculations that when the neutron number increases, the contribution of the neutrons at the nuclear surface become predominant. The low-lying dipole states for Ni isotopes were studied [15] by making a comparison between the QRPA with Gogny DS1 interaction and a continuum RPA with a SLy4 Skyrme interaction [144]. The results of such systematic is shown in Fig. 12 where the dimension of the isoscalar disc (green) and isovector circle (open black) indicate their transition strength as function of the excitation energy for all the considered Ni isotopes. The IVGDR lays around the 20 MeV energy region and it seems not to be particularly affected by the variations in neutrons number except for a small effect on the fragmentation. The ISGDR shows in contrast an accountable variation around 30 MeV. A different outcome for the low-lying region is evident in the isoscalar strength around and below 10 MeV appearing to become stronger as the number of neutrons increases. Note also that the states in this region are not purely isoscalar as one can see from the fact that also the black open circle are relevant. Similar results were obtained when using two different interactions.

4.2.3. Relativistic RPA and QRPA

The time-dependent relativistic mean-field model developed in the seminal work of Walecka [145] can describe the dynamic of collective motion [146]. The nucleus is described as a system of Dirac spinors and their interaction is mediate by the exchange of virtual mesons and photons. The Lagrangian of the system incorporate the fields of the σ-meson, the ω-meson and the ρ-meson and the photons to account for the electromagnetic interaction. The coupled equations of motion are given by the Dirac equation for the nucleons and by the Klein–Gordon equation for the mesons. The solution

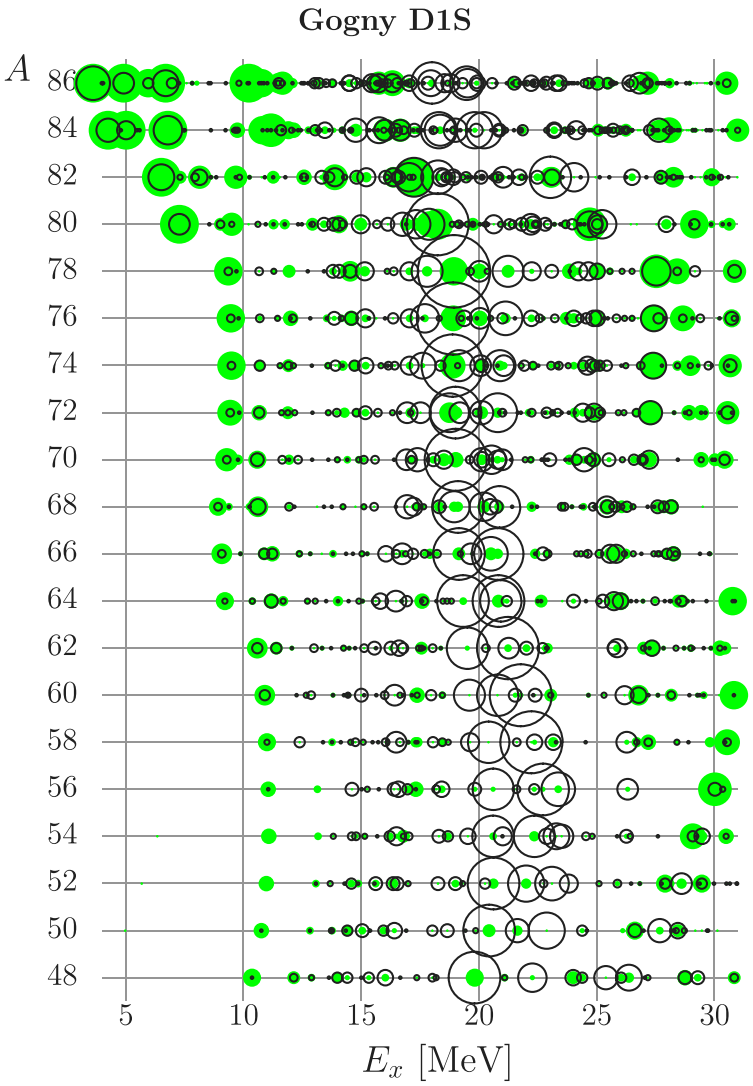

Fig. 12. Isoscalar (green disc) and isovector (open black circle) transition strength calculated within a QRPA with Gogny DS1 interaction. They are plotted as function of the excitation energy and of the even Ni isotopes shown in the vertical axes. The area of the disc and circle are proportional to the strength.
Source: Taken from Ref. [15].

for these coupled equations are found by applying approximations such as the mean-field approximation, where the meson-field are substituted by their expectation value, and the so-called no-sea approximation where the antiparticle states are not taken into consideration. These relativistic models have been successfully applied in the description of the static properties of stable nuclei and in nuclei far from the stability valley. The static case provide the stationary solution used as initial condition for the time dependent equations. After an initial boost the system is then followed in time.

The Relativistic Random Phase Approximation (RRPA) represent the small amplitude limit of the time-dependent relativistic mean-field theory. A way to obtain it is to calculate the linear response of the density matrix to an external field [148]. The RRPA equation can be cast in a similar matrix form like in Eq. (13). Several nuclear structure phenomena are well described by the RRPA and special attention has been given to the PDR [11,47,50,149,150]. In the description of open-shell nuclei pairing correlation needs to be included. One way of doing so it is to derive the pairing interaction from the one-meson exchange and including it in a density functional theory to derive a relativistic Hartree–Bogoliubov model [151]. The Relativistic Quasi-particle Random Phase Approximation (RQRPA) can be derived, in the limit of small oscillations, from the Relativistic Hartree–Bogoliubov theory. To simplify the solution the RQRPA equations in Ref. [147] were solved in the canonical basis; this was done by writing the relativistic Hartree–Bogoliubov wave functions in the terms of BCS-like wave functions. All these relativistic calculations are strongly dependent from the effective Lagrangian chosen to perform the calculations. The most used relativistic effective interactions are pure phenomenological and their

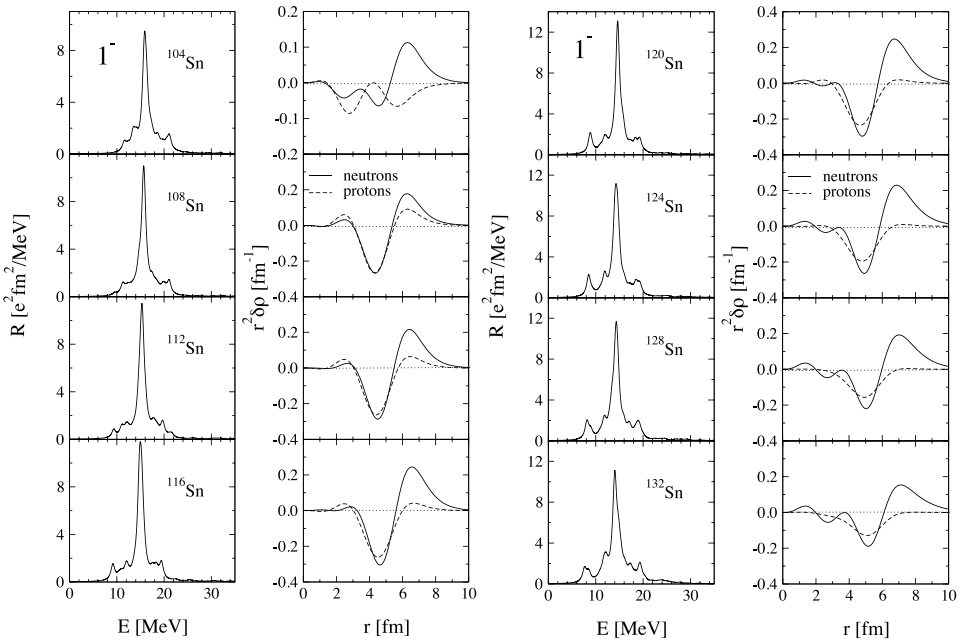

Fig. 13. Isovector dipole distribution (first and third columns) and the proton (dashed line) and neutron (solid line) transition densities (second and fourth columns) calculated within an RHBB + RQRPA model using a NL3 + D1S effective interaction, for some Sn isotopes.
Source: Adapted from Ref. [147].

parameters are adjusted to reproduce the main global properties of spherical nuclei. The evolution of the isovector dipole strength in the Sn isotopes has been studied in Ref. [147] within a RQRPA using an NL3 effective interaction [152] for the relativistic mean-field of the effective Lagrangian and a Gogny D1S [142] for the phenomenological pairing interaction. The results are shown in Fig. 13 for the isovector dipole distribution (first and third columns) and for the proton and neutron transition densities (second and fourth columns). In the dipole strength distribution one can clearly see the appearance of a peak in the low energy region as the neutrons number increases. At the same time, the rise of the neutron excess modifies the relative shapes of the proton and neutron transition densities towards the familiar shapes shown in panel (a) of Fig. 11. In particular, with the increasing neutron number the contribution of the protons at the nuclear surface goes slowly to zero while the neutron one is the only surviving. As a general behaviour it has been found that when increasing the neutron number the strength exhausted by the low-lying dipole is also increasing, and the centroid position of the low-lying modes shifts towards lower energies. It should be noted that the peak of the PDR moves slightly to lower energies when the pairing interaction is included in the description of the dipole excitation.

4.2.4. Second RPA (SRPA) and subtracted SRPA (SSRPA)

The RPA models provide a good description of the nuclear collective excitations in terms of coherent superposition of one-particle one-hole (1p–1h) configurations. In particular they are able to describe, with good accuracy, the main feature of the giant resonances like their centroid energies, EWSR and strengths. On the other hand they struggle to describe other important properties as the damping mechanism which manifests as a spreading width of the strength distribution. The spreading width is generated by the coupling of 1p–1h configurations with states formed by more complex configurations as 2p–2h, 3p–3h and more. It is clear that to obtained a proper description of the spreading width this coupling (regulated by the residual interaction) needs to be accounted for in the calculations. The natural way of doing so is achieved in the so-called Second RPA (SRPA) where the 2p–2h configurations are explicitly coupled with the 1p–1h configurations. In this way one is expecting to give, at the same time, a better description of the giant resonances as well as of the low-lying states and a correct description of the width. Many approaches have been based on boson mapping procedure as a natural extension of the RPA. These kind of approaches will require higher terms in the expansion in order to take properly into account the correction for the Pauli principle. In this extension, the excitation operator of Eq. (10) contains now a superposition of 1p–1h and 2p–2h configurations

$$q^\dagger_\nu = \sum_{ph}\left[X^\nu_{ph}a^\dagger_p a_h - Y^\nu_{ph}a^\dagger_h a_p\right] + \sum_{p<p',h<h'}\left[X^\nu_{php'h'}a^\dagger_p a_h a^\dagger_{p'}a_{h'} - Y^\nu_{php'h'}a^\dagger_h a_p a^\dagger_{h'}a_{p'}\right] \tag{26}$$

The SRPA equation can be formally written like the RPA ones with the matrices A and B containing the coupling between the 1p–1h and 2p–2h configurations [153]. Full SRPA calculations have been performed for O and Ca isotopes [154–156]. In the one for ^{40}Ca and ^{48}Ca [156] using the SGII Skyrme interaction the strength distribution for the giant

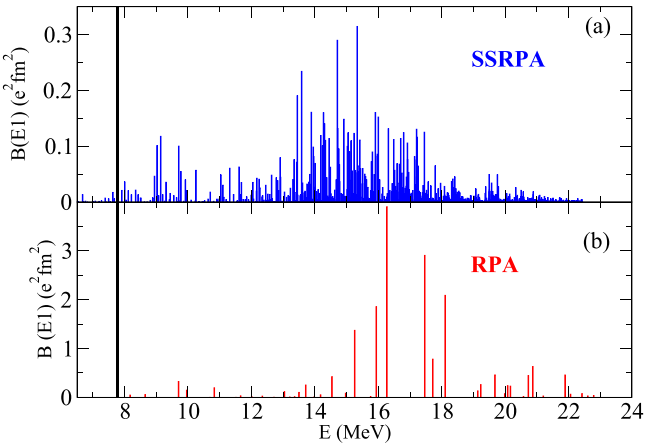

Fig. 14. Isovector dipole strength distribution calculated within a SSRPA (upper frame) and RPA (lower frame) model using a SGII effective interaction for the ^{68}Ni isotope. The vertical black line indicates the neutron emission threshold.
Source: Taken from Ref. [158].

resonances are shifted by several MeV with respect to the RPA results decreasing the agreement with the experimental values. The low-lying strength obtained for ^{48}Ca, in contrast to what found with RPA and RRPA, seems to reproduce better the experimental results in terms of the energy position but not for the integrated B(E1) that is predicted to be greater than the measured one. Although this approach is able to obtain some strength for the dipole states at low energies, the results are not satisfactory because of the shift to low energy of the entire distribution strength. The dipole strength in the $N = 82$ isotones ^{140}Ce, ^{142}Nd and ^{144}Sm was calculated using the second random-phase approximation with a SIII Skyrme interaction [157]. In this case the spreading width showed a further increment while maintaining the strength distribution similar to the RPA ones. This can be ascribed to the different use of the residual interaction which is not consistent with the one used to calculated the single particle wave functions [157].

The origin of the shift towards a lower-energy region was related to some other correlations which are implicit added in the ground state by the SRPA procedure. The self-consistent RPA is based on the Energy Density Functional (EDF) theories that provide density dependent interactions whose parameters are defined with mean-field calculations to reproduce the fundamental properties of nuclei. Therefore, the EDF contains a part of the complex configurations which are explicitly introduced in the extended RPA. When higher-order correlations are added to the mean-field approximations the parameters of the interactions should be adjusted to avoid this double counting. The correlations contained in the EDF should be thought as static correlations, while the one introduced to get the excitations of the resonances can be considered as dynamic. Often then the ground and the excited states are described by different interactions. An efficient way to solve this problem is the so-called "subtraction" model [159,160]. In brief for the SRPA, this procedure consists in modifying the SRPA matrix in order to get the RPA response in the zero frequency limit (for details see also Ref. [161]). That is, by imposing that the eigenvalue equation for the RPA and for the SRPA produce the same results for the ground state properties. This can be achieved by subtracting the static interaction amplitude from the part containing the contribution of more complex configurations [160]. An application of the Subtracted Second RPA (SSRPA) model, on nuclei with neutron excess to study the low-lying dipole states, can be found in Refs. [158,162] where the calculations have been performed using a SGII Skyrme interaction. The difference between the RPA and SSRPA results for the ^{68}Ni isotope are shown in Fig. 14. In the extended RPA, the dipole strength is spread over a large energy interval with respect to the RPA reaching down to the neutron emission threshold (indicated with the vertical black line in figure). In the SSRPA spectrum the centroid of the IVGDR is shifted lower in energy and overall more strength with higher EWSR is present. In the lower part of the spectrum the SSRPA shows structures between 9 and 11 MeV which in the RPA results (lower panel) are concentrated in few states. The typical feature of the pygmy states of an isospin mixing generated by the dominant contribution of the neutrons at the nuclear surface is also observed in the SSRPA transition densities as found in other theoretical approaches illustrated before. This isospin mixing is more evident in Fig. 15 where the isovector (panel (a)) and isoscalar (panel (b)) are plotted for the ^{68}Ni in the low-energy range 0–13 MeV. The solid black line are obtained with the correction for the spurious states while the dashed red lines without this correction. The authors infer the presence of the PDR isospin splitting from the comparison of the isoscalar and isovector distributions: in fact while the isovector distribution show similar values of the strength over the full energy range, the isoscalar one is stronger in the lower part compared to higher energies. From the experimental point of view, the presence of the PDR splitting for ^{68}Ni is still not clear because the only data available [89] do not clarify this aspect.

4.2.5. Multiphonons models

Higher order configurations can be taken into account by introducing explicitly the coupling between simple 1p–1h configurations and more complex configurations as two- or three-phonons. The particle-vibration coupling was introduced

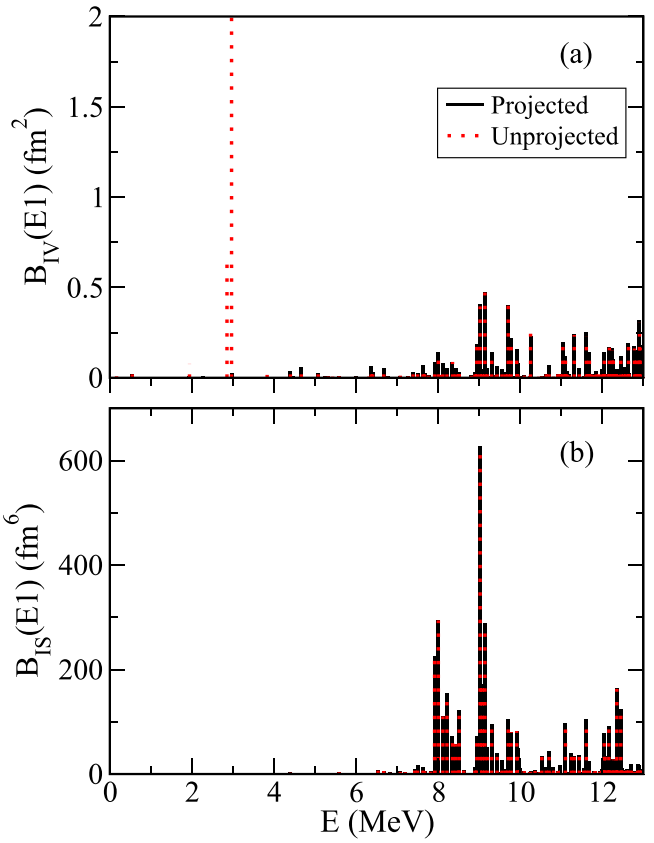

Fig. 15. Calculated SSRPA isovector (upper frame) and isoscalar (lower frame) dipole strength distribution for the ^{68}Ni isotope. The solid black line are the projected results while the dashed red lines are the results obtained without the correction for the spurious states.
Source: Taken from Ref. [158].

for the first time in the Nuclear Field Theory [163] where the coupling between the nucleons and the collective states were described by a field theory. There are several way to implement this coupling in the mean-field approximation. As explanatory example we will discuss the boson mapping method which was used in the study of the Double GDR [164–166]. The RPA can be seen as the lowest order of a boson expansion [123,167]. Here after we will follow the procedure proposed in Ref. [167] to map the fermion particle–hole operators $a^\dagger_p a_h$ into boson operators $B^\dagger_{ph}$

$$a^\dagger_p a_h \to B^\dagger_{ph} + (1-\sqrt{2})\sum_{p'h'} B^\dagger_{p'h'} B^\dagger_{p'h} B_{ph'} + \cdots . \tag{27}$$

In the RPA Hamiltonian only the $V_{ph,p'h'}$ and $V_{pp',hh'}$ terms of the residual interaction are taken into account. To consider the other terms $V_{pp',p''p'''}$, $V_{hh',h''h'''}$, $V_{pp',p''h}$ and $V_{ph,h'h''}$ one has to introduce the following mapping

$$a^\dagger_p a_{p'} \to \sum_h B^\dagger_{ph} B_{p'h} \ , \quad a_h a^\dagger_{h'} \to \sum_p B^\dagger_{ph} B_{ph'} \tag{28}$$

The second term on the right-hand side of Eq. (27) is a correction applied to take care of the Pauli principle. The boson image of the Hamiltonian, truncated to the fourth order in the $B^\dagger$ and B operators, can be written as (dropping the indices)

$$\begin{aligned} H_B = {} & H_{10}B^\dagger + H_{11}B^\dagger B + H_{20}B^\dagger B^\dagger + H_{21}B^\dagger B^\dagger B + \\ & H_{22}B^\dagger B^\dagger BB + H_{31}B^\dagger B^\dagger B^\dagger B + h.c. \end{aligned} \tag{29}$$

the term H_{10} vanishes in the H–F basis. Collective phonon operators are introduced by means of the Bogoliubov transformation

$$Q^\dagger_\nu \equiv \sum_{p,h} (X^\nu_{ph} B^\dagger_{ph} - Y^\nu_{ph} B_{ph}) \tag{30}$$

by imposing the quadratic term of the boson Hamiltonian to be diagonal, the RPA equation and the amplitudes X and Y are obtained

$$H_{RPA} = \sum_{\nu} E_{\nu} Q_{\nu}^{\dagger} Q_{\nu} \ . \tag{31}$$

From the inversion of Eq. (30) the Hamiltonian H_B can be written in terms of the $Q^{\dagger}$ and Q collective operators

$$\begin{aligned} H_B = & \ \mathcal{H}_{11} Q^{\dagger} Q + (\mathcal{H}_{21} Q^{\dagger} Q^{\dagger} Q + h.c.) + \mathcal{H}_{22} Q^{\dagger} Q^{\dagger} Q Q \\ & + (\mathcal{H}_{30} Q^{\dagger} Q^{\dagger} Q^{\dagger} + h.c.) + (\mathcal{H}_{31} Q^{\dagger} Q^{\dagger} Q^{\dagger} Q + h.c.) \\ & + (\mathcal{H}_{40} Q^{\dagger} Q^{\dagger} Q^{\dagger} Q^{\dagger} + h.c.) + \cdots \end{aligned} \tag{32}$$

The matrices $\mathcal{H}$ in general contain the amplitudes X and Y however in this case the ones in the first line have only the X amplitude. Since the ratio X/Y is small for nuclei with closed shells one can retain only the terms in the first line ($\mathcal{H}_{11}$, $\mathcal{H}_{21}$ and $\mathcal{H}_{22}$). In the space spanned by one- and two-phonon states the bosonic Hamiltonian can be written as

$$\begin{aligned} H = & \sum_{\nu} E_{\nu} Q_{\nu}^{\dagger} Q_{\nu} + \Bigg[\sum_{\nu_1 \nu_2 \nu_3} V^{21} Q_{\nu_1}^{\dagger} Q_{\nu_2}^{\dagger} Q_{\nu_3}^{\dagger} \\ & + \sum_{\nu_1 \nu_2 \nu_3 \nu_4} V^{22} Q_{\nu_1}^{\dagger} Q_{\nu_2}^{\dagger} Q_{\nu_3} Q_{\nu_4} \Bigg] + H.C. \end{aligned} \tag{33}$$

The eigenstates and eigenvalues are then found by diagonalising the Hamiltonian in the space of the states containing up to a certain number N of phonons. The V^{21} represent the matrix elements that mix states having the number of phonons differing by one while the V^{22} term mixes multiphonon states with the same number of phonons. The procedure adopted to perform the calculations selects the most important RPA one-phonon states, namely the ones with a consistent (5%) EWSR, to construct, out of them, all the possible two- and three-phonon states. Then the Hamiltonian (33) is diagonalised in the space spanned by such states. The eigenstates are mixed states whose components are of one-, two-, and three-phonon type:

$$|\Phi_{\alpha}\rangle = \sum_{\nu_1} c_{\nu_1}^{\alpha} |\nu_1\rangle + \sum_{\nu_1 \nu_2} c_{\nu_1 \nu_2}^{\alpha} |\nu_1 \nu_2\rangle + \sum_{\nu_1 \nu_2 \nu_3} c_{\nu_1 \nu_2 \nu_3}^{\alpha} |\nu_1 \nu_2 \nu_3\rangle \ . \tag{34}$$

Calculations for the relativistic Coulomb excitation for the system ^{132}Sn + ^{208}Pb at 500 MeV/u measured at GSI [88], have been performed within this approach. The inelastic excitation cross section was evaluated within the semiclassical model described in Section 5. It was investigated the possible contributions to the PDR peak of other low-lying multiphonon states, like the ones obtained by coupling the 2^+ with the 3^-. The contribution of other states were estimated to be between 3 and 21%, depending on the isotopes and interactions used [49].

4.2.6. Quasiparticle Phonon Model

Another approach very similar to the one just described is the Quasi-particle Phonon Model (QPM) [168,169] whose description for the PDR below the neutron emission threshold has been extremely useful. In this approach, the Hamiltonian is taken as the sum of three terms [169]. The first one describes the single particle motion for neutrons and protons. The pairing for non-magic nuclei is described by a residual interaction taken as a monopole pairing. The residual interaction responsible for the coupling of 1p–1h configuration with more complex ones is given by a sum of isoscalar and isovector separable multipole interactions with radial form factor given by r^L or with the Bohr and Mottelson form, $\partial U/\partial r$. The one-phonon basis is obtained as a solution of a QRPA, starting blocks for the construction of the two- and three-phonon configurations. A boson mapping procedure – similar to the one described in Section 4.2.5 – is applied, and a phonon creation operator can be written in term of quasi-boson operators, achieving an expression similar to the one in Eq. (30). The Hamiltonian is then diagonalised in this enlarged basis and the eigenfunctions are similar to the ones in Eq. (34). For a practical applications, a superposition of central and spin–orbit phenomenological Woods–Saxon potential is preferred to the use of the density functional interaction such as the Skyrme one. This has the advantage to fix the parameters by getting the nuclear ground states properties with great accuracy. Although this approach looses the fully microscopic picture and the self consistency it is able to describe with good accuracy some of the main features of the PDR.

The main effect of the coupling of one-phonon state with more complicated configurations is that the strength distribution is fragmented into many states towards lower energies, as seen also for the SRPA and SSRPA theories. This is how the coupling contributes to the determination of the spreading width. The dipole strength distributions calculated with the QRPA and the QPM [170] for two Sn isotopes are plotted in Fig. 16 for the low energy region. The first column display the QRPA E1 distributions while the QPM ones are shown in the second column. The fragmentation of the strength produced in ^{122}Sn by the QPM results can be clearly appreciated in the comparison of the two top panels. In the second row, the same effect can be seen for the ^{130}Sn nucleus. The lowest QPM 1^- states are not present in the QRPA calculations since they represent the quadrupole–octupole two-phonon states. A more detailed studies on the tin isotopes have been done in Ref. [171].

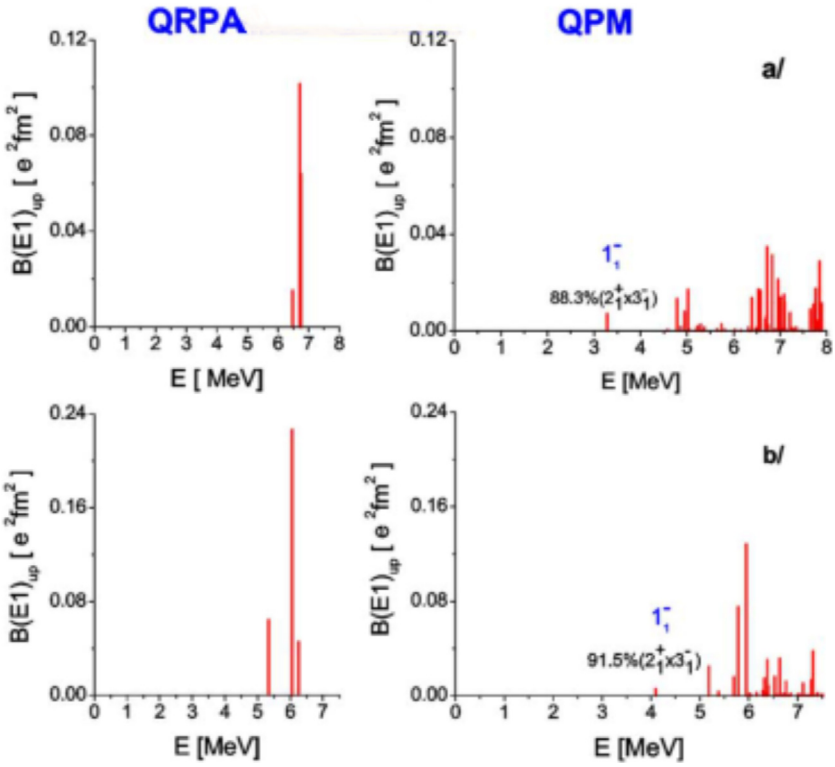

Fig. 16. Dipole reduced transition probabilities B(E1) calculated within the QRPA (left columns) and within the QPM (right columns) for ^{122}Sn (upper row) and for ^{130}Sn (lower row).
Source: Taken from Ref. [170].

A beautiful example of how the coupling to configurations of increasing complexity modify the theoretical dipole strength distribution is shown in Fig. 17 where the fragmentation of the reduced electric transition probability for ^{136}Xe have been obtained within the QPM. The calculations have been done by V. Yu Ponomarev [94] taking as basis phonons with multipolarity up to 9. In the top panel of Fig. 17 the B(E1) distribution is obtained including only the one-phonon states. This result should be equivalent to the RPA calculation. The few states are strongly fragmented when the coupling with the two-phonon configurations are included (middle panel) and a wide energy range is filled with hundreds of states. The fragmentation is increasing when also the three-phonon states are considered (lower panel) while the summed strength in almost unchanged. These last results are in quantitative agreement with the experimental values [94] in Fig. 18 where the B(E1) distributions for five stable even N = 82 isotones are shown.

The QPM has been extended to describe the β decay used as another method to excite the pygmy dipole states [80] (see Section 2.2.1). The β decay was measured for the transition ^{136}I to ^{136}Xe whose photon scattering (γ, γ') has been largely studied [94], hence a comparison between the two set of data could be done. The intensity of the population of the dipole states was calculated considering – in the QPM formulation – the reduced matrix element of the Fermi β decay instead of the electromagnetic ones. Such calculations have shown that the β decay dominantly populates 2-phonon components which is in contrast with the results of the excitation of the ^{136}Xe via electromagnetic probes (see also Fig. 17).

4.2.7. Relativistic Quasiparticle Time Blocking Approximation (RQTBA)

The QPM provides a good description of the experimental data of the low-lying dipole strength. However the approximations used, like the choice of separable interaction and the lack of self-consistency, are not satisfactory from a pure theoretical point of view. Another model which gives a good description of the PDR features is the Relativistic Quasiparticle Time Blocking Approximations (RQTBA) where the RQRPA is modified by including the coupling to the low-lying vibrations. This, in contrast to the QPM, is a full self-consistent model and the coupling with more complex configurations allows the description of the width of the GDR as well as the fragmentation of the dipole strength of the PDR.

The nuclear energy density functional approaches are designed to treat nuclear static properties and the time dependent version is suited for the description of excited states. In presence of pairing interaction, the small amplitude limit correspond to the RQRPA. The inclusion of coupling the 1p–1h to more complex configurations, in particular the coupling of quasiparticle with phonons, can be dealt with the Green function formalism. The time representation of the

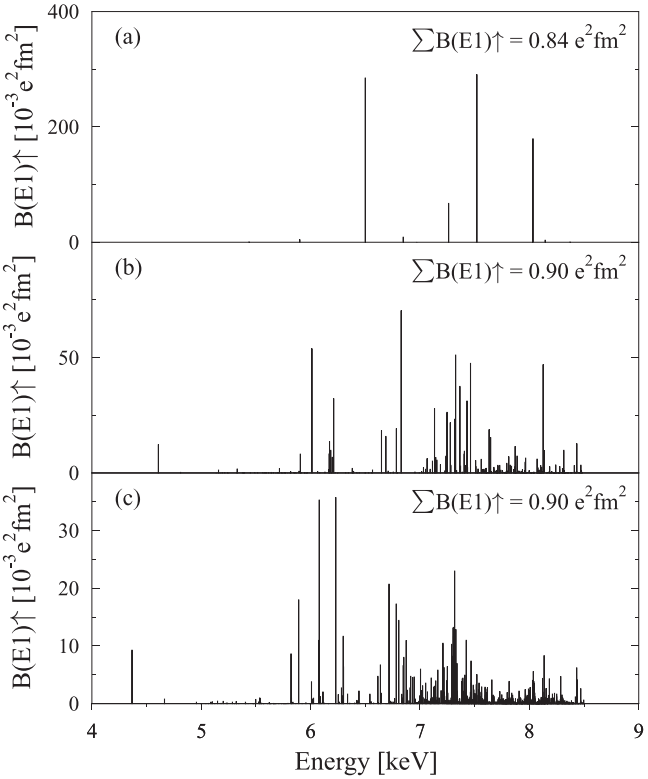

Fig. 17. Dipole reduced transition probabilities B(E1) calculated within the QPM for ^{136}Xe for several approximation. In the top frame are shown the results when only one-phonon states are taken into account. Calculations when also the two-phonons and the two- and three-phonons are considered are shown in the middle and lower frame, respectively.
Source: Taken from Ref. [94].

Green function allows to chronologically order the contribution of all the complex configurations [159]. Therefore, the equation of motion can be solved including only the appropriate coupling, while the more complicated ones – like the two quasiparticle with 3-phonon – are blocked in the time representation. This method to couple the quasi-particle states to collective degree of freedom is called Relativistic Quasiparticle Time Blocking Approximation (RQTBA) [71,159,172]. The truncation of the more complex structures makes the calculations of the response function feasible. Another approximation included in the RQTBA is the subtraction procedure already described in Section 4.2.4. Indeed, the relativistic mean-field ground state is obtained by fitting the experimental static properties and containing in this way many correlations. When the complex configurations are explicitly introduced in the theory then some correlations can be double counted. The subtraction procedure [160] can avoid this double counting. The calculations of the dipole strength within the RQTBA [48,71], done for several isotopes of Sn, Ni, and for some N = 50 isotones, show a more fragmented distribution in the low energy region when compared with the RQRPA, maintaining the structure of the IVGDR peak almost unchanged. In Fig. 19 two different calculations for the spectra and the photo absorption for three N = 50 isotones are shown. The dashed lines correspond to the RQRPA calculations whose spectra is related to the excitation of the two-quasiparticle states. When these are coupled with the collective vibrational states the spectra of the low-lying dipole states are fragmented and they are shifted towards lower energies as can be seen in the left column of Fig. 19. A new version of the relativistic time blocking approximation RQTBA-2 [173,174], which allows the coupling between two-quasiparticle and two-phonon configurations was developed. Calculations performed within this full self consistent approach for several Sn and Ni isotopes show a different distribution of the dipole strength for the low-lying dipole states. A comparison among the RQRPA calculations and the previous two-quasiparticle RQTBA approach is shown in Fig. 20. The distributions obtained with the QRPA for the ^{68}Ni, ^{70}Ni, ^{72}Ni, are shown in the same figure as dotted black lines (panel (b), (c), and (d)). The RQRPA strength have a pronounced peak which is smeared out by the coupling with one-phonon states considered in the RQTBA calculations (dashed blue lines). When the two-quasiparticle configurations are allowed to couple with the two-phonon states – as in the RQTBA-2 approach – the fragmentation is further modified especially in the low energy part as shown by the red solid lines in Fig. 20. The RQTBA-2 results for ^{68}Ni are compared in panel (a) of Fig. 20 with the experimental data extracted from Ref. [82]. Among the three calculations in panel (b) the one performed with the RQTBA-2 are the one more in agreement with the data. However, the direct comparison between B(E1) and differential cross section has a quantitative meaning only for the Coulomb cross sections (see discussion in Section 5.2). The question arising, for these kind of approaches, is the limit for convergence when more complex configurations are added.

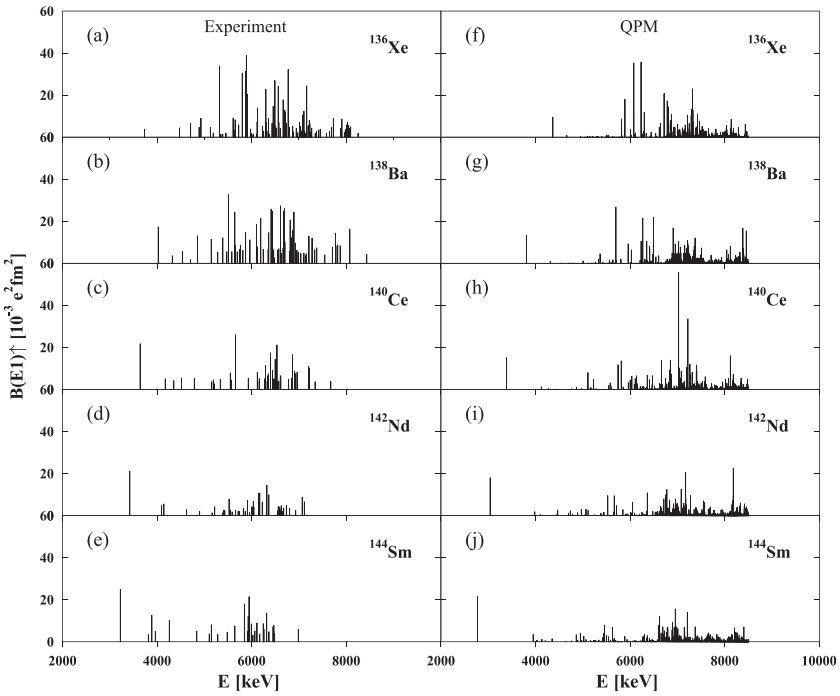

Fig. 18. Dipole reduced transition probabilities B(E1) measured in a photon scattering experiment for five stable even N = 82 isotones (left column). On the right column the calculation within the QPM for the corresponding nuclei.
Source: Taken from Ref. [94].

4.2.8. Equation of Motion Phonon Method (EMPM)

Another way to introduce complex configuration in the description of the PDR is the so-called Equation of Motion Phonon Method (EMPM). The multiphonon basis is generated by an iterative set of equation of motion and they are built on phonons obtained in a Tamm–Dancoff Approximation (TDA). The method can adopt general Hamiltonians whose matrices have a simple structure and they can be cast in diagonal form. In Ref. [176] the method was applied to the study of the electric dipole response to the ^{132}Sn isotope. The nucleon–nucleon chiral potential NNLO$_{opt}$ was adopted, with an extra repulsive, density dependent, term to get the dipole spectra close to the experimental values. This extra term is not necessary when dealing with light nuclei. In the calculation were included only two-phonon states producing a fragmentation of the PDR and IVGDR. The analysis of the transition densities show for the two excitations the same typical behaviour described in previous Sections. The disregard of the ground-state correlations – due to the use of the TDA – can, in principle, be compensated by the coupling of one-phonon with the two- and three-phonon basis. However, the inclusion of the three-phonon basis can be achieved, in this method, only by a drastic cut of the phonon basis. This is a severe limitation because, as it was shown in the approach of Section 4.2.5, the inclusion of the three-phonon states stabilise the results produced by the two-phonon states [166]. An extension of the model to treat open-shell nuclei was derived in Ref. [177]. The canonical basis was generated within the Hartree–Fock–Bogoliubov (HFB) model and the phonon within the TDA. This quasi-particle version is formally very close to the p–h version. The application to the ^{20}O isotope was possible after a truncation of the two-phonon states which produces, in any case, a strong fragmentation of the dipole strength qualitative close to the experimental data.

4.3. The case of deformed nuclei

Recent interest has been raised on the effect of deformation on the dipole strength distribution in the low-energy region for neutron-rich nuclei. The effect of deformation is well known for the IVGDR, where due to the coupling of dipole and quadrupole degrees of freedom the total strength is split into two or three humps in the case of axial or triaxial deformations, respectively. In the hydrodynamical model these different structures correspond to vibrations of the nuclear matter along the different principal axis of the system [163,178,179]. The splitting of the IVGDR can also be obtained within the Interacting Boson Model (IBM) [180] where a p-boson (L = 1) is coupled to a system of interacting s (L = 0) and d (L = 2) bosons. The ratio between the strength of the two peaks depends on the number of active bosons (N); however for large values of N it coincide with the hydrodynamical value [181]. In the hydrodynamical model the normal dipole modes consist of out-of-phase oscillations of the proton and neutron densities along the symmetry axis and along the two orthogonal axis, characterised by the quantum numbers $K^\pi = 0^-$ and $K^\pi = \pm 1^-$ in the intrinsic frame. These

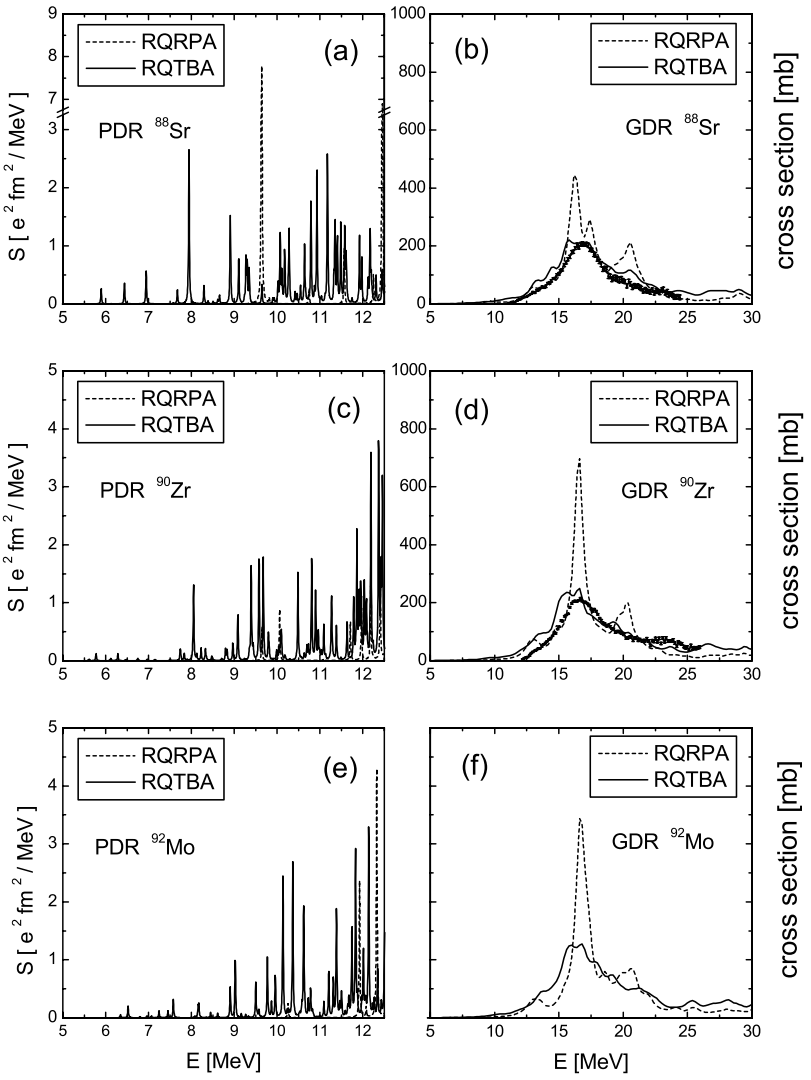

Fig. 19. Dipole spectra and photo absorption cross section for ^{88}Sr, ^{90}Zr and ^{92}Mo calculated with the RQRPA (dashed lines) and RQTBA (solid lines). The black dot are experimental data taken from Ref. [175].
Source: Taken from Ref. [71].

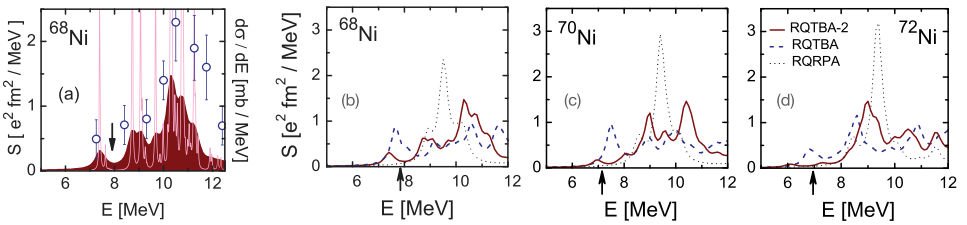

Fig. 20. Dipole spectra for Ni isotopes calculated with the QRPA (dotted black lines), RQTBA (dashed blue lines) and RQTBA-2 (solid red lines). In frame (a), the theoretical result for the RQTBBA-2 for ^{68}Ni, shown also on frame (b), are compared with the experimental data (open circle) taken from Ref. [82].
Source: Adapted from Ref. [174].

quantum numbers K are the projection of the total angular momentum onto the symmetry axis, the intrinsic (body-fixed) frame of the nuclear system. In the laboratory frame this gives rise to two distinct dipole bands with different energy compared to the "spherical" value E_1, whose distance is associated to the parallel ($R^{\parallel}$) and perpendicular lengths ($R^{\perp}$) of

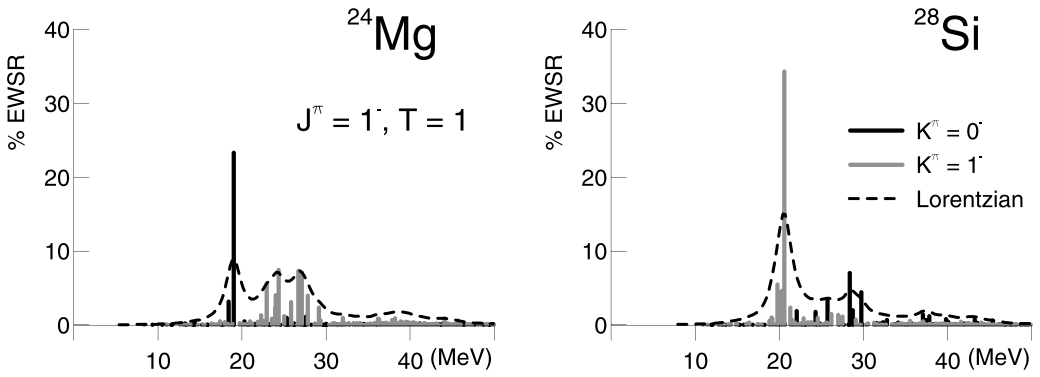

Fig. 21. Fraction of the EWSR for the isovector E1 states for ^{24}Mg and ^{28}Si for the two components $K^{\pi} = 0^-$ (black lines) and $K^{\pi} = 1^-$ (grey lines). The dashed line is obtained with a smooth procedure with Lorentzian functions.
Source: Taken from Ref. [182].

the symmetry axis, namely

$$\frac{\Delta E}{E_1} = \frac{E_1^{\perp} - E_1^{\parallel}}{E_1} = \frac{R^{\parallel} - R^{\perp}}{R_0} = \frac{3}{2}\sqrt{\frac{5}{4\pi}}\,\beta = 0.95\,\beta \tag{35}$$

resulting to be approximately proportional to the deformation parameter β [163,179].

If the common view of the PDR, seen as an oscillation of a neutron skin against an inert core, is valid, then one could imagine that the deformation may induce a splitting of the PDR strength as found for the IVGDR. This investigation was experimental attempted in ^{76}Se [108] using a $(\vec{\gamma}, \gamma')$ polarised photon scattering method (see Section 3.4). Even though this nucleus has a relatively small neutron excess the splitting of the IVGDR have been observed. An enhancement was noticed in two low energy regions but no clear indication of a splitting was observed. Detailed experimental aspects of the PDR in deformed nuclei have been discussed in Section 3.4.

Several theoretical works focused on the effect of the deformation in the structure of the low-lying dipole states. Among them, a microscopic quasi-particle random phase approximation (QRPA) built on top of self consistent Hartree–Fock–Bogoliubov (HFB) mean field has been extended [183] to study the isovector dipole response in deformed neutron-rich nuclei, employing the Skyrme effective interaction SkM* [184]. In this approach the full velocity dependence of the residual interaction was included but the spin–orbit and Coulomb two-body forces were not accounted for. The Skyrme-HFB mean field was calculated in the coordinate-space representation to improve the spatial structure description of the quasiparticle wave functions. This alternative approach prevents the inaccurate description of loosely bound wave functions that can originate when an expansion of the quasiparticle wave function in terms of harmonic oscillator is used. For states near the Fermi level in neutron drip-line nuclei, a good description of the wave functions is of great importance. The isovector and isoscalar response was calculated for medium heavy nuclei as ^{20}O, ^{26}Ne and several Mg isotopes [185]. The peaks corresponding to the two quantum numbers $K^{\pi} = 0^-$ and $K^{\pi} = 1^-$ are slightly separated but no clear splitting can be observed.

A fully consistent axially-symmetric deformed Hartree–Fock–Bogoliubov (HFB) + QRPA approach was developed [182,186,187] using the D1S Gogny effective interaction [126]. The same effective nucleon–nucleon force is used to solve both the HFB and the QRPA equations in all p–h, p–p, and h–h channels. Since the Coulomb exchange field in not included in the HFB calculations this term was omitted also in the QRPA to preserve self-consistency. Although this approach has the drawback discussed above, namely the HFB equations are solved in a finite harmonic oscillator basis, it can be used to described an extended variate of nuclei, including open- and closed-shell nuclei both spherical and deformed. Calculations have been performed for Ne isotopes and N = 16 isotones [182,186,187]. In deformed nuclei, theoretical isovector dipole responses are found separated into two major components as expected and the strength is predicted to be almost equally distributed between the two components. In the prolate ^{22,24}Mg nuclei the lower-energy peak is associated to $K^{\pi} = 0^-$ states (which should correspond to oscillation along the symmetry axis) whereas the higher one corresponds to $K^{\pi} = 1^-$ states (oscillation along the perpendicular axis). For oblate nuclei, the $K^{\pi} = 1^-$ components are found at lower energies. Fraction of the EWSR for the isovector E1 states for ^{24}Mg and ^{28}Si are shown in Fig. 21 for the two components $K^{\pi} = 0^-$ (black lines) and $K^{\pi} = 1^-$ (grey lines). The relative positions of the two contributions are swapped between prolate (^{24}Mg) to oblate (^{28}Si) nuclei. The energy split between $K = 0$ and $K = 1$ states is governed by the intrinsic deformation of the ground state. In the two spherical nuclei analysed, ^{28}Mg and ^{30}Si, only the $K^{\pi} = 0^-$ component is calculated as $K^{\pi} = 1^-$ states are degenerated. The transition densities for the low-energy dipole states for the N = 16 isotones present the same features at peripheral value of the nuclear radius where only the neutron transition densities give a contribution as previously discussed. Furthermore, a similar behaviour as observed for spherical nuclei was found: the energy of the low-lying peak decreases with the isospin asymmetry while the B(E1) strength increases.

While these studies were dealing with medium heavy nuclei, a specific investigation on the electric dipole response in the GDR and PDR energy regions was performed for several tin isotopes by using a relativistic Hartree–Bogoliubov (RHB) mean field plus a relativistic QRPA microscopic calculations [188,189]. The deformation and pairing correlations were included in a fully self-consistent fashion in a relativistic deformed QRPA approach. The use of the RPA to calculate the excitation of deformed nuclei is formally the same as for spherical nuclei. The difference lays only in the single particle wave functions that do not satisfy the rotational symmetry, due to the absence of a good quantum angular momentum. The only symmetry preserved is the axial symmetry and the projection K of the angular momentum on the symmetry axis becomes a good quantum number. By taking this symmetry consideration into account the relativistic RPA equation can be derived as per standard procedure. The first step is to construct the energy functional from the effective Lagrangian build with the σ, ρ and ω meson fields. The corresponding equation of motion can then be extracted and linearised to obtain the RPA equations (the relativistic case is more complicated and all the details are in Ref. [188]). Open-shell nuclei can be described by introducing the contribution of a pairing potential. This can be done by quantising the mesons fields or by mean of an effective pairing interaction. The latter was the choice in Ref. [189] where a monopole–monopole pairing interaction was adopted. The transition densities in the intrinsic reference frame depend on the distance to the symmetry axis and angular coordinates. The individual radial transition densities are obtained by expanding the intrinsic one in spherical harmonics. These quantities describe the excitation from the 0^+ state of the ground-state rotational band to each member of the different dipole rotational bands. The intrinsic transition densities for $K^\pi = 1^-$ state at 7.3 MeV of ^{150}Sn are shown in the upper panel of Fig. 22. Note that in the case of axially deformed nuclei the transition density depends on the two coordinates z and r that represent the distances along and perpendicular to the symmetry axis, respectively. Since this is a $K^\pi = 1^-$ mode the excitation (oscillation) happens along a direction perpendicular to the symmetry axis z. In the inner part of the nucleus the neutron transition density (left panel) is in phase with the proton one (right panel), while at the surface (outside the red dashed line) the only contribution comes from the neutrons. The transition densities in the intrinsic frame depends on the good quantum number K and they contain a mixture of many angular momenta. The transition densities in the laboratory frame are obtained after the projection to the dipole angular momentum. The proton (dotted red line) and neutron (blue solid line) radial transition densities in the laboratory frame are presented in the bottom panel of Fig. 22. These transition densities have a pattern similar to those found in spherical nuclei. This behaviour common in all low-lying dipole peaks for both K-modes and for all the Sn isotopes analysed in Ref. [189]. This suggests that also in the case of deformed nuclei the combined use of isovector and isoscalar probes could provide new insight in the understanding of the PDR (see discussion in Section 3.4).

An analysis of the summed B(E1) as function of the mass number was done for the Sn isotopes and the result is shown in Fig. 23. The blue circles and red squares refer to spherical and deformed nuclei, respectively. For each isotope the partial contributions to the total strength of the two K-modes is indicated by dashed orange vertical lines for the $K^\pi = 0^-$ mode and solid cyan lines for the $K^\pi = 1^-$ mode. The contribution of the $K^\pi = 1^-$ mode is double the one of $K^\pi = 0^-$ in the spherical cases. The dashed black line, which is a least squares fit to the data points of the spherical nuclei, indicates almost a linear increase with neutron number. On the contrary, in correspondence of nuclei with great deformation – as ^{152}Sn – the summed low-lying strength is reduced. Based on these results, one may conclude that deformation quenches the dipole response in the low-lying energy region.

An opposite view is given by the calculations performed within an HFB plus QRPA with Skyrme interactions [190] for Nd and Sm isotopes, where the summed low-lying dipole strength is found to be five times larger than in spherical nuclei. A strong enhancement has been found also for the isoscalar dipole transition strengths for Mg isotopes in the same low-energy region [185]. In this work the residual spin–orbit interaction was implemented in the HFB + QRPA approach developed in Ref. [183] without including the Coulomb interaction for computational limitation. Nevertheless this approximation should only move the centroid of the IVGDR by few hundreds of keV. The HFB equations were solved in the coordinate space using cylindrical coordinates and the SkM* [184] was used to determine the particle–hole wave function of the EDT. The procedure in Ref. [192], which depends on both the isoscalar and isovector densities, was followed to account for the pairing interaction. The calculations reproduce quite well the experimental photo-absorption cross section for the excitation of the IVGDR in Nd and Sm isotopes, and in particular the evolution of the observed splitting from spherical to deformed nuclei was predicted with good agreement.

The contribution of the two K-mode for the low-lying dipole are separately shown in Fig. 24 for two deformed Sm isotopes, ^{152}Sm and ^{154}Sm. The comparison of these results with the spherical ^{144}Sm nucleus, in panel (a), shows a remarkable fragmentation of the low-energy dipole states for the deformed isotopes. Furthermore, the fragmentation enhances the total strength in the low energy region: the summed B(E1) strength – summed up to 10 MeV – is about five times greater than the one for the spherical case. This is quite opposite to what has been found in Refs. [188,189] and discussed above. The two calculations are based on different theoretical approaches. Different pairing interaction are used: one [190,191] implements the Bogoliubov method while the other [188,189] the BCS formalism. In Refs. [188,189] the wave function are expanded in terms of harmonic oscillator basis while in Refs. [190,191] they are calculated in coordinate space, therefore the treatment of the continuum and of the weakly bound states is different. Finally the use of self-consistent treatment adopted in Refs. [188,189] makes this approach free from the contamination of the spurious centre of mass motion. These opposite contradictory results need further studies to clarify the reasoning behind such discordances.

The isoscalar response was also studies for Nd and Sm isotopes by paying more attention on the evolution of the strength distribution with deformation [191]. The onset of deformation produces a fragmentation of the isoscalar E1

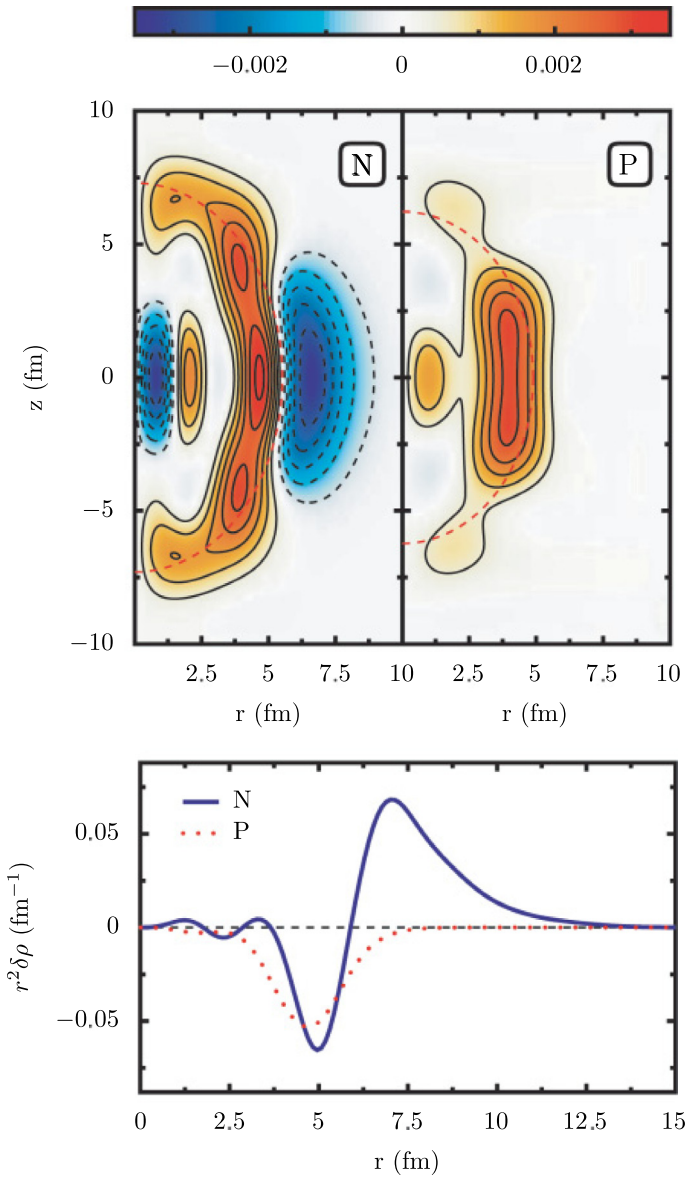

Fig. 22. Transition densities for $K^\pi = 1^-$ at 7.3 MeV of ^{150}Sn in the intrinsic (upper panel) and in the laboratory (lower panel) frame. The dashed circle is a reference for the non deformed nucleus.
Source: Taken from Ref. [189].

strength as can be seen in Fig. 25 where the $K^\pi = 0^-$ (black bars) and $K^\pi = 1^-$ (red bars) contributions are plotted for the Sm isotopes. For the two spherical nuclei, ^{146}Sm and ^{144}Sm, the K-modes contributions are equal. The isoscalar response shows a separation between K = 0 and K = 1 components which is similar to what happens for the IVGDR of deformed nuclei. As the deformation increases the fragmentation extends to lower energies and the splitting is more pronounced. This aspect is worth to be investigate and some experiment are designed to attempt this study (see discussion in Section 3.4). It is clear from the results presented that even from a theoretical point of view the effect of the deformation on the dipole response is not yet conclusive and the development of additional investigation are important.

4.4. Other models

This section is dedicated to additional models that do not strictly belong to the previous ones. As for the Toroidal Dipole Resonance (TDR) – original investigated within a fluid-dynamic model – nowadays is studied within the microscopic mean-field approaches. The location of this approach in this section is justified by the alternative point of view with respect to the PDR nature.

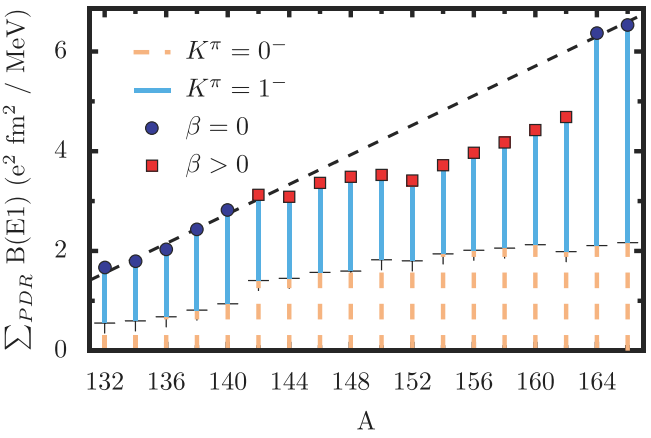

Fig. 23. Summed B(E1) strength for PDR states as function of the mass number for the Sn isotopes. Results for spherical (blue circles) and deformed (red squares) nuclei are shown together with their composition: dashed vertical lines indicates the $K^\pi = 0^-$ contribution while the solid cyan lines the $K^\pi = 1^-$ mode. Note that, for spherical nuclei, the $K^\pi = 1^-$ contributions are the double of the $K^\pi = 0^-$ one. The dashed black line is the least square fit to the data point for spherical nuclei.
Source: Taken from Ref. [189].

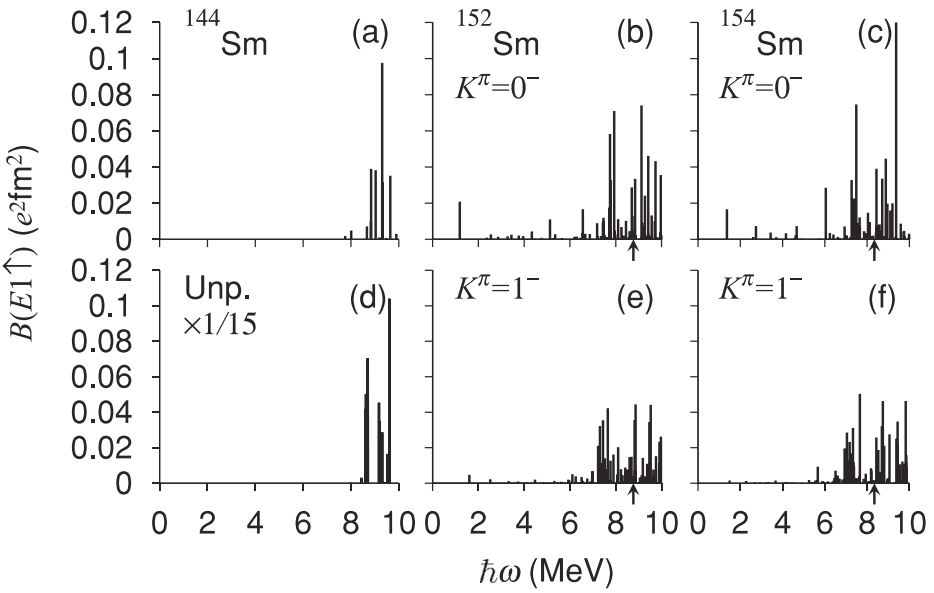

Fig. 24. Low-energy isovector dipole strengths B(E1) for ^{144,152,154}Sm. The arrow indicates the neutron emission threshold energy. In panel (d) the unperturbed strengths multiplied by 1/15 are shown for ^{142}Sm.
Source: Taken from Ref. [190].

4.4.1. Toroidal Dipole Resonances

Several work are aimed to show that the PDR can be treated as a manifestation of the Toroidal Dipole Resonance [193–197]. This isoscalar mode is characterised by a toroidal shaped velocity field. This mode was predict by a nuclear fluid-dynamics model where the transverse oscillation of the nucleons generates a new macroscopic mechanism of dipole resonance excitation [198]. It is estimated to be found at an excitation energy of $E_{tor} = (65 - 85)A^{-1/3}$. The isoscalar dipole channel receive contributions from the toroidal and compressional modes. A schematic picture of the toroidal and compressional velocity fields are shown in Fig. 26 compared to the usual representation of the macroscopic picture of the PDR. The operators generating the toroidal and compressional modes are obtained as a second-order terms in a low momentum expansion, or long wavelength limit, of the electric multipole operator. The toroidal operator can be written in the integral form as [195]

$$O_{1M}^{(Tor)} = -\frac{1}{10\sqrt{2}} \int d^3r \left[r^3 - \frac{5}{3}\langle r^2 \rangle r \right] \vec{Y}_{11M}(\hat{r}) \cdot \left(\vec{\nabla} \times \vec{j}(\vec{r}) \right) \tag{36}$$

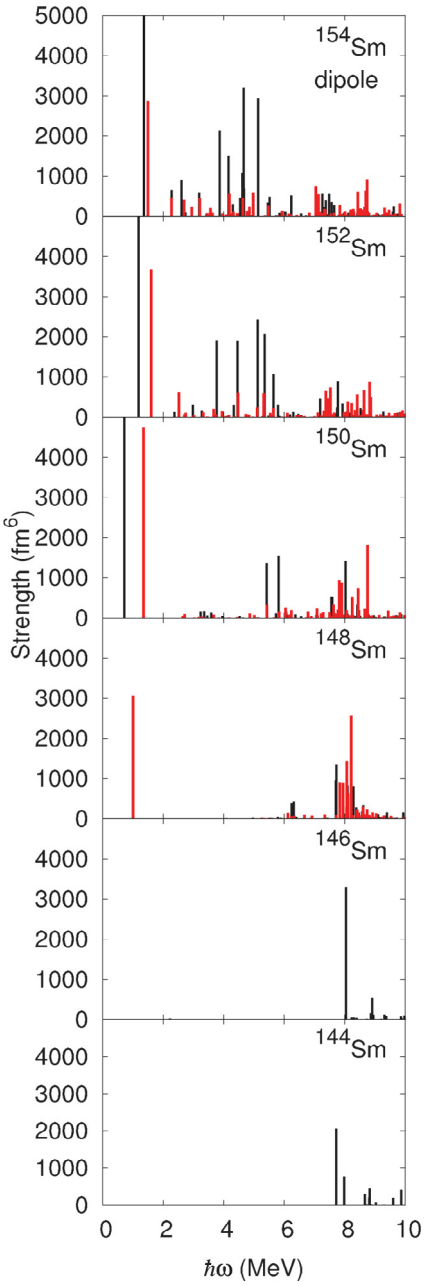

Fig. 25. The low-lying isoscalar dipole for the SM isotopes. The two contribution corresponding to $K^\pi = 0^-$ and $K^\pi = 1^-$ are shown as black and red bars, respectively. For the spherical nuclei, ^{146}Sm and ^{144}Sm, the two K-mode contributions are equal.
Source: Adapted from Ref. [191].

where $\vec{Y}_{11M}(\hat{r})$ is the vector spherical harmonic and $\vec{j}(\vec{r})$ is the nuclear current. The compressional operator can be cast in the usual form as in Eq. (17). Numerical calculations have been done using fully self consistent relativistic RPA [193], self-consistent separable RPA and QRPA approaches based on the factorised Skyrme residual interaction [194–196]. A more recent paper replaced the separable residual interaction approaches of the latter quoted works with a full self-consistent QRPA [197]. Numerous stable and exotic nuclei have been studied showing the presence of a broad distribution of the isoscalar toroidal strength independently from the neutrons to protons ratio. The concentration of strength in the energy interval 6–20 MeV has been called Toroidal Dipole Resonance (TDR). Since this TDR strength is located at the same energy region of the PDR it was suggested that the PDR could be a peripheral manifestation of the TDR even though these are irrotational and vortical kind of nuclear motion. It is worth noticing that the PDR manifests in nuclei with N>Z while the TDR is present in all nuclei. The TDR transition densities for the states found in energy region corresponding to the PDR

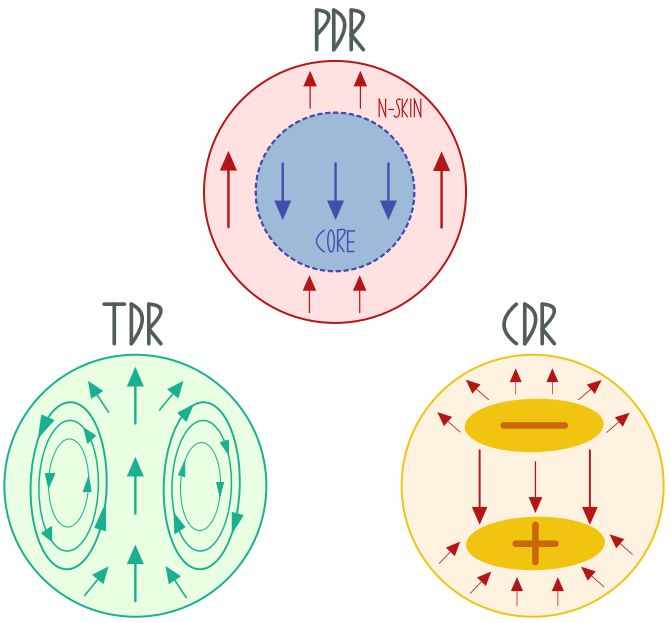

Fig. 26. Schematic velocity fields for dipole Pygmy (PDR) toroidal (TDR) and compressional (CDR) modes.

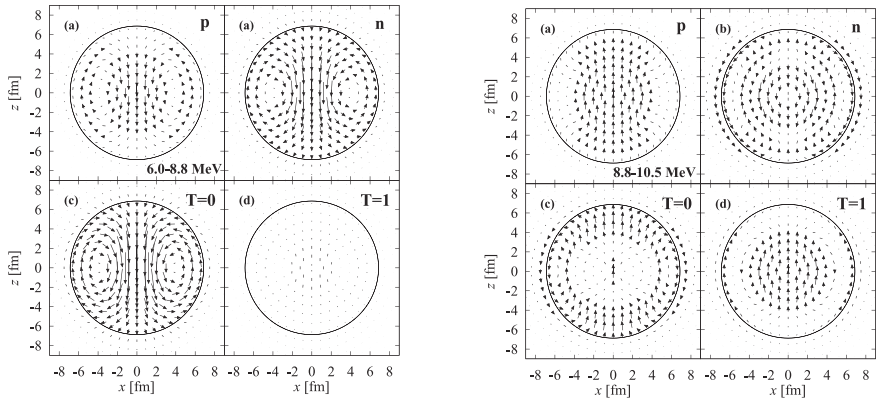

Fig. 27. Current transition densities for the ^{208}Pb summed over two low energy interval: 6–8.8 MeV (the four panels on the left) and 8.8–10.5 MeV (the four panels on the right). In each group, the upper frames show the average velocity fields for proton (left) and neutron (right), while in the lower frames there are the isoscalar (left) and isovector (right) distributions.
Source: Adapted from Ref. [195].

show the same shapes described in the previous sections although this is not surprisingly since the transition densities do not depend on the toroidal operator but on the RPA wave functions. A more in depth look to the current field can reveal details on this distribution. As an example the current transition densities (or velocity field) for ^{208}Pb calculated using a RPA approach [195] with an SLy6 Skyrme interaction [136] are shown in Fig. 27. In order to have informations which do not depend on the single states characteristics, an average over a given energy range are performed. In the results for two energy intervals 6–8.8 MeV and 8.8–10.5 MeV presented in the figure, two peaks in the E1 (T = 1) strength distribution are found. For the lower interval, the neutrons show a typical velocity field of the toroidal mode (see Fig. 26); they are more important in the interior and at the surface of the nucleus, and by moving in phase with the protons the total flow is found to be predominantly isoscalar. For the higher-energy interval, the neutrons contribution is again the most relevant especially at the surface and the total flow is strongly isospin mixed. In the PDR energy region there is a complicated mixture of different kind of dipole motion, the question of the presence of the TDR is under debate and selective experimental observation has yet to come.

4.4.2. Interacting boson approximation

The Interacting Boson Model (IBM) [180] is able to describe a great variety of collective nuclear excitations. The first version of the model (IBM-1) does not differentiate between protons and neutrons. Since treating the two type of nucleons

proved to be very important in some microscopic theories, this approximation has been amended by introducing in the model an effective boson number. The original IBM-1 can only describe positive-parity states being based on the s and d bosons with positive parity. The extension to negative-parity states, as those associated with the dipole or octupole degrees of freedom, implies the inclusion in the model of p (L = 1) and f (L = 3) bosons (IBM-spdf). With this extension it is then possible to describe octupole deformed systems and GDR-like states. The region energetically associated to the PDR was also studied in the framework of the IBM-spdf, where a number of effective boson have been employed to reproduce the main features of the PDR for stable even–even N = 82 isotones [199]. The IBM Hamiltonian including the p and f bosons degree of freedom is written as

$$H_{spdf} = \epsilon_d n_d + \epsilon_p n_p + \epsilon_f n_f + \kappa(Q_{spdf} \cdot Q_{spdf}) + a_3\left[(d^\dagger d)^{(3)} \cdot (d^\dagger d)^{(3)}\right]^{(0)} + a_4\left[(d^\dagger d)^{(4)} \cdot (d^\dagger d)^{(4)}\right]^{(0)} \tag{37}$$

here ϵ_d, ϵ_p and ϵ_f are the energies of the bosons while n_d, n_p and n_f are the boson-number operators. The other two parameters a_3 and a_4 are the strengths associated with the $l = 3$ and $l = 4$ interactions. The parameter κ is the quadrupole interaction strength of the quadrupole operator

$$Q_{spdf} = Q_{sd} + Q_{pf} = \left[(s^\dagger d + d^\dagger s)^{(2)} - \frac{\sqrt{7}}{2}(d^\dagger d)^{(2)}\right] + \left[\frac{3\sqrt{7}}{5}(p^\dagger f + f^\dagger p)^{(2)} - \frac{9\sqrt{3}}{10}(p^\dagger p)^{(2)} - \frac{3\sqrt{42}}{10}(f^\dagger f)^{(2)}\right] \tag{38}$$

In the spdf algebra more than one operator is responsible for dipole transitions, and the general E1 transition operator is therefore written as

$$T(E1) = e_1\left[\chi_{sp}^{(1)}(s^\dagger p + p^\dagger s)^{(1)} + (p^\dagger d + d^\dagger p)^{(1)} + \chi_{df}^{(1)}(d^\dagger f + f^\dagger d)^{(1)}\right] \tag{39}$$

where e_1 is the effective charge of the dipole transition and $\chi_{sp}^{(1)}$ and $\chi_{df}^{(1)}$ are two additional parameters of the model opportunely adjusted to reproduced the experimental B(E1) value for each studied nucleus. In the three equations above, the bosons are coupled to the value of the angular momentum indicated by the superscripts. The fit of the IBM parameters were done for the N = 82 isotones ^{136}Xe, ^{138}Ba, ^{140}Ce, ^{142}Nd, and ^{144}Sm. Their experimental B(E1) strength distributions are shown in the left column of Fig. 28 and are compared with the results of the IBM-spdf calculations [199]. The IBM is able to reproduce the shape of the distributions that is only affected by a small energy shift. The slightly increase of the centroid of the strength distributions from ^{144}Sm to ^{136}Xe is also reproduced. It is relevant to underline that the results depend on the choice of the effective bosons number. In fact, in the calculations of Ref. [199] it was found that a single set of effective bosons number was giving a good agreement with the experimental values.

The same model has been used to interpret the experimental E1 strength distribution below 4 MeV in rare-earth nuclei [201,202]. In particular the B(E1) distribution and the variation of the excitation energy in the Nd isotopes is well reproduced by the model. An analysis done in terms of the fraction of p- and f-bosons have shown, for all Nd isotopes, a major contribution from p-bosons. The same feature has been found also for the other rare-earth nuclei analysed. The enhancement for the dipole state below 4 MeV has been associated to the presence of α clustering suggesting a new excitation mode for these low-energy states. The existence of α clustering in heavy nuclei is still an open question that needs to be investigated further. The studies of the E1 strength distribution seems to provide a further means for the investigation of the α clustering in heavy nuclei.

4.4.3. Semiclassical model

The full microscopic approaches described in the previous sections may require substantial computational power. An accurate estimation of the fundamental properties of the nuclei can be obtained by implementing semiclassical approximations to the microscopic theories. One of the most successful semiclassical approaches is the Vlasov equation. If one writes the Time Dependent Hartree Fock (TDHF) equations in terms of the density matrix then the Vlasov equation can be obtained by imposing the semiclassical limit ($\hbar \to 0$) to the TDHF [123]. This method has been used for the description of different collective modes with satisfactory results [203,204]. The Vlasov equation is expressed in terms of the distribution function $f(\vec{r}, \vec{p}, t)$ being the Wigner transform of the densities. Since the density matrix for protons and neutrons are different, the two coupled Vlasov equation for neutrons and protons are written separately

$$\frac{\partial f_i}{\partial t} + \frac{\vec{p}}{m}\frac{\partial f_i}{\partial r} + \frac{\partial U_i}{\partial r}\frac{\partial f_i}{\partial p} = 0 \tag{40}$$

with the indices $i = n, p$, and the mean field U dependent on the densities. To solve numerically the Vlasov equation it is employed the so-called test-particle method [205] which consists in writing the distribution function f as a finite number of δ functions. From that, each of the test particles should follow the classical trajectories given by the classical equation of motion governed by the Wigner transform of the mean field hamiltonian. The δ functions are usually replaced with finite range functions, as for example Gaussians, to get a smooth density function. Such procedure transforms the mean field in an effective finite range interaction. The test-particle position and momentum are randomly initialised with the conditions to reproduce the density and the Fermi momentum. To describe the collective motion, the ground-state density is perturbed at the initial time and the oscillation of the nucleus is followed in time by the Vlasov equation. To study the E1 response of the nuclear system the isoscalar and isovector operator, like the ones in Eqs. (16) and (17), are used to

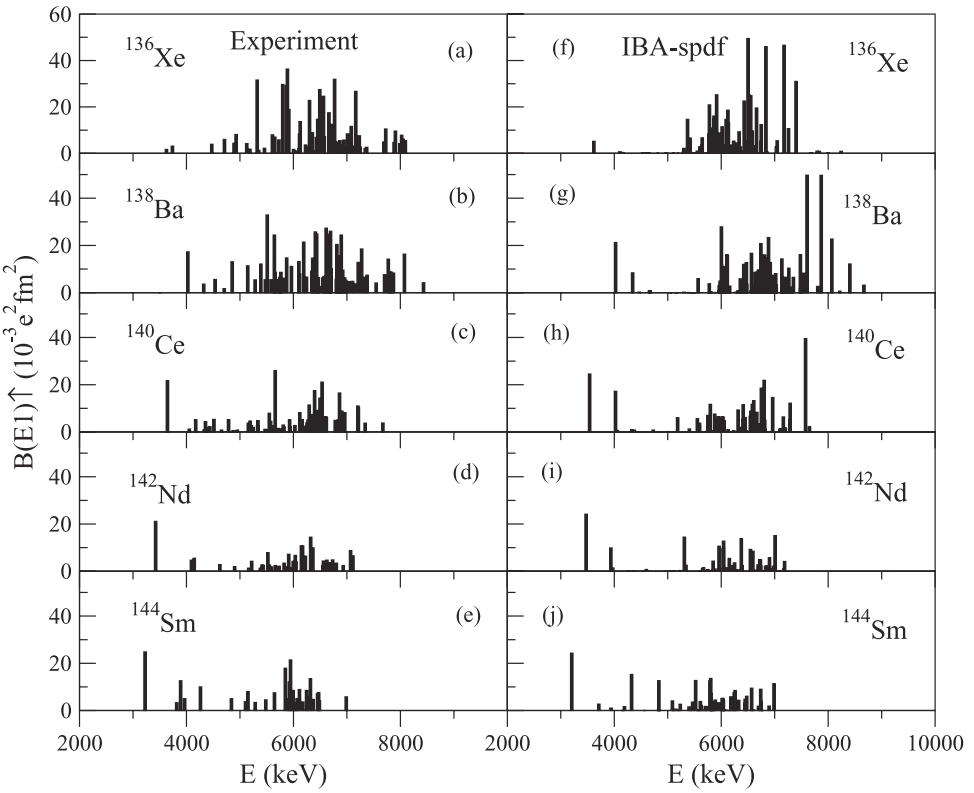

Fig. 28. Experimental B(E1) strength distribution (left columns) compared with the IBM$_{spdf}$ calculations (right columns) for the N = 82 isotones ^{136}Xe, ^{138}Ba, ^{140}Ce, ^{142}Nd, and ^{144}Sm. The experimental data are from Refs. [94,200].
Source: Taken from Ref. [199].

determine the initial boost. In the isovector case, the boost correspond to displace all the neutrons against all the protons maintaining the centre of mass of the system unchanged. A more complete and detailed description of this method can be found in Ref. [206] where the Vlasov equation approach have been used to study the PDR in the O and Sn isotopes. In this work the ground state was set to be a Thomas–Fermi approximation with the so-called Barcelona–Catania–Paris effective interaction [207] used also in the Vlasov calculations. The expectation value of the electric dipole operator as a function of time is obtained from the solution of the classical equation of motion and its value is shown in the left panel of Fig. 29 for three Sn isotopes. An oscillator behaviour that exponentially damps with time is evident for all nuclei. The corresponding strength functions are obtained as a Fourier transform of the expectation values of the dipole operator and are shown in the right panel of Fig. 29. A small enhancement in the isovector dipole strength function below the IVGDR centroid is present for the N>Z nuclei selected while it is absent for nuclei with N = Z. The centroids of the IVGDR are in reasonable agreement with experimental values, whereas the widths are predicted to be smaller due to the fact that the only damping mechanism present in this calculations is the Landau damping as per RPA. The introduction of a collision term in the Vlasov equation could produce some effect similar to the 2p–2h excitation in the mean field approaches.

By making some additional approximations one can extract the radial transition densities and the velocity fields. Being in the linear response regime implies that the amplitudes of the oscillations are small and therefore the angular dependence of the transition densities can be separated from the radial part due to the symmetry of the dipole operator. The azimuthal angle can be integrated out because of the cylindrical symmetry of the system and the polar angle can be averaged. The initial perturbation induce simultaneously oscillations of all possible modes excited by the selected operator, therefore to extract the transition densities of a state with a given energy, a Fourier transform of the density oscillation has to be performed. The derived transition densities [206] have the typical PDR-like shapes. This result is not so trivial since in the Vlasov approach the transition densities are deduced from the densities oscillations induced by the isoscalar or isovector operator. This might suggests that they might depend on the initial boost. However, the fact that they show a PDR-like shape support the strong relation of these quantities with the properties of the nucleus and the dependency on the wave function of the considered state as in the case of microscopic mean field approaches.

In Ref. [206] the velocity fields have been calculated for an isoscalar toroidal operator and similar results to the one described in Section 4.4.1 have been found.

The Vlasov equation approach have been followed also in Ref. [208] where the isovector dipole response was studied varying the density dependence of the symmetry energy. A Skyrme parametrisation of the nuclear mean field was

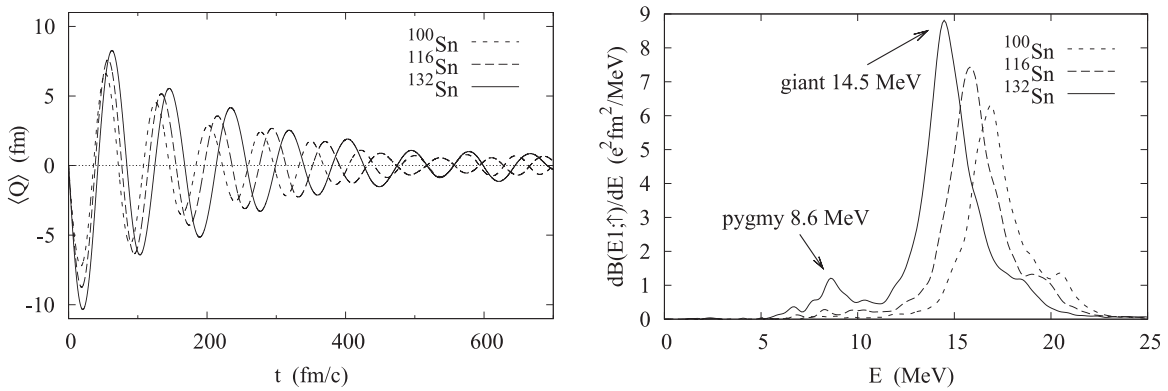

Fig. 29. Time dependent expectation values of the electric dipole operator (left frame) for the three Sn isotopes indicated in the figure. The corresponding electric dipole strengths are shown in the left panel.
Source: Adapted from Ref. [206].

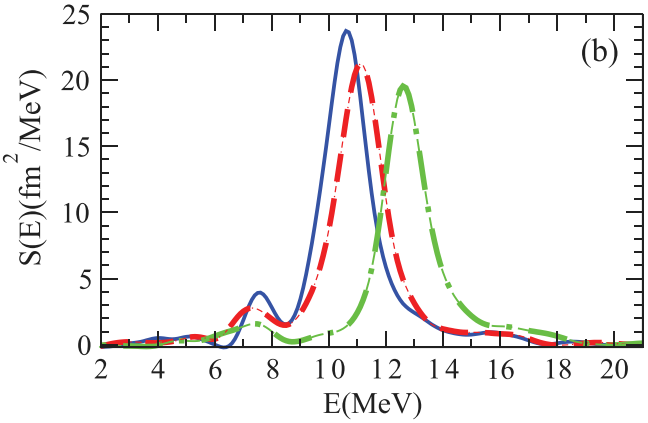

Fig. 30. The strength function for ^{140}Sn for the asysoft (green dashed-dot line), asystiff (dashed red line) and asysuperstiff (blue solid line) symmetry energy slope adopted.
Source: Adapted from Ref. [208].

considered. The symmetry energy at the saturation density was kept constant and the three different expressions for the density away from equilibrium were considered. Three Equation Of State (EOF) with different symmetry energy slope parameters L, defined as the derivative of the symmetry energy with respect to the density, were selected. According to the L values used, the EOS are identified with different names: asystiff for L = 72 MeV, asysoft with L = 14.4 MeV and asysuperstiff with L = 96.6 MeV. The calculations of the isovector strength function for the ^{140}Sn are shown in Fig. 30. For increasing slope parameters the IVGDR peak shifts lower in energy while the peak around 8 MeV – which correspond to the PDR – maintains its energy value. The position of the PDR is found to correspond to the ones in Ref. [209] where the isotopic dependence of the PDR energy was studied within HFB + RQRPA approach (note that in this reference also a good agreement of the IVGDR centroids was found simultaneously).

The Vlasov equation method with a different effective interaction of the Skyrme type, the SAMi-J interaction [18,210], has been used to study the dipole response for the three standard closed-shell nuclei: ^{68}Ni, ^{132}Sn and ^{208}Pb [211]. As shown in the case described above the larger the value of the symmetry energy L is, the higher the peaks in the low-energy region corresponding to the PDR are found, see Fig. 30. The centroid of the IVGDR peak does not seems to be affected by the SAMi-J parametrisations.

The RPA is the small amplitude limit of the quantal time-dependent Hartree–Fock method and both of them have their semiclassical counterpart in the Vlasov equation. An interesting comparison of the low-lying dipole states description obtained with these approaches is discussed in Ref. [212]. In this work three commonly used microscopic theories – TDHF, RPA and Vlasov – were presented.

In the TDHF method the nuclear system is described using the time evolution of the one body density matrix

$$i\hbar\frac{\partial\rho(t)}{\partial t} = \left[h[\rho], \rho(t)\right] \tag{41}$$

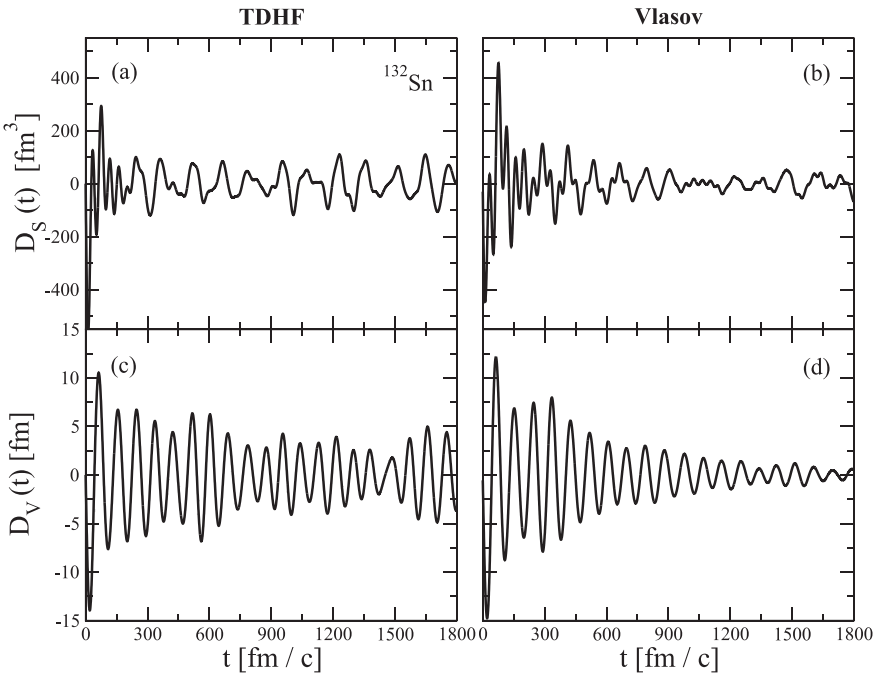

Fig. 31. Time evolution of the isoscalar (upper panels) and isovector (lower panels) dipole moment for ^{132}Sn obtained in a TDHF (left column) and Vlasov (right column) calculations.
Source: Taken from Ref. [212].

where the one body density functional h is the non relativistic single particle Hamiltonian

$$h[\rho] = \frac{\vec{p}^{\,2}}{2m} + U[\rho] \tag{42}$$

with $U[\rho]$ being the self-consistent mean field interaction. To study the collective modes the limit to a small deviations from the equilibrium density needs to be applied. This is obtained by linearising the TDHF equation to obtain the RPA ones. The semiclassical counterpart of the TDHF is the Vlasov equation which in the case of small amplitude limit become the semiclassical representation of the RPA. In this comparison, the same Skyrme functionals were used in the three approaches to maintain the same approximation with the exception of the spin–orbit terms present only in the RPA and TDHF. The calculations for the three methods were carried out with the SAMi-J parametrisation [18] of the interaction and including the Coulomb potential. The ground-state configurations of the different models were modulated to reproduce the experimental values of both proton root-mean-square radius and binding energy. The time evolution of the dipole moments for ^{132}Sn is shown in Fig. 31 for the two time dependent methods: the TDHF (left column) and Vlasov (right column) approaches. The isoscalar (D_S) and isovector (D_V) dipole moments are presented in the upper and lower panels, respectively. The Vlasov calculation shows a larger damping effect in both moment evolutions. Like in the Vlasov method, the dipole strength distributions in TDHF are obtained by taking the Fourier transform of the time expectation value of the isoscalar or isovector dipole moments. These distributions are shown in Fig. 32. The isovector response results obtained in the two methods are very similar especially for the IVGDR where both strength and centroids are very close to each other. In the PDR region, a shift between the two results is evident: the TDHF gives a lower energy values. For the isoscalar response the differences are substantial over all the energy range studied. In particular, the two peaks predicted in the low energy region by the TDHF calculations are not reproduced by the Vlasov method. This discrepancy may be connected with shell effects but this will not explain why these effects should influence only the isoscalar results. An excellent agreement is obtained when a combined comparison of the TDHF and RPA findings for the isovector and isoscalar dipole strength distributions is given [212].

In TDHF the transition densities can be extract with the same procedure described above for the Vlasov method. A comparison with the other approaches shows that the semiclassical calculations can reproduce the gross features of the dipole states in the three energy region discussed at length in the previous sections, namely the PDR, IVGDR and ISGDR regions. An analysis of the low energy modes has been performed as function of the isospin mixing for three isotope of Sn. For the ^{120}Sn (N>Z) the isoscalar dipole strength is strongly enhanced compared with the ^{100}Sn (N = Z) case. This was already shown in the investigation of the evolution of the isoscalar dipole strength for the Ca isotopes in Ref. [131]

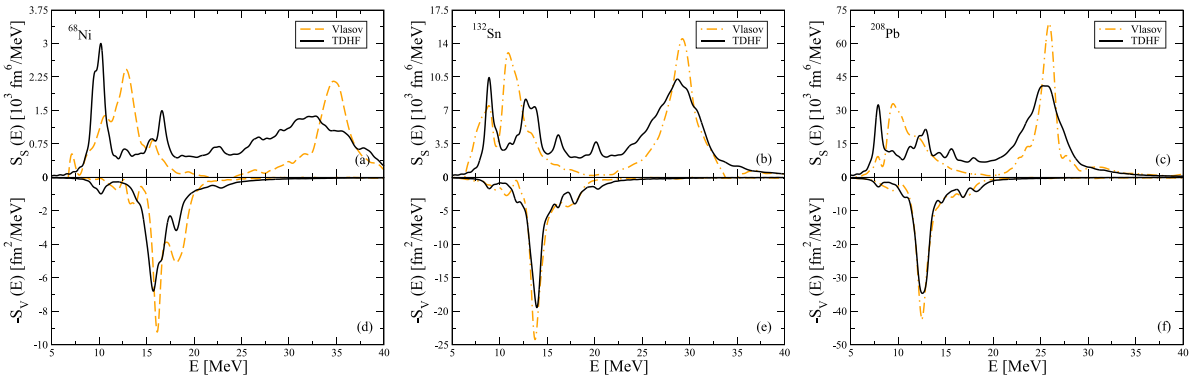

Fig. 32. Strength distributions for the dipole isoscalar (upper panels) and isovector (lower panels) responses for ^{68}Ni, ^{132}Sn and ^{208}Pb obtained in a TDHF (black solid line) and Vlasov (dashed orange line) calculations.
Source: Taken from Ref. [212].

(see Fig. 8). The transition densities for states belonging to different energy ranges show once again the different modes present in the dipole strength distributions. For the low-lying dipole states for N = Z nuclei the transition densities are pure isoscalar while for nuclei with N>Z the typical pattern of the PDR states is found. Even for the transition densities, the results from TDHF give results compatible with the RPA method.

5. Cross section calculations

The majority of experimental findings for the low-lying dipole states comes from electromagnetic excitation processes (see Section 2 and Refs. [7,10]). The main information that can be extracted from these methods is the multipole transition rate B(EL) while information on wave functions and transition densities of the excited states cannot be directly deduced. A more effective way to investigate the latter two quantities is to use reactions where the nuclear interaction is involved. The strong isoscalar component of the low-lying dipole strength makes the PDR states good candidates for the study of the interplay between isoscalar and isovector modes. The theoretical approaches presented in Section 4 give a detailed and exhaustive description of the nuclear structure of the PDR mode. To have a complete comprehension of the experimental data it is compulsory to evaluate the cross sections predicted by the different theoretical models especially when dealing with isoscalar probes like the ones illustrated in Section 2.2.

The most complete theory to estimate the reaction cross section is the Coupled Channel (CC) method where the elastic and inelastic cross section are calculated by explicitly account the most important channels participating in the nuclear scattering. Taking into account only the first order terms in the non-diagonal elements of the interaction matrix, the CC equations can be approximate to the so-called Distorted Wave Born Approximation (DWBA) [115]. The name come from the exchange of the scattering wave functions – plane waves in the Born Approximation – with waves "distorted" by the optical potential governing the entrance and exit channels. For heavy ions reactions, it is preferred for the calculations the use of semiclassical approximations of the inelastic process because it allows a description of the nuclear reaction process where the most important ingredients can be easily identified.

The semiclassical models assumes the centre of mass motion to be described with the classical Newton equation of motion. The condition for the applicability of these models depends (for the Coulomb case) from the Sommerfeld parameter

$$\eta = \frac{Z_a Z_A e^2}{\hbar v} \tag{43}$$

where v is the asymptotic relative velocity. This parameter can be thought as the ratio between half the distance of closest approach (for impact parameter zero) d_0 and the de Broglie wave length $\lambda\!\!\!^{-}$ associate with the incident projectile

$$d_0 = \frac{Z_a Z_A e^2}{\mu v^2} \;\; ; \;\; \lambda\!\!\!^{-} = \frac{\hbar}{\mu v} \, . \tag{44}$$

When $\eta \gg 1$ the nuclei can be considered as moving on classical trajectories. When the nuclear interaction is also contributing to the scattering the condition is more complex. The validity of the semiclassical model lies in the de Broglie wave length being small compared to characteristic reaction quantities such as the distance of closest approach or the distance where the nuclear potential is substantially changing (i.e. the diffuseness of the Saxon–Woods potential). These conditions are well satisfy for heavy ion with incident energy above the Coulomb barrier.

In the semiclassical models, while the nuclei are moving according to the classical equation of motion, the internal degree of freedom are treated according to quantum mechanics. Suppose one has two nuclei a and A, partners of a nuclear reaction, and let us assume that one can distinguish them along the entire classical trajectory. The Hamiltonian of the system can be written as

$$H = H_a + H_A \qquad \text{where} \qquad H_i = H_i^0 + W_i(t)\,, \quad \text{with } i = a, A \tag{45}$$

The internal Hamiltonian for the nuclei A (similar for a) is

$$H_A^0 = \sum_i \epsilon_i a_i^\dagger a_i + \sum_{ij,lk} V_{ij,lk} a_i^\dagger a_j^\dagger a_l a_k \tag{46}$$

The external field $W_A(t)$ describes the excitation of the nucleus A due to the mean field U_a of the nucleus a whose matrix element are depending on time via the relative trajectory $R(t)$

$$W_A(t) = \sum_{ij} \langle i|U_a(R(t))|j\rangle a_i^\dagger a_j + h.c. \tag{47}$$

The complete eigenfunction of the Hamiltonian H can be written as the product of the two eigenfunctions of H_a and H_A

$$|\Psi(t)\rangle = |\psi_a(t)\rangle|\psi_A(t)\rangle. \tag{48}$$

The next step is to solve the Schrödinger equation for the nucleus target A

$$i\hbar \frac{\partial|\psi_A(t)\rangle}{\partial t} = H_A|\psi_A(t)\rangle \tag{49}$$

with the initial condition $|\psi_A(-\infty)\rangle = |\psi_A^0\rangle$ with $|\psi_A^0\rangle$ being the ground state of the target A. Taking out the indices a and A one can write the time dependent wave function as a sum of the eigenfunctions ϕ_α of H^0,

$$|\psi(t)\rangle = \sum_\alpha a_\alpha(t) e^{-\frac{i}{\hbar}E_\alpha t}|\phi_\alpha\rangle \tag{50}$$

where $H^0|\phi_\alpha\rangle = E_\alpha|\phi_\alpha\rangle$. Substituting the $|\psi(t)\rangle$ in the Schrödinger equation, a coupled-channel equations for the amplitude $a_\alpha(t)$ is obtained

$$\dot{a}_\alpha(b,t) = -\frac{i}{\hbar}\sum_{\alpha'} e^{-\frac{i}{\hbar}(E_\alpha - E_{\alpha'})t}\langle\phi_\alpha|W(t)|\phi_{\alpha'}\rangle a_{\alpha'}(b,t)\,. \tag{51}$$

Therefore, the probability amplitude gets a contribution from all the possible channels involved in the excitation process. In this relation the dependence on the impact parameter b comes from the fact that the classical trajectories have to be solved for each impact parameters. The semiclassical coupled channel equations, Eq. (51), are equivalent to the Schrödinger equation and their solution for each excited state α gives the amplitudes $a_\alpha(b,t)$ as function of b whose values at the end of the scattering process ($t = +\infty$) determine the probability to excite the state α

$$P_\alpha(b) = |a_\alpha(b,+\infty)|^2 \tag{52}$$

The cross section for the inelastic excitation of the state α is obtained by integrating $P_\alpha(b)$ over the impact parameter range

$$\sigma_\alpha = 2\pi \int_0^{+\infty} P_\alpha(b)\, T(b)\, b\, db\ . \tag{53}$$

The transmission coefficient $T(b)$ takes into account processes not explicitly included in the model space. It is usually taken as a depletion factor that falls to zero as the overlap between the two nuclei increases. It can be constructed from an integral along the classical trajectory as

$$T(b) = \exp\left\{-\frac{2}{\hbar}\int_{-\infty}^{+\infty} U_I(R(t'))\, dt'\right\} \tag{54}$$

where U_I is the imaginary part of the appropriate optical potential to describe the elastic scattering of the reaction of interest. When the imaginary part is not available from the experimental data it is usual practice to set it as half the magnitude of the real part. In this semiclassical model the optical potential determine the trajectory as well as part of the absorption.

The coupled channels equations Eq. (51) are an infinite set of equations (the summation index α' could run, in principle, up to infinity). For practical numerical calculations one has to make some approximations, in particular one can truncate the equations by choosing the most important channels. The effect of the discharged channels are taking into account by the imaginary part of the optical potential in (54). To perform the calculations one has to specify the states α that are actively participating to the reaction process and the structure of the matrix elements $\langle\phi_\alpha|W(t)|\phi_{\alpha'}\rangle$ which determines

the excitation process of these states commonly referred to – for the radial part – as form factors. Following the choice done in Refs. [49,56,164] the internal structure of the colliding nuclei can be obtained using the HF + RPA approach. In principle one is interested to compute the cross section only for those states that have a significant $B(E\lambda)$ values. To reduce the complexity of the problem – maintaining the essential feature of the reaction – a good approximation is to consider in the coupled-channel calculations only the states with a sizeable EWSR percentage. The number of coupled equations is subsequently reduced by grouping together states with significant strength that are found close in energy. The average of their energy – obtained by weighting the energy of the single states by their $B(E\lambda)$ – define the energy of the new single "doorway" state. Its p–h components are obtained with the constraint that the new state exhausts the fraction of EWSR given by the sum of the EWSR of the constituent states. This *bunching* procedure permits to include in the calculation many states with different multipolarities.

The real part of the optical potential, which together with the Coulomb interaction determines the classical trajectory, is constructed with the double-folding procedure [115,213]. The same procedure has been adopted to compute the radial form factor which are the fundamental part of the transition matrix elements $\langle\phi_\alpha|W(t)|\phi_{\alpha'}\rangle$. We will discuss the importance of the radial form factor and how to calculate them in Section 5.1.

In Ref. [49] a calculation for the system ^{132}Sn + ^{208}Pb at 500 MeV/u was performed to analyse the peak at low energy that was supposed to correspond to the PDR. It is worth noticing that this measurements [12,88,100], see Section 2.2.1, has a limitation in disentangle the contributions from other multipolarities. This amount was estimate as follow. The calculation for this relativistic Coulomb excitation was performed within an approach where anharmonicities and nonlinearities were introduced by the coupling among one- and two- and three-phonon configurations (see Section 4.2.5). The non linearity is a consequence of the use of the Boson mapping briefly described in Section 4.2.5. In fact in this case the excitation operator can be written as

$$W = W^{00} + \sum_{\nu} W^{10}_{\nu} Q^{\dagger}_{\nu} + h.c. + \sum_{\nu\nu'} W^{11}_{\nu\nu'}\, Q^{\dagger}_{\nu} Q_{\nu} + \sum_{\nu\nu'} W^{20}_{\nu\nu'}\, Q^{\dagger}_{\nu} Q^{\dagger}_{\nu} + h.c. \tag{55}$$

The first term in this equation represents the interaction of the two colliding nuclei in their ground state. The W^{10}_{ν} part connects states differing by one phonon, the $W^{11}_{\nu\nu'}$ term couples excited states with the same number of phonons, while $W^{20}_{\nu\nu'}$ allows transitions between states differing by two phonons. The calculation [49] was done using the two different Skyrme interaction and were considered up to nine states of multipolarity lower or equal to 3. In the low-energy region (up to 12 MeV) a 3 to 21% increase, due to the other two- and three-phonon configurations, was found.

5.1. Importance of radial form factor

Independently on the choice of method used to calculate the inelastic excitation cross section – first order DWBA, all order Coupled channel equations or semiclassical methods – the basic and fundamental quantities to describe the excitations are the transition matrix elements which contain – beside the coupling angular momentum terms – the radial form factors. These are the quantity responsible for the transition from one state to another and they determine the entire nuclear reaction together to the dynamic of the process. The form factors depend very much on the model chosen to describe the nuclear structure. However, the common property that distinguish them from the Coulomb form factor is the dependence on the multipolarity λ of the excited states. In fact, the radial Coulomb form factor is proportional to $1/r^{\lambda+1}$ and to $\sqrt{B(E\lambda)}$ (see for instance Refs. [115,214,215]), reason why the Coulomb cross section provides information on the reduced electromagnetic transition probability. The nuclear form factors does not have any explicit dependence on the isoscalar $B(E\lambda)$ nor on the multipole. For instance, in the collective model the radial dependence of the form factor is usually described by the derivative of the nuclear interaction in the distance r and the multipolarity of the state enters into account through the deformation parameter.

In the coupled channel equations (51) the general matrix elements $\langle\phi_\alpha|W(t)|\phi_{\alpha'}\rangle$ describe the excitation between two generic states α and α'. In the equations to follow, only the transitions between the ground states and the dipole states will be taken into consideration. Indeed, in most of the recent experiments using isoscalar probes, the selection of the excited dipole states are achieved by measuring the γ-decay following the de-excitation of the nuclei to their ground states. One of the most used and precise way to calculate the form factor is by mean of the so-called double-folding procedure [115,213]. This method is also employed for the calculation of the real part of the optical potential between two heavy ions and it is obtained by integrating the nucleon–nucleon interaction over the densities of the two nuclei. Following the notation of Satchler's book [115] and accounting for the isospin dependent part of the nucleon–nucleon interaction, the central part of the local effective interaction v_{12} can be written as the sum of two terms: the isoscalar part v_0 generating the isoscalar ion–ion potential and an isovector term v_1 giving the isospin dependent folding potential. Denoting with τ_i's the isospin of the nucleons

$$v_{12} = v_0(r_{12}) + v_1(r_{12})\tau_{\mathbf{1}} \cdot \tau_{\mathbf{2}} \tag{56}$$

Therefore the neutron–neutron, proton–proton and neutron–proton interaction will be

$$v_{nn} = v_{pp} = v_0 + v_1,\ \ v_{np} = v_0 - v_1. \tag{57}$$

Then for the double folding potential we have

$$\begin{aligned} U_F &= \iint \rho_a(r_1)\rho_A(r_2)v_{12}\, d\mathbf{r_1}d\mathbf{r_2} \\ &= \iint \Big[(\rho_{a_n}(r_1)\rho_{A_n}(r_2)) + (\rho_{a_p}(r_1)\rho_{A_p}(r_2))\Big](v_0+v_1)d\mathbf{r_1}d\mathbf{r_2} \\ &+ \iint \Big[(\rho_{a_n}(r_1)\rho_{A_p}(r_2)) + (\rho_{a_p}(r_1)\rho_{A_n}(r_2))\Big](v_0-v_1)d\mathbf{r_1}d\mathbf{r_2} \end{aligned} \tag{58}$$

hence

$$U_{F_0} = \iint \rho_a(r_1)\rho_A(r_2)v_0(r_{12})\, d\mathbf{r_1}d\mathbf{r_2} \tag{59}$$

$$U_{F_1} = \iint \{\rho_{a_n}(r_1) - \rho_{a_p}(r_1)\}\{\rho_{A_n}(r_2) - \rho_{A_p}(r_2)\}v_1(r_{12})\, d\mathbf{r_1}d\mathbf{r_2} \tag{60}$$

Note that in the particular case when $\rho_n = \rho_p(N/Z) = \rho(N/A)$ the last expression reduces to

$$U_{F_1} = \left(\frac{N_A - Z_A}{A_A}\right)\left(\frac{N_a - Z_a}{A_a}\right)\iint \rho_a(r_1)\rho_A(r_1)v_1(r_{12})d\mathbf{r_1}d\mathbf{r}_2. \tag{61}$$

This implies that when one of the two partner of the reaction has $N = Z$ the isovector part of the interaction U_{F_1} is zero. For v_0 and v_1 one can use the M3Y nucleon–nucleon interaction, Reid type [216], whose explicit expressions (in MeV and r in fm) are [213]

$$v_0(r) = \left[7999\frac{e^{-4r}}{4r} - 2134\frac{e^{-2.5r}}{2.5r}\right] - 262\,\delta(\mathbf{r}) \tag{62}$$

and

$$v_1(r) = -\left[4886\frac{e^{-4r}}{4r} - 1176\frac{e^{-2.5r}}{2.5r}\right] + 217\,\delta(\mathbf{r})\,, \tag{63}$$

Here the zero range term is the pseudo-potential which takes into account, in an effective way, the single nucleon exchange [213].

In a similar way the form factors are constructed with the double-folding procedure by using the density of one nucleus and the transition densities of the other excited nucleus, including the nucleon–nucleon interaction for both isoscalar and isovector terms. Only transition densities from the ground state to the excited dipole states will be considered here. Proceeding as for the real part of the potential, the following expression for the form factors are obtained

$$F_0 = \iint \Big[\delta\rho_{a_n}(r_1) + \delta\rho_{a_p}(r_1)\Big]v_0(r_{12})\Big[\rho_{A_p}(r_2) + \rho_{A_n}(r_2)\Big]r_1^2\, dr_1\, r_2^2\, dr_2 \tag{64}$$

$$F_1 = \iint \Big[\delta\rho_{a_n}(r_1) - \delta\rho_{a_p}(r_1)\Big]v_1(r_{12})\Big[\rho_{A_n}(r_2) - \rho_{A_p}(r_2)\Big]r_1^2\, dr_1\, r_2^2\, dr_2 \tag{65}$$

note that, if one of the two nuclei has $N = Z$ then F_1 goes to zero as for the potential.

The next step is to decide which form of the transition density should be used to compute the radial form factors. In macroscopic models the collective vibrational modes are considered as oscillations of the nuclear surface. These modes are viewed as a deformation of the surface and therefore they are usually described in terms of the derivative of the ground-state density. A different approach is to use the microscopic transition density computed within the mean field theories, as it is described in Section 4. In Ref. [56] the form factors for the three systems ^{132}Sn + (α, ^{40}Ca, ^{48}Ca) were calculated using microscopic transition densities derived from the HF + RPA approach with a SGII Skyrme interaction and are here presented in Fig. 33. The upper panels show the form factors for the PDR state of ^{132}Sn for each target where the contribution of the Coulomb (red dotted–dashed line) and nuclear components (dashed blue and dotted black lines) are shown together with the total one (solid black line). In the lower panel the form factors for the IVGDR is shown. The nuclear contribution for the PDR is more important – almost an order of magnitude – than the Coulomb one in all three cases. For the IVGDR the two components are comparable at least in the peripheral region. The difference is due to the isospin mixing which is stronger in the low-lying dipole states. Note that, for the case where one of the two partner of the reaction has N = Z, the F_1 is very small. The nuclear and Coulomb parts interfere destructively at small radii and constructively at large radii. This is mainly due to the fact that the isoscalar dipole transition density displays nodes [130,131].

Considering the PDR as due to an oscillation of the neutron excess against a N = Z core, a very simple model is presented in Ref. [217] to describe the PDR excitation with the help of a modified Goldhaber–Teller model. To eliminate

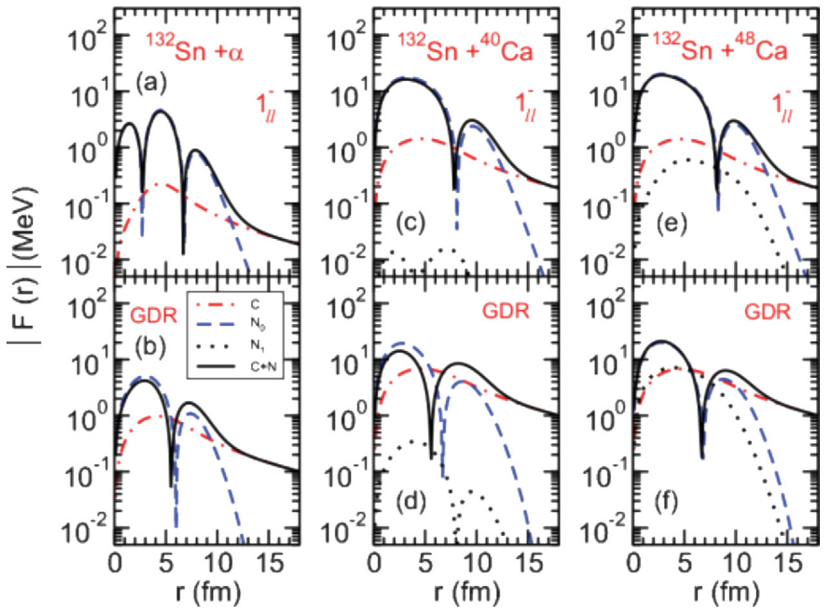

Fig. 33. Form factors for three different systems ^{132}Sn + (α, ^{40}Ca, ^{48}Ca), from the left to the right columns. The upper frames show the ones for PDR states while the lower panels are for the IVGDR. The different components are indicated in the legend together with the total one.
Source: Taken from Ref. [56].

the centre of mass motion, the displacement of the core (C) and the skin (S) along the axis joining the centre of mass of the two oscillating objects should be written as

$$\Delta x_S = -x\frac{Z+N_C}{A}\ ; \quad \Delta x_C = x\frac{N_S}{A} \tag{66}$$

The total number of neutron is given by the sum of the neutron in the core N_C and the neutron in the skin N_S. The density is given by the sum of three terms

$$\rho(r) = \rho_p(r) + \rho_n^C(r) + \rho_n^S(r) \tag{67}$$

and the transition densities are given by a modified Goldhaber–Teller model

$$\delta\rho_n(r) = \delta\left[\frac{N_S}{A}\frac{d\rho_n^C(r)}{dr} - \frac{N_C+Z}{A}\frac{d\rho_n^S(r)}{dr}\right] \tag{68}$$

$$\delta\rho_p(r) = \delta\left[\frac{N_S}{A}\frac{d\rho_p(r)}{dr}\right] \tag{69}$$

where δ is the deformation length. The isoscalar and isovector transition densities can then be constructed as

$$\delta\rho_{PDR}^{is} = \delta\left[\frac{N_S}{A}\frac{d(\rho_n^C+\rho_p)}{dr} - \frac{N_C+Z}{A}\frac{d\rho_n^S}{dr}\right] \tag{70}$$

$$\delta\rho_{PDR}^{iv} = \delta\left[\frac{N_S}{A}\frac{d(\rho_n^C-\rho_p)}{dr} - \frac{N_C+Z}{A}\frac{d\rho_n^S}{dr}\right] \tag{71}$$

Another way to calculate the transition densities and the form factor for the low-lying dipole states is to assume that these states are purely isoscalar and therefore the same method to describe the ISGDR can be adopted [218,219]. In this method it is assumed that the isoscalar dipole energy-weighted sum rule is fully exhausted by a single collective state and the corresponding isoscalar transition density can then be derived. In the work of Harakeh and Diepering (HD) it is written as [219]

$$\delta\rho_{ISGDR}^{HD}(r) = -\frac{\beta_1}{R\sqrt{3}}\left[3r^2\frac{d}{dr} + 10r - \frac{5}{3}\langle r^2\rangle\frac{d}{dr} + \epsilon(r\frac{d^2}{dr^2} + 4\frac{d}{dr})\right]\rho_0(r) \tag{72}$$

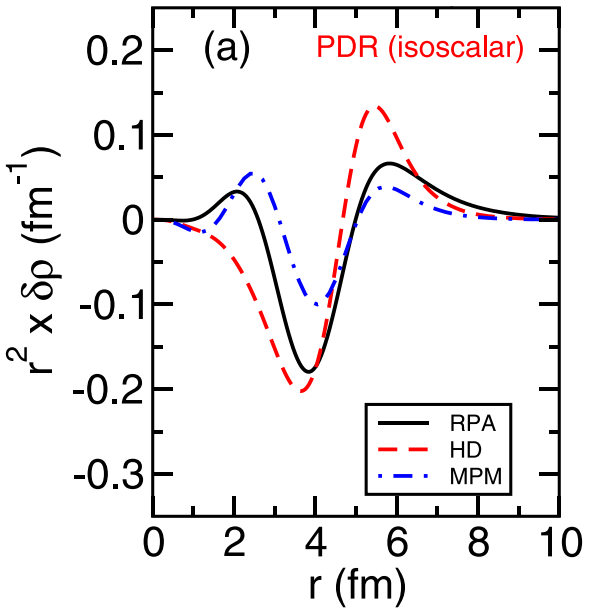

Fig. 34. Isoscalar transition densities for ^{68}Ni calculated with three different approaches: microscopic RPA (solid black line), Harakeh and Diepering method (HD) (dashed red line) and the Macroscopic Pygmy Model (MPM) (dotted–dashed blue line) described in the text.
Source: Adapted from Ref. [217].

where the coupling parameter β_1 is

$$\beta_1^2 = -\left(\frac{6\pi\hbar^2}{mAE_x}\right)\frac{R^2}{(11\langle r^4\rangle - \frac{25}{3}\langle r^2\rangle^2 - 10\epsilon\langle r^2\rangle)} \tag{73}$$

with

$$\epsilon = \left(\frac{4}{E_2} + \frac{5}{E_0}\right)\frac{\hbar^2}{3\ mA} \tag{74}$$

E_2 and E_0 being the giant quadrupole and giant monopole excitation energies, respectively. The distance R is the half-density radius of the mass distribution. The transition density expression Eq. (72) contains the centre of mass correction and the terms with ϵ can be omitted for nuclei with $A \geq 40$. It is strait forward to show that the condition of translational invariance ($\int \delta\rho^{HD}(r)r^3dr = 0$) is satisfied.

The transition densities calculated according to the three methods illustrated above can be compared among themselves once a proper normalisation is implemented, for instance to the microscopic result obtained with the RPA calculations. The neutron and proton ground state densities are computed with the H–F method. The three isoscalar transition densities for the nucleus ^{68}Ni are shown in Fig. 34 and they show some difference in the entire radial nuclear region. All of them follow the same trend but the transition density calculated by the Harakeh and Dieperink (HD) method (dashed red line) shows a substantial difference at the surface nuclear region.

These apparently little differences have appreciable effects in the radial form factor functions as shown in Fig. 35. All these calculation were performed with the double-folding procedure described above for the system ^{68}Ni + ^{12}C. The choice of the target has been done to select an isoscalar probe able to explore in a nuclear reaction the grazing region of the two nuclei where the differences between the transition densities are larger. From the figure it is evident that in the region 7–9 fm – which is the region explored by the selected ^{68}Ni + ^{12}C reaction – the difference among the three form factors is prominent. DWBA calculations performed with the DWUCK4 code [220,221] for the system ^{68}Ni + ^{12}C at 10 MeV/nucleon using the form factors shown in Fig. 35, are plotted in Fig. 36. The result obtained with the HD form factor gives larger value (more than 3 times) than the microscopic one in the relevant forward angular region. The results for the MPM are also in disagreement with the microscopic calculations with the additional difference that the discrepancy is extended to the full angular region considered. It is important to stress that the contribution from the forward angular region is dominant in this process since it is directly related with the prevalent surface excitation. In fact, the almost factor of 2 in the surface region of the form factors is generating a factor of almost 4 in the cross section. The microscopic form factor has been successfully employed in the analysis of various experiments performed with ^{17}O as isoscalar probe [8,10,64,66–68]. In these papers, only the use of the microscopic form factor has allowed the extraction of the isoscalar components of the low-lying dipole excited states.

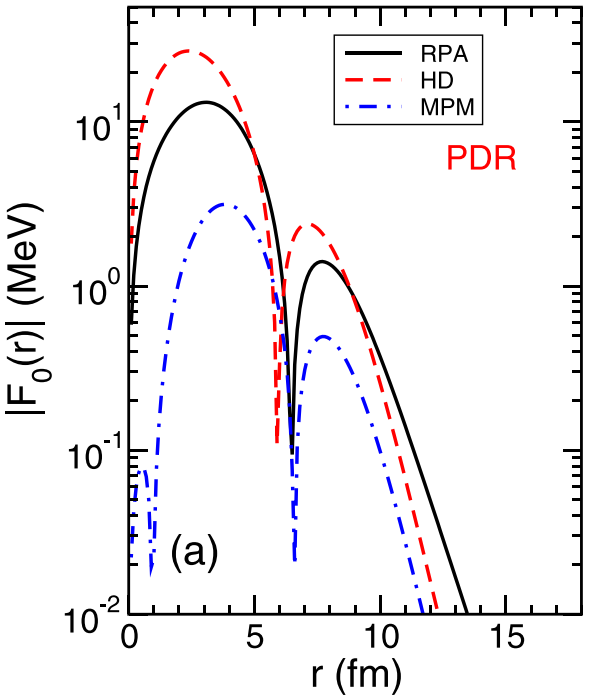

Fig. 35. Radial form factors for the system ^{68}Ni + ^{12}C for the PDR state calculated with the double folding procedure with the transition densities of Fig. 34.
Source: Adapted from Ref. [217].

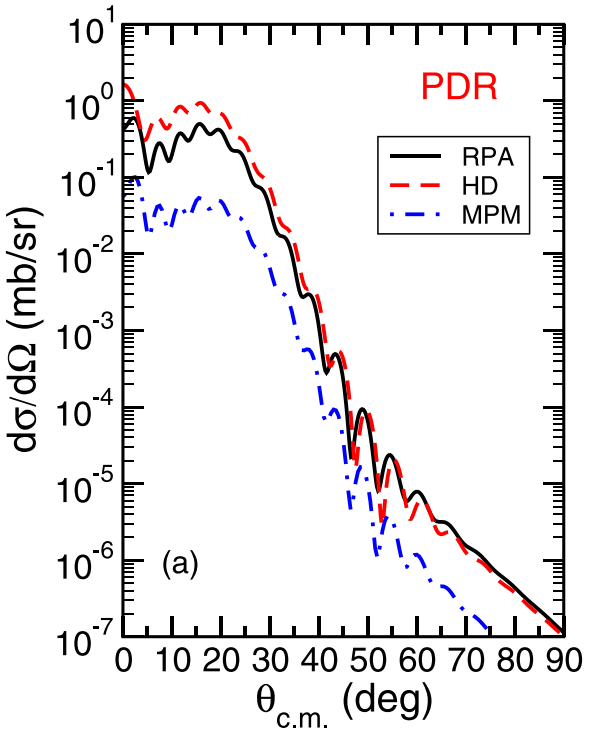

Fig. 36. Differential cross section for the system ^{68}Ni + ^{12}C at 10 MeV/nucleon for the PDR state calculated using the form factors shown in Fig. 35. Calculation done with the DWUCK4 code.
Source: Adapted from Ref. [217].

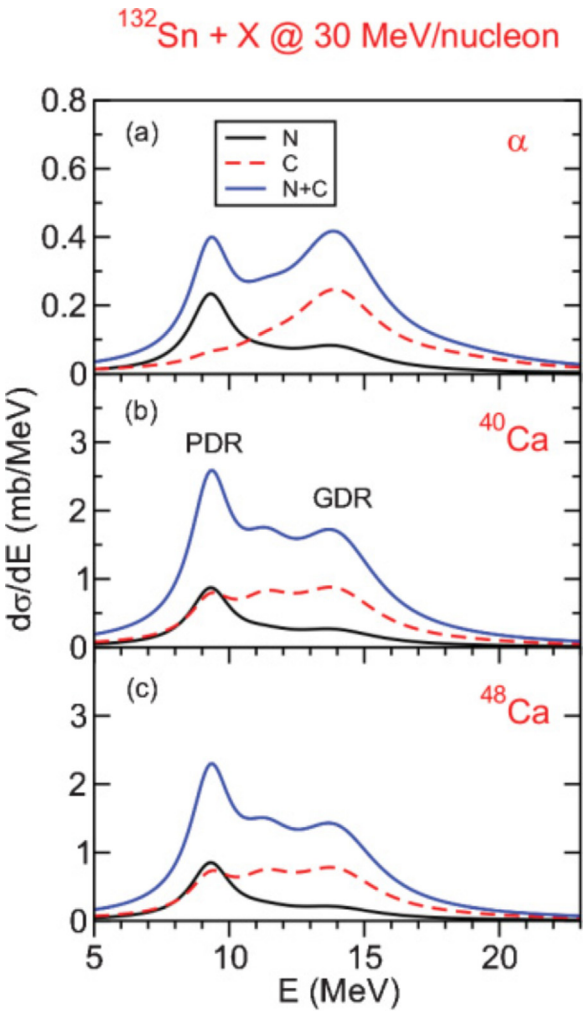

Fig. 37. Excitation function for the dipole states of ^{132}Sn at 30 MeV/u incident energy with three different targets: α (top frame), ^{40}Ca (middle frame) and ^{48}Ca (bottom frame). The Coulomb contribution is the dashed red line, the nuclear one is the black solid line. The blue line is for the total cross section.
Source: Taken from Ref. [56].

5.2. Coulomb and nuclear excitations

As discussed in previous sections, the main characteristic of the Pygmy states can be identified in the strong isospin mixing at the nuclear surface making the contribution to the excitation given by the nuclear interaction possibly relevant. By tuning the projectile mass, charge, bombarding energy and scattering angle, the relative role of the nuclear and Coulomb components can be modified together with the isoscalar and isovector contributions. The knowledge of this interplay may be of paramount importance in to design an experimental measure. Calculations for the excitation of dipole of ^{132}Sn with different partner and including both Coulomb and nuclear interaction were performed with three targets – α particle, ^{40}Ca and ^{48}Ca – and at different incident energies [56]. The energy differential total cross sections for the dipole states are shown in Fig. 37 at 30 MeV/nucleon incident energy. The discrete total cross sections obtained with Eq. (53) are folded with Lorentzians with energy dependent widths. The nuclear and Coulomb contribution are shown separately with solid black and dashed red lines, respectively. The blue lines represent the total result. Changing the partners of the reaction, the relative strength between PDR and IVGDR varies appreciably; for the Ca isotopes at this incident energy the PDR peak is higher than the IVGDR one. This can be interpreted as being the IVGDR always dominated by the Coulomb interaction, while for the PDR the nuclear component strongly contribute, especially for the case of alpha particles.

The ratios between PDR and IVGDR cross section can be better understood by looking at the differential angular distributions. In the semiclassical picture, this quantity is associated to different ranges of impact parameters. The "partial-wave cross sections" – the integrand in the cross section expression (53) – are plotted as functions of the impact parameter

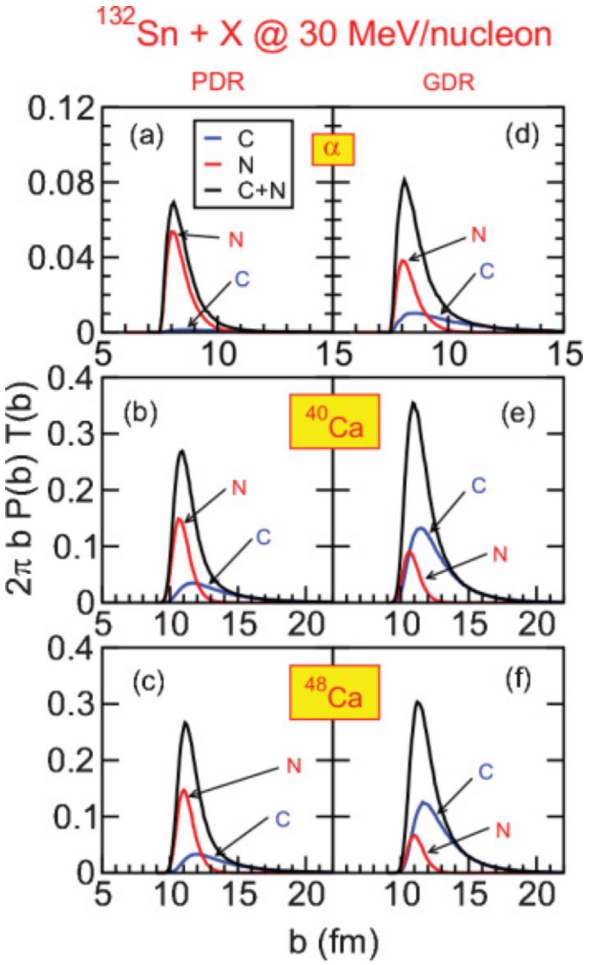

Fig. 38. "Partial wave cross section" as function of the impact parameter b for the dipole excitation of ^{132}Sn at 30 MeV/u incident energy with three different targets: α (top panels), ^{40}Ca (middle panels) and ^{48}Ca (bottom panels). In the left columns are shown the results for the PDR and in the right columns the ones for the GDR. The Coulomb and nuclear contribution are explicitly indicated in all the frames.
Source: Taken from Ref. [56].

in Fig. 38. A limited range of impact parameters, corresponding to the grazing angles, is associated to nuclear component of the excitation while the Coulomb interaction is present for a larger range of impact parameters. In all systems studied, the nuclear contribution to the PDR is higher than the Coulomb one. A different behaviour is seen for the IVGDR with the exception of the α particles where the Coulomb excitation plays a less important role for both PDR and IVGDR.

Another variable of the reaction process that can change the relative importance of the excited states can be the incident energy. In the semiclassical model of Ref. [56] it is possible to calculate the contribution of other multiple states. The differential cross sections as function of the excitation energy for the systems $^{17}O + ^{208}Pb$ and two values of incident energies are shown in Fig. 39. The different multipole contributions are separately shown: The pale (green) shaded area corresponds to the $L = 2$ multipole states while the dark (red) area is the dipole contribution. The thin (blue) and the thick (black) line correspond to the L = 3 and total contributions, respectively. The low-lying 2^+ and 3^- states are much more excited and their intensity do not change for the energy selected; the PDR and IVGDR peaks increase with increasing energy.

A global vision of the effects on the inelastic excitation due to the variation of the incident energy can be seen by looking at Fig. 40 where the nuclear, Coulomb and total inelastic cross sections for different multipole states are plotted as function of the incident energy [222] for the $^{17}O + ^{208}Pb$ system. The excitation of the pure isoscalar states is enhanced by the nuclear field (panel (a)) and a similar behaviour is shown by the PDR mode. The mixed isoscalar and isovector components in the low-lying dipole states allow for greater excitation at lower incident energies where the probability to excite the PDR is sensibly higher than for the GDR. The middle panel (b) shows the inelastic cross section induced by the Coulomb field. For the low-lying 2^+ and 3^- states it is clear the effects due to the strong angular momentum dependence of the Coulomb form factors and of the adiabatic cut-off effect. When the two interactions are acting together (frame (c))

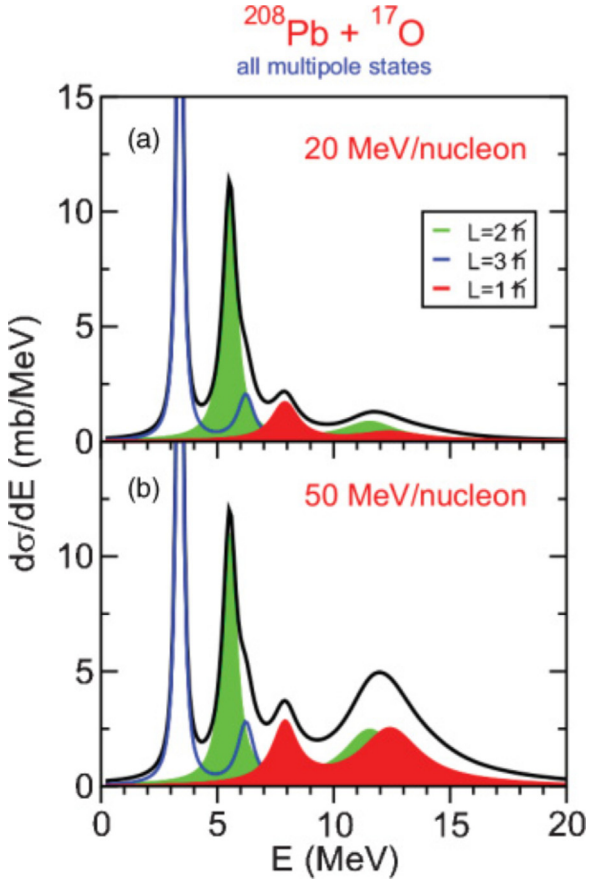

Fig. 39. Excitation function for the systems $^{17}O + {}^{208}Pb$ for two different incident energies. In each frame the multipole contributions are shown. The red area corresponds to the dipole multipole states while the green area is the L = 2 contribution. The thin (blue) solid line and the thick (black) line correspond to the L = 3 and total, respectively.
Source: Taken from Ref. [56].

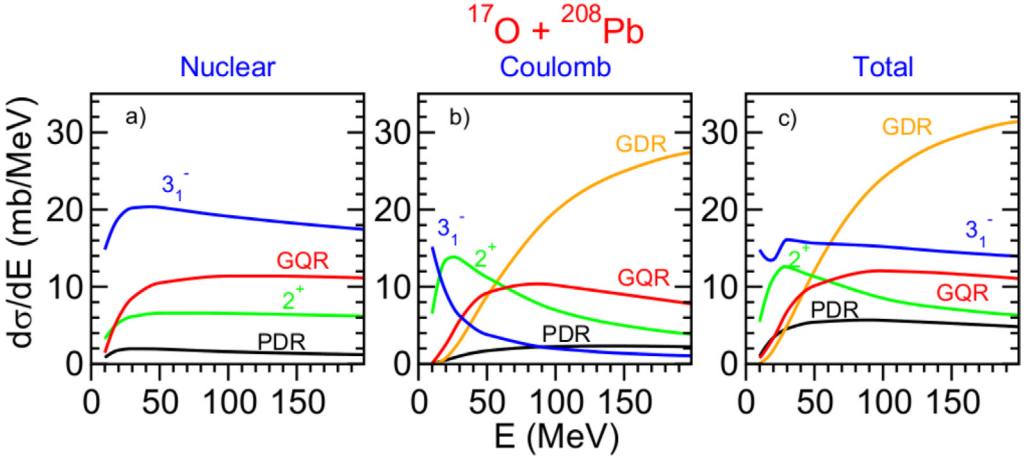

Fig. 40. Excitation function for the systems $^{17}O + {}^{208}Pb$ as a function of the incident energy per nucleon for the multipole states indicated in the figure. The nuclear (a) and Coulomb (b) contributions, as well as the total one (c), are shown in separate frames. The contributions of each multipole state are indicated with the corresponding labels.
Source: Taken from Ref. [222].

a strong positive interference is observed for the PDR excitation. These results suggest that the investigation of the PDR state, explored with isoscalar probes, can be better carried out at low incident energy (below or around 50 MeV/nucleon).

The description of the excitation of the PDR and of its internal structure via the microscopic mean field theories, sketched in Section 4, together with the quantitative inelastic cross section calculations, described in this section, allows a comprehensive understanding of the phenomenon. Furthermore, the study of the response to different external fields may help in testing various aspects of the wave functions of the involved excitations. This experimental approach has revealed one of the most interesting aspect of the PDR states, the so-called isospin splitting, a structural splitting of the low-lying E1 strength (for the experimental part see Section 3). As stated in the previous sections, this consists in the separation of the PDR energy region in two parts, the low-lying part where the states have a strong isospin mixing and they can be excited by both isoscalar and isovector probes and a high-lying region where the population of the states occur only through electromagnetic interactions. This behaviour has been reproduced by the theoretical calculation within the QPM and RQTBA models that take into account the coupling of simple 1p–1h configurations to complex configuration going beyond the quasi-particle RPA. The inclusion of the coupling to multiphonon states allows a fragmentation of the strength and a shift towards energies below the neutron emission threshold (see Sections 4.2.6 and 4.2.7). The calculations of the isoscalar and isovector reduced transition probabilities have been compared to the $(\alpha, \alpha'\gamma)$ inelastic cross section and the measured $B(E1)$ in a (γ, γ') reaction for ^{124}Sn [223]. However, as discussed in this section, the α scattering cross section cannot be directly compared with the calculated isoscalar $B_{is}(E1)$. In order to have a quantitative comparison, a calculation within the semiclassical model described above was performed for the system $\alpha + {}^{124}$Sn at 136 MeV [224]. The transition densities used to construct the form factors were obtained by the RQTBA calculation. To show the fundamental difference between the cross section and the isoscalar and isovector $B(E1)$ a quantity, that is independent from the biases introduced by the dynamics of the process, needs to be identified. Such quantity was found in the ratio between the Coulomb (nuclear) cross section and the isovector (isoscalar) reduced transition probability, for each dipole state. The Q-value dynamical effects have been completely removed by setting to zero the energies of the states. Therefore, the ratio $\sigma_x^i(E_i = 0)/B_x^i(E1)$ – where the indices i and x denote the dipole states and the isospin nature, respectively – show a constant value for all the states only for the Coulomb cross section. Therefore, in the case of isoscalar probes one has to perform inelastic cross section calculations in order to extract information from the comparison between experimental data and theoretical calculations. However, the comparison between the theoretical and experimental cross section shows [224] a strong reduction of the experimental α cross section at higher excitation energy compared to the isovector channel, confirming the structural splitting of the low-lying E1 strength.

A systematic investigation of the PDR in ^{140}Ce using different probes has been carried out in Ref. [62] and the results are shown in Fig. 41. The figure depicts all the available results for the low-lying dipole energy region for ^{140}Ce: the $(\alpha, \alpha'\gamma)$ [225], the $(p, p'\gamma)$ [62], the NRF reaction (γ, γ') [200,226] and the measured averaged branching ratio to the first excited state [97]. The cross section for the alpha and low-energy heavy-ion reactions is sensitive to the isoscalar component of the excited states; the proton reaction $(p, p'\gamma)$ at a bombarding energy of 80 MeV provides more informations since the proton scattering is sensitive to isovector components and its surface-peaked interaction is less pronounced. The theoretical calculations for the reduced transition probability have been performed within the QPM framework taking into account the coupling to one-, two-, and three-phonon configurations and they are shown in the right part of panel (c). The (α, α') cross sections have been calculate within the semiclassical model described above. The ground state densities and the transition densities used to build the form factors were obtained by the QPM approach. The integral in Eq. (53) has been carried out over the interval of impact parameters that lead to the scattered projectile in the measured angular range. The (p, p') cross sections have been computed within the DWBA employing the DWBA07 code [227]. The effective nucleon–nucleon interaction of Love and Franey [228,229] has been used as input to calculate both the optical potential and transition amplitudes. The experimental data show the presence of what has been called PDR splitting, an indication of different isospin properties of the states, in this low energy range. To investigate this point the cross section calculations for both reactions have been repeated for nuclear and Coulomb interaction separately. The results are presented in the upper two rows of Fig. 42 while last row shows the complete calculation. In both reactions the nuclear part dominates the lower part of the PDR energy range producing large cross section; on the contrary the Coulomb interaction seems to give a stronger contribution to states in the higher part of the spectrum. The structural behaviour of the results of the p and α reactions seem very similar except for different order of magnitude measured in the cross section, aspects also reproduced in the theoretical calculations. The overall and simultaneous agreement between the experimental data and the theoretical calculations on an absolute scale for all observables is satisfactory and corroborates the present interpretation of the PDR. However there are some aspects of this excitation mode still uncertain and to be clarified, some of these open questions will be discussed in the next section.

6. Open problems

The extensive experimental and theoretical work done to investigate the low-lying dipole states has produced a lot of information on the structure and excitation of these states. Reviewing these works made clear that the main characteristics and features of this electric dipole strength were identified. However, there are still some aspects that need to be clarified. One strongly debated point, still unresolved, is about the collectivity property of the PDR. Another one is the interplay between the isoscalar and isovector contribution which mixes the isospin nature of these states and makes the investigation of this mode complicated although more interesting. In our opinion, the manifestation of the PDR splitting needs further clarification especially above particle emission threshold.

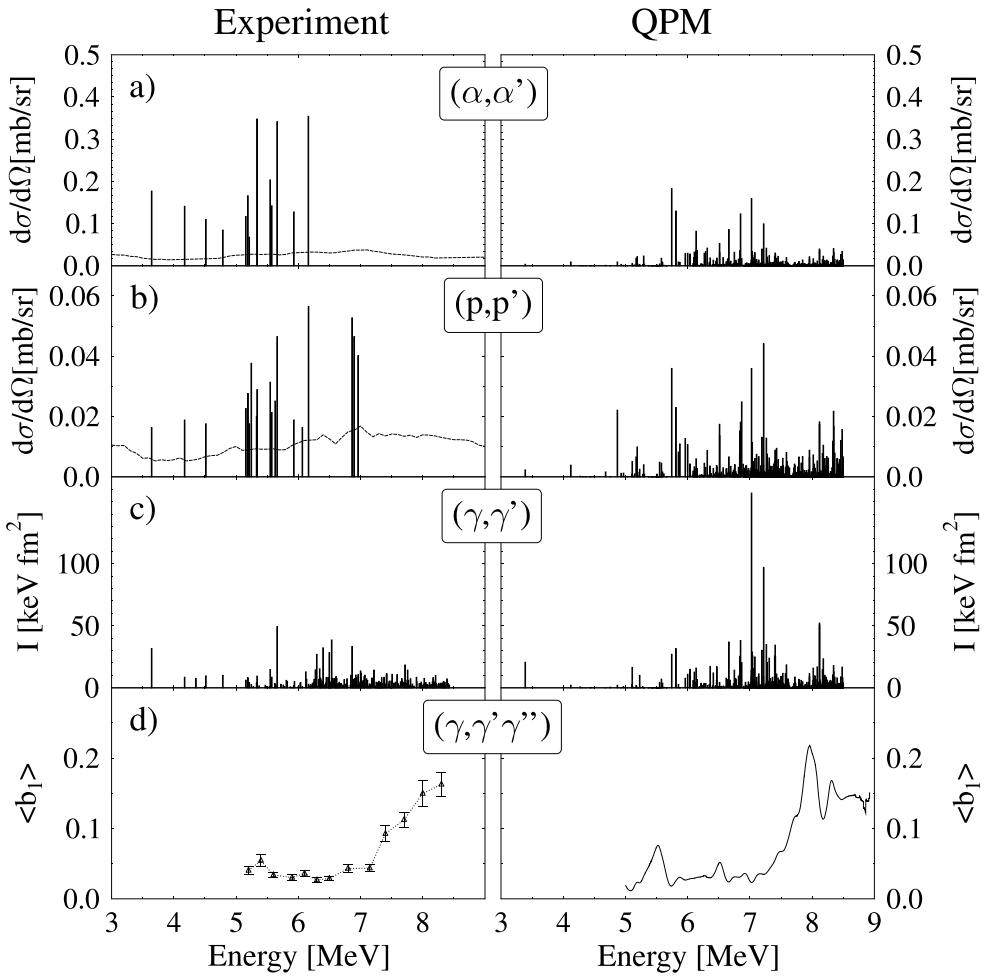

Fig. 41. The experimental results (left columns) for ^{140}Ce using different probes are compared to the theoretical calculations (right columns). In the lowest panels the averaged branching ratio to the first excited state. For more details and references see text.
Source: Taken from Ref. [62].

6.1. Are they collective or single particle excitations?

One of the first question on the PDR was whether these states could be considered or not collective modes. From the theoretical point of view, asserting the collective nature of a state is strongly connected to the model adopted for its description. The use of a macroscopic collective model implicitly assumes that – for instance in the IVGDR – the neutrons and protons move coherently one against the other. For a microscopic model – like RPA – this is not the case. For these approaches one has to determine first how many p–h configurations contribute to the state and then investigate their coherency. Among the quantities commonly used to identify the collectivity, it is important to underline that the EWSR is not an appropriate index. In the case of a collective low-lying quadrupole state, even though its percentage of the EWSR is only around 10% – compared to the one exhausted by the GQR (60% and above) – the low-lying 2^+ cannot be considered less collective state than the GQR. The Weisskopf units also can give only a simple estimation of the collectivity degree. Since no clear answer could be drawn from these quantities a deeper investigation on the composition of these states must be conducted before concluding anything on their collective nature. The first step is to quantify how many configurations contribute to the construction of the pygmy states in a mean-field approach. In a RPA calculation, with NL3 interaction, one can estimate [47] for a state ν the contribution of a particle–hole configuration by defining the amplitude

$$A^{\nu}_{ph} = |X^{\nu}_{ph}|^2 - |Y^{\nu}_{ph}|^2 \tag{75}$$

with X and Y being the amplitudes defined by the RRPA equations and with the normalisation condition

$$\sum_{ph} A^{\nu}_{ph} = 1\,. \tag{76}$$

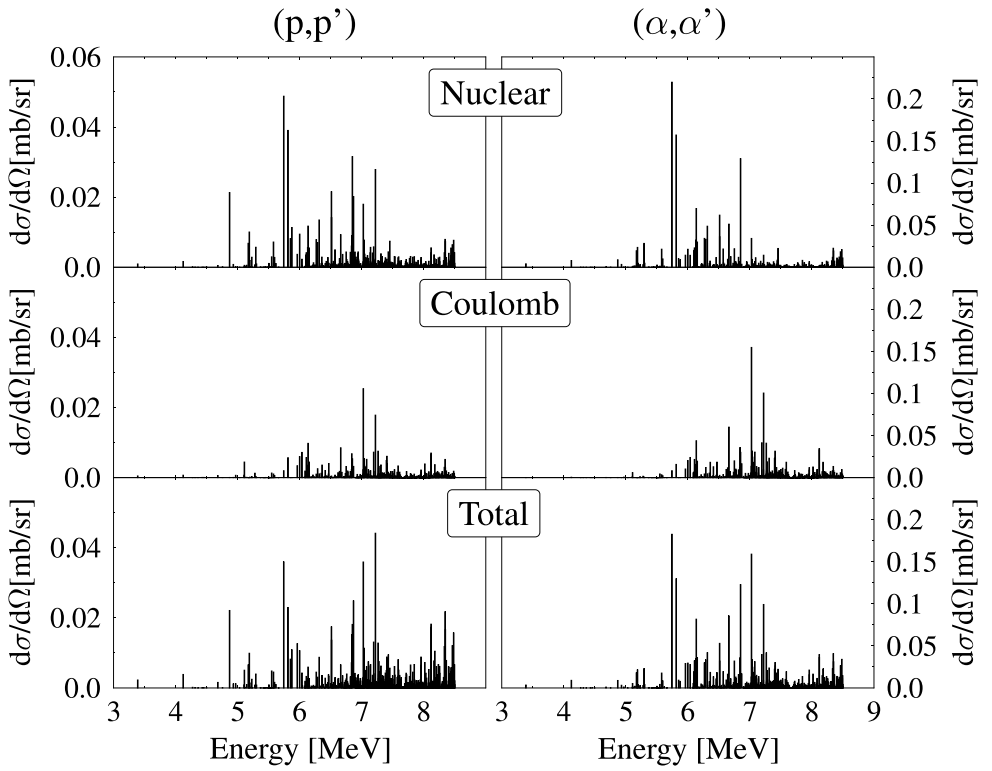

Fig. 42. Inelastic cross section for ^{140}Ce(α, α') and ^{140}Ce(p, p') reaction for only nuclear interaction (top rows), only Coulomb interaction (middle row) and total one (bottom row).
Source: Taken from Ref. [62].

The second step is to calculate the percentage contribution of a p–h configuration in the formation of the state ν. In Ref. [47], nine p–h configurations – with a contribution more than 1% – have been found for ^{68}Ni and ^{132}Sn nuclei. An alternative way to estimate the p–h contribution is to follow the method adopted in Ref. [138] where an index is defined to measure the degree of collectivity of a specific excited state. In this work an RPA approach was used where the single particle basis were constructed on a Woods–Saxon well and expanded in a harmonic oscillator basis. This index $\mathcal{D}$ is defined in terms of the total number of p–h configuration N_{ph} and the number of states with $[|X^{\nu}_{ph}|^2 - |Y^{\nu}_{ph}|^2] \geq 1/N_{ph}$, named N^*

$$\mathcal{D} = \frac{N^*}{N_{ph}} \tag{77}$$

Two extreme case can be obtained: $\mathcal{D} = 1$ when all the p–h configuration give a contribution and it is $\mathcal{D} = 1/N_{ph}$ when only one single p–h contributes. The analysis based on the amplitude A^{ν}_{ph} and the index $\mathcal{D}$ are not exhaustive because they are missing the fundamental concept that defines collectivity: coherence. This was noted in Ref. [49] where the reduced transition probability was written as (see Eq. (18))

$$B(E\lambda) = \left| \sum_{ph} b_{ph}(E\lambda) \right|^2 = \left| \sum_{ph} (X^{\nu}_{ph} - Y^{\nu}_{ph}) T^{\lambda}_{ph} \right|^2 \tag{78}$$

where T^{λ}_{ph} are the 2^{λ} multipole transition amplitudes associated with the elementary p–h configurations. An analysis carried out on ^{132}Sn, with the $B(E\lambda)$ calculated with an HF + RPA with a SGII interaction, shows [49] that p–h configurations with small A^{ν}_{ph} may have big values of $b_{ph}(E\lambda)$. For the same nucleus a calculation of the index $\mathcal{D}$ gives a value of 0.28, with $N^* = 90$, to be compared to the value of 0.53, with $N^* = 169$, corresponding to the IVGDR, where the total number of p–h configurations for the dipole states give $1/N_{ph} = 0.003$. One should be critical in concluding something at this stage because these quantity do not take into account the amplitude T^{λ}_{ph} nor the relative signs of the separate contributions. Fig. 43 shows the partial contributions $b_{ph}(E\lambda)$ plotted against the order number of the p–h configurations used in the RPA calculations. Each $b_{ph}(E\lambda)$ value is represented by a bar while the continuous thin blue line is the cumulative sum of the contributions. The dashed lines divide the protons from the neutron configurations. The top rows show the isovector responses for few selected dipole states in ^{208}Pb whose excitation energy are written in the

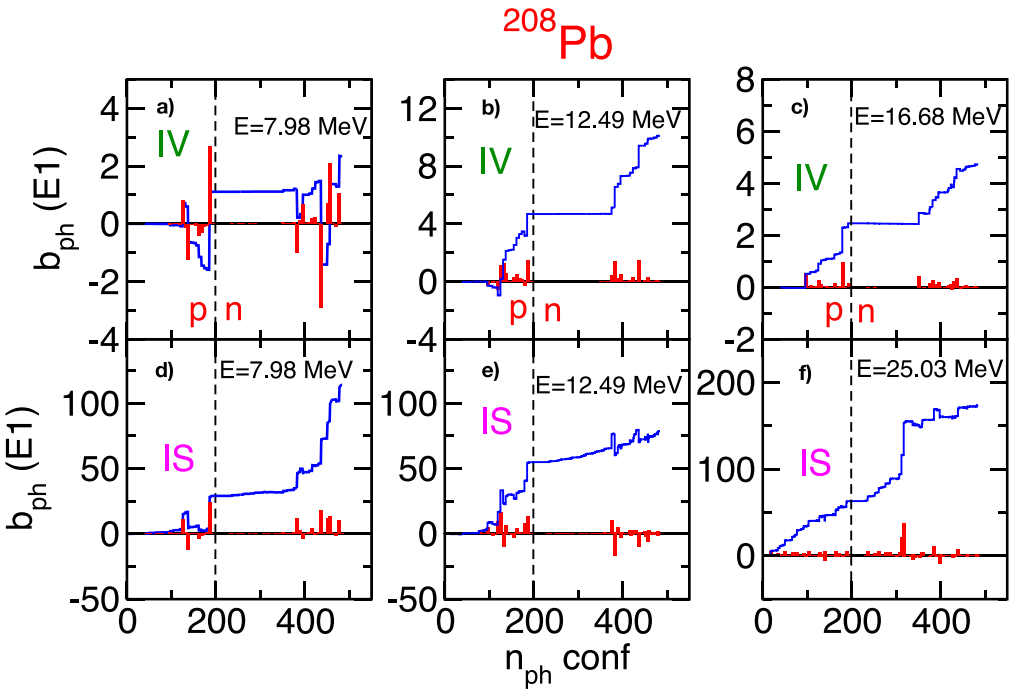

Fig. 43. Partial contributions b_{ph} of the reduced transition probability vs the order number of the p–h configurations n_{ph} used in the RPA calculations for some dipole states of ^{208}Pb. The dashed vertical lines divide the protons from the neutron configurations. The order goes from the most to the less bound ones. The bars corresponds to the individual b_{ph} contributions; the continuous thin line is the cumulative sum of the contributions. The top rows are for isovector dipole states responses whose excitation energy are written in the panels; in the bottom rows the results for isoscalar responses.

panels; while the bottom rows shows the results for isoscalar responses. From the figure, one can see how the $B(E1)$ of all the dipole states except the one in panel (a), are composed from small contributions of many p–h configurations which add coherently. The low-lying states in frame (a) shows a different behaviour: several p–h configurations participate in the formation of the $B(E1)$ but some of them contribute with opposite sign, giving rise to a small total value. From this analysis, it emerges that the isoscalar response for the three states considered shows a collective behaviour. The same can be observed for the IVGDR (frame b) and the higher dipole state at 16.68 MeV (frame c). Although the low-lying states cannot be considered collective, they also cannot be described as of single p–h nature. In fact, they are generated by the cooperative, although not coherent, effect of several particle–hole excitations. To confirm the efficiency of the method, the same analysis was applied to the low-lying quadrupole state of ^{132}Sn. In panel (a) of Fig. 44, the transition densities for protons (black dashed line) and neutrons (red dashed–dotted line) are plotted together with the isoscalar (black solid line) and isovector (blue solid line) ones. Protons and neutrons oscillate in phase giving rise to a pure isoscalar state. Its collective nature is clearly shown in panel (b), similar to Fig. 43, since many p–h configurations form the state, hundreds of them, and they add coherently as shown by the cumulative sum.

A similar analysis with compatible results was performed for ^{68}Ni, ^{132}Sn and ^{208}Pb closed-shell nuclei in a full self consistent HF + RPA approach using three different Skyrme interactions: SGII [133], SLy5 [136] and SkI3 [137]. The isovector (a) and isoscalar (b) dipole responses of the pygmy states in ^{208}Pb are presented in Fig. 45 for the three interactions. All the neutron (black) and proton (red) p–h contributions to the reduced amplitude A_{ph} – equivalent to the b_{ph} defined above – are shown as a function of their excitation energy. Similar results are reproduced by all the interaction considered. In the isovector response a destructive interference between contributions is predicted while the isoscalar response shows a more evident collective behaviour due to the coherent sum of the individual amplitudes. Similar results were obtained for the other nuclei studied. No difference in the results was find when using a full self consistent RRPA with the DD-ME1 [230] or DD-ME2 [231] effective interactions [50].

Although an agreement has been found among these works, other approaches seems to indicate an alternative scenario. A schematic modified Brown–Bosterly model [233], with separable interactions and condition on different coupling constant for the particle–hole interaction, was introduced in Ref. [52]. In calculating the response within the TDA and RPA approaches, it was assumed that, for a subsystem of particle–hole pairs belonging to a core c, the interaction $A_{ij} = \lambda_1 Q_i Q_j^*$, with $i, j < i_c$ corresponds to a potential symmetry energy at saturation density (ρ_0). For the subsystem outside the core, with $i, j > i_c$, the interaction $A_{ij} = \lambda_3 Q_i Q_j^*$ is associated to a density $\rho_e < \rho_0$. For particle–hole pair between the two subsystems the interaction is $A_{ij} = \lambda_2 Q_i Q_j^*$. Of the two states found, n_1 and n_2, the energy of one was pushed up while for

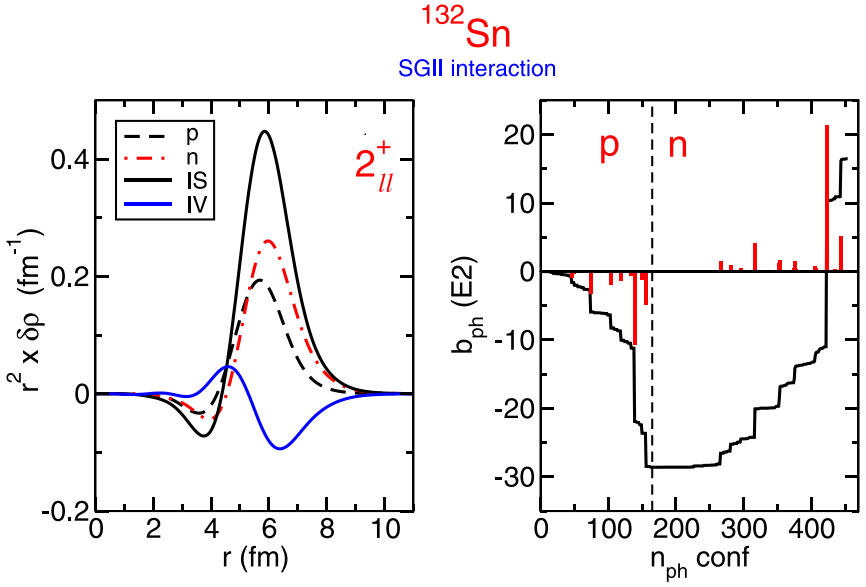

Fig. 44. Panel a: Proton (black dashed line) and neutron (red dashed-dotted line) transition densities for the low-lying quadrupole state of ^{132}Sn at E = 5.03 MeV. The black and blue solid lines are the isoscalar and isovector transition densities, respectively. Panel b: Same as Fig. 43 for the low-lying quadrupole state of ^{132}Sn.

the other the energy was close to the unperturbed value. The energy independent sum rule was distributed only between these two states

$$\sum_i |Q_i|^2 = |\langle n_1|Q|0\rangle|^2 + |\langle n_2|Q|0\rangle|^2 \tag{79}$$

This was taken by the authors as an indication of a collective behaviour of both states. Similar results are obtained for the schematic RPA model. Conclusions based on such schematic models need to be corroborated by more sophisticated investigations.

The problem could be investigated also by means of a correlation analysis based on data analysis methods. By using a self-consistent nuclear density functional theory in the Skyrme-Hartree–Fock plus RPA with recent EDF parameterisations adjusted to a large collection of various nuclear data known as SV-bas [17], an analysis for the collectivity property of the PDR states have been carried out in Ref. [232]. Fig. 46 shows the energy distribution of the transition densities for ^{208}Pb averaged over the energy:

$$\rho^{(T)}(E, r) = 4\pi \sum_\nu \int_0^\infty dq\, q^2\, j_1(qr) F^{(T)}(q)\, G_\Gamma(E - E_\nu) \tag{80}$$

where $F^{(T)}(q)$ is the dipole transition form factor whose Fourier transform gives the transition density. The $G_\Gamma(E - E_\nu)$ is a Gaussian folding function with an energy-dependent width Γ. This width simulates the nuclear damping effects and its value increases with energy. The $T = 1$ transition densities (lower panel of Fig. 46) shows a hump in the energy range of 12–17 MeV which correspond to the IVGDR excitation as indicated in figure. The other collective state can be observed in the upper panel, corresponding to the $T = 0$ cases, where the ellipse indicate the ISGDR in the energy region of 22–27 MeV. Opposite to what found in the two previously considered cases, in the region below 12 MeV (indicate with a dotted red line) the $\rho^{(T)}$ varies rapidly with E, exhibiting a complex multinodal behaviour in both isospin channels. This strong state dependence suggests a weak collectivity.

From the experimental point of view this problem is much more complicate to resolve because there is not an associated measurable quantity to this problem. As discussed in Section 3.3 one possible way is to investigate the spectroscopic factors of single-particle states in the region of interest and compare the results with theoretical calculations and other experimental methods to attempt a rational interpretation. However, these experimental findings, together with the theoretical results described above, strongly suggest that the isovector response of the PDR excitation mode cannot clearly be considered collective. This implies that the traditional picture of the PDR generated by the excess neutrons moving against the rest of the nucleus is far to be real.

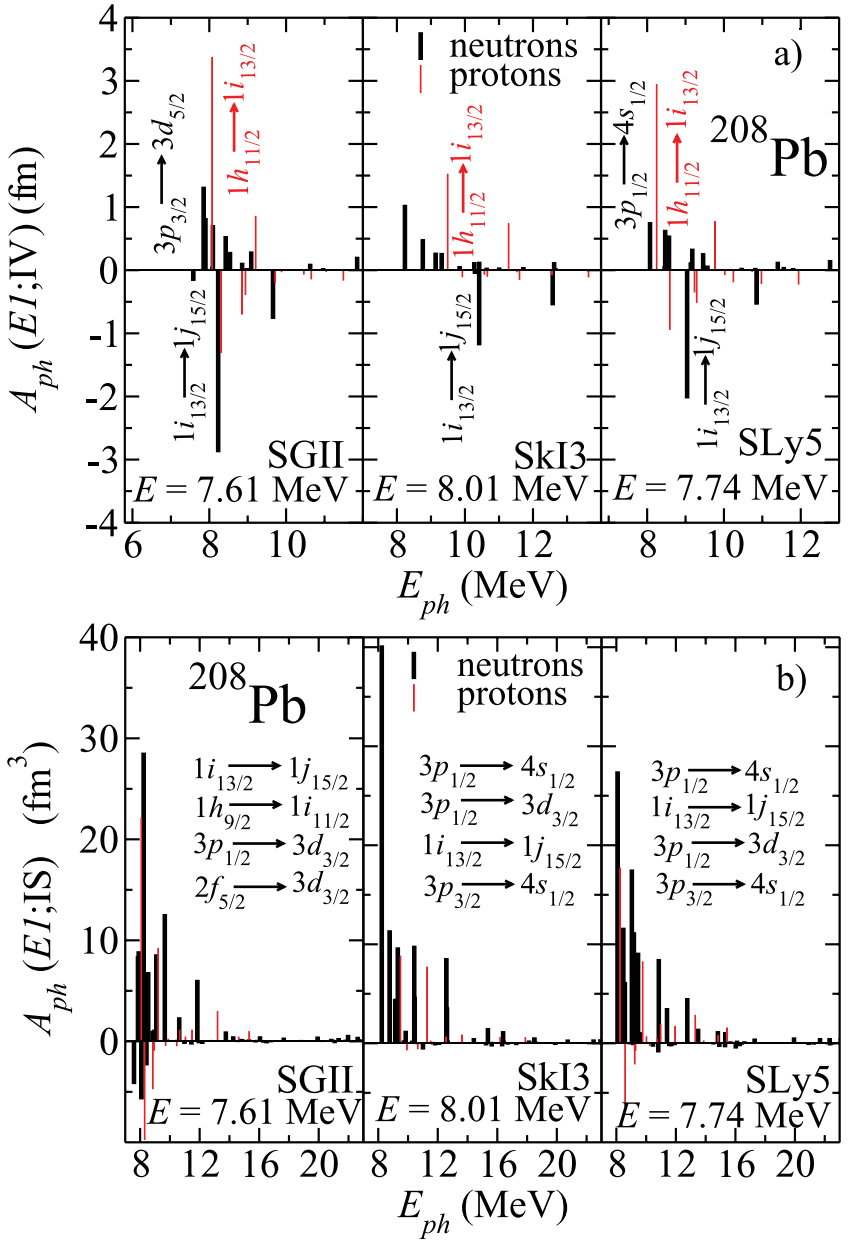

Fig. 45. All p–h contributions to the isovector reduced amplitude corresponding to the ^{208}Pb pygmy state as a function of the p–h excitation energy (a) and for the three Skyrme interactions used in the RPA calculations. Largest neutron p–h contributions are also listed in decreasing order from top to bottom. In the lower panels the same as in panels (a) but for the isoscalar reduced amplitude.
Source: Adapted from Ref. [14].

6.2. Interplay between isoscalar and isovector contribution

We have seen in the previous sections that the transition densities show a strong isospin mixing, especially in the nuclear surface region, which allow to investigate the dipole excitation with isoscalar probes. The use of both isoscalar and isovector probes have revealed a new aspect of this mode usually refer to as PDR (or isospin) splitting (see Section 3). Such phenomenon has been observed experimentally only for dipole states lying in the energy region below the neutron emission threshold until now. A recent measurement showed that dipole states observed below the IVGDR energy but above the neutron emission threshold can be excited by an isoscalar probe indicating therefore an appreciable isospin mixing also for these states. At this point one can summarise the situation in this way: there is a region of the excitation spectrum – the low energy region below the neutron emission threshold – where the low-lying dipole states show

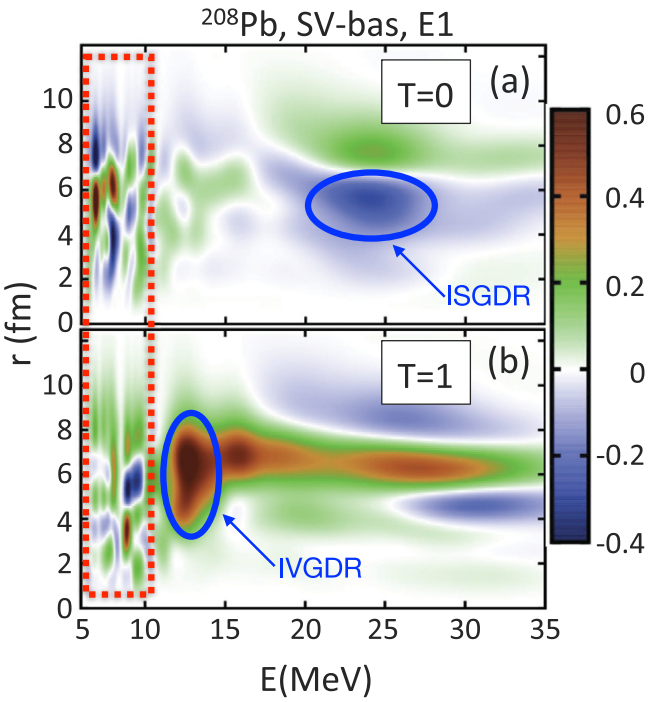

Fig. 46. Energy-averaged E1 transition density in ^{208}Pb calculated within a RPA with a SV-bas interaction as a function of E and r for (a) $T = 0$ and (b) $T = 1$.
Source: Adapted from Ref. [232].

a strong isospin mixing. For these states their excitation can be achieved via electromagnetic and nuclear interaction. Above that region the dipole states found are excited only by an isovector probe. At higher energy, above the neutron emission threshold, it has been found a group of dipole states which can be excited with both probes. From the theoretical point of view this is not surprising since – as discussed in the previous sections – these dipole states with high degree of isospin mixing have been found for stable and unstable nuclei with neutron excess, above and below the neutron emission threshold. From the experimental point of view it will be important to investigate the region above and below the neutron emission threshold for the same nucleus. In fact, there are very few evidence until now, but while waiting for further confirmations it is worthy to ask ourself what is the cause of this sequence of different structural behaviour of the low-lying dipole states with respect to their isospin content. What is clear up to now is that the isospin mixing is a property of the single dipole states. This has been verified from the theoretical and experimental findings. There is a component of the isospin mixing due to the presence of "intruder" states, namely pure isoscalar states in the region of predominantly isovector states, and viceversa, which give rise to a mixing when a folding procedure is applied. This component is not present when, for dipole states below the neutron emission threshold, the γ detection – in the (γ, γ') and (α, α') reactions – allows to clearly separate the states with pure isospin character.

The role of isospin in the excitation of collective states is very important and the maximum response is achieved when an isovector (isoscalar) interaction is exciting an isovector (isoscalar) mode. It is well known that in the case of nuclei with N≠Z the use of one definite isospin interaction can excite mode with both isospin character [234]. For the low-lying dipole states and for nuclei with N>Z, the authors of Ref. [235] have investigated the interplay of the isoscalar and isovector interaction by enabling one at the time in a HF + RPA approach with a SLy4 Skyrme interaction. Using the operators of Eqs. (16) and (17) the isoscalar and isovector strength distributions for the dipole states for ^{22}O and ^{24}O were calculated. Note that there are no RPA solutions below the neutron emission threshold energy. When the isovector interaction is included together with the isoscalar one, the heights of several low-lying isoscalar peaks decrease and their energies shift to slightly higher energies due to the repulsive nature of the isovector interaction. In contrast, many isovector peaks around 16 MeV, obtained by including only the isovector interaction, seem to be grouped in a one broad peak at an energy of 14 MeV when the isoscalar interaction is included.

It is important to understand the isospin content of the PDR region. Several ways can be adopted to investigate this point but as a general guideline one should study the proton $(\delta\rho_p)$ and neutron $(\delta\rho_n)$ transition densities and their relative behaviour. For instance one may scrutinise for each dipole state whether $\delta\rho_p$ and $\delta\rho_n$ are in phase or out of phase over some extended region within the nuclear volume, and estimating the percentage. These calculations have been done with a fully self-consistent RHB + RQRPA for the ^{140}Ce [72]. When the proton and neutron transition densities, for each particular state, are found in phase over more than 70% (80% or 90%) within a given radial interval the state is denoted IS

70% (IS 80% or IS 90%). This analysis was done for two different nuclear radial regions and the results are shown in Fig. 1 and Fig. 2 of Ref. [72] where the isovector dipole strength distribution is plotted for ^{140}Ce. The IS 70%, the IS 80% and the IS 90% are plotted for the radial region between 0 and 8 fm and for the 4.25–8 fm region. From the figures, it is clear that the states belonging to the peak of the PDR – below the neutron emission threshold S_n – consist of between 70%–80% of isoscalar constituent. The results for the surface nuclear region, on the contrary, indicate that the peak has its maximum contribution from the IS 90% states. This is the region which is tested when the isoscalar probes – like α particle, ^{17}O and ^{12}C – are used to investigate the PDR. Another method can be used to establish the amount of isospin mixing present in the PDR peak which relays on the difference between the isoscalar and isovector transition densities. In particular, a state ν is defined to be 70% isoscalar if the relation $|\delta\rho_\nu^{IS}(r)| > |\delta\rho_\nu^{IV}(r)|$ is satisfied by the 70% of the point in the region chosen for this analysis. The fully self-consistent non relativistic mean-field approach based on Skyrme Hartree–Fock plus random phase approximation of Ref. [14] (already quoted in the previous sections) has been used for the nuclei ^{68}Ni, ^{132}Sn, and ^{208}Pb with three different Skyrme interactions. Such analysis has been carried out for three different radial distances and are shown in Fig. 47 for the entire nucleus (from 0 to the nuclear radius R, left frame), the most internal part (from 0 to R/2, middle frame) and the most external region (from R/2 to R, right frame). The dashed lines indicate the partial contribution to the isovector distribution given by the states which are at least 70% isoscalar plotted as solid black line. In the figure, the Skyrme interactions used for the three nuclei for the analysis are indicated. Other used interactions give similar results. For these nuclei the surface regions show again a relevant isoscalar contribution confirming the picture of the PDR states described in the previous sections.

The methodology of using different probes to extract complementary information on the interplay between the isoscalar and isovector components of the low-lying dipole states have been largely employed in the studies of the PDR states. Recently, such experimental method has been used to investigate the isoscalar character of the 1^- states in ^{90,94}Zr [63]. A $(p, p'\gamma)$ at 80 MeV and a $(\alpha, \alpha'\gamma)$ at 130 MeV reactions on the two Zr isotopes have been performed and the results have been compared with (γ, γ') measurement [236,237]. The proton and α scattering can be considered good isoscalar probes in the same way as light heavy-ion projectiles like ^{17}O and ^{12}C (see Section 2.2). Both reactions probe the nuclear surface as it was inferred from calculations performed within the semiclassical model described above. These reactions result to be well described within the DWBA approach. The radial form factors needed for the calculations of the inelastic scattering cross sections were constructed within the double folding approach (see Section 5.1) with the transition densities calculated using the RPA with a SGII interaction. The DWBA calculations performed for one of the dipole state were fitted to the data by varying the E1 ISEWSR strength of the state from the original theoretical value. Under the assumption that the information extracted with the $(\alpha, \alpha'\gamma)$ can be extended to the p reactions, the calculations for the cross section for the $(p, p'\gamma)$ reaction have been done with the values of the ISEWSR obtained from the α reaction. These results are shown in Fig. 48 where the experimental data (orange bars) are plotted together with the prediction obtained using the ISEWSR deduced from the $(\alpha, \alpha'\gamma)$ reaction (blue bars). The general trend has been reproduced except for few states for the ^{90}Zr case. These differences are probably reflecting the stronger mixed character of the $(p, p'\gamma)$ excitation. This coupled analysis shows that the mixing of isoscalar and isovector components is not the same for all the 1^- states below the particle binding energy. It is worthwhile to apply this analysis – improving the modelling – to other nuclei, to try to understand better the intrinsic structure of these low-lying states.

7. Pygmy quadrupole resonance

As we have seen in the previous sections, the properties of the PDR – although some of them are not fully understood – have been extensively studied from both theoretical and experimental point of view. What is clear from these studies is that this excitation mode are due to the neutron excess present in stable and unstable nuclei. Can the presence of neutron or proton skin affect the excitation of states with other multipolarities? Which would be their characteristic properties? If we conform to an indication of their presence as found for the PDR, we should look in neutron-rich nuclei for a bunch of states with same multipolarity (e.g. 2^+) at an excitation energy lower than the corresponding giant resonance (e.g. ISGQR) with a considerable isospin mixing.

Theoretical calculation based on a phenomenological energy-density functional (EDF), use the QRPA prediction based on HFB theory to calculate the excited states within the multiphonon description of the QPM. Such calculations have been performed for studying the low-energy quadrupole excitations in charge asymmetric nuclei like the Sn isotopic chain [238]. Fig. 49 shows as example the QRPA prediction of the B(E2) transition probability calculated for the nucleus ^{124}Sn. The isospin character of the 2^+ excited states was assigned by calculating the multipole transition matrix elements $M_0(\lambda\mu)$ (isoscalar) and $M_1(\lambda\mu)$ (isovector) contributions [65]. A similar figure is shown in Ref. [238] for other Sn isotopes. These results show a sharp separation between the isoscalar and isovector contributions which is in contradiction with early findings [131] where a clear separations of the quadrupole states was observed only for the N = Z nuclei. This net division seems to indicate that these states are mostly of isoscalar nature. Differing from what happens for the summed low-lying B(E1), the summed B(E2) decreases as function of the neutron number until the value of $A = 120$ when it starts to increase (see Fig. 3 of Ref. [238]).

Guided by these theoretical results the experimental work of Pellegri et al. [65] was aimed to measure the low-lying quadrupole states for the ^{124}Sn isotope via a (^{17}O, ^{17}O$'$ γ) reaction at 340 MeV incident energy. Besides the already known 2^+ states, they found new states whose quadrupole nature has been unambiguously established via the angular

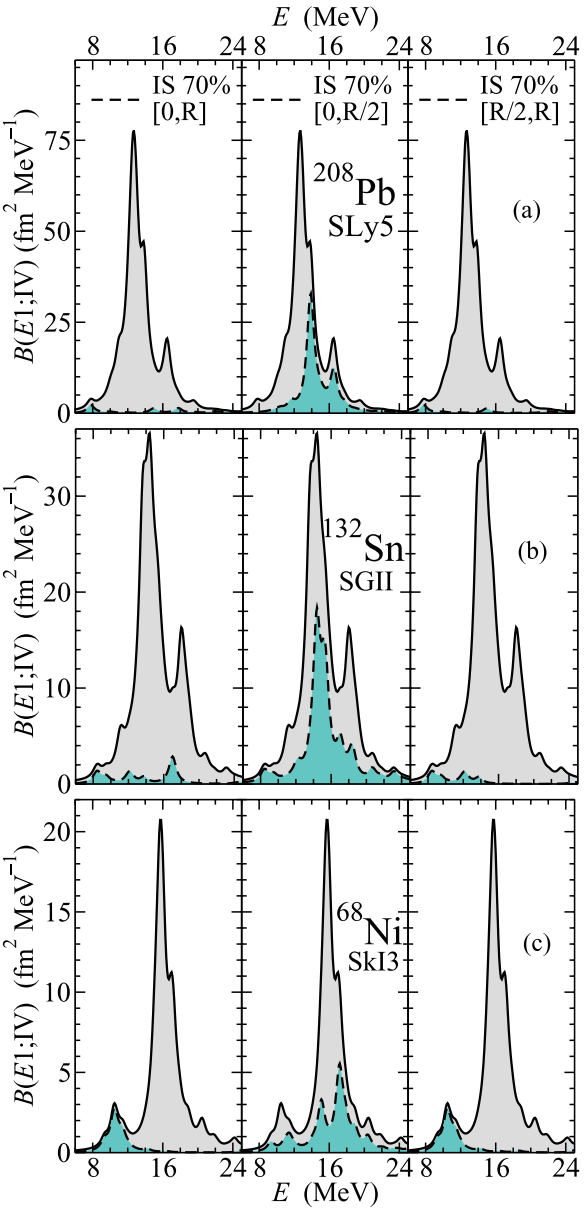

Fig. 47. Isovector dipole strength function of ^{208}Pb (a), ^{132}Sn (b) and ^{68}Ni (c) as a function of the excitation energy (solid lines). The dashed lines indicate the partial contribution due to those states which are at least 70% isoscalar (see text for the definition). The panels for each nucleus are divided in three frames corresponding to three different radial distances: between 0 and R (left frame), between 0 and R/2 (middle frame) and between R/2 and R (right frame). In the figures are indicated also the Skyrme interaction used for each nucleus.
Source: Taken from [14].

distribution of the detected γ rays. The analysis of the cross sections populating these 2^+ states within the DWBA has allowed to infer the values of the E2 transition probability. The calculations assume a pure isoscalar character for these states.

The QPM calculations predicts a large fragmentation of the single particle strength due to the coupling of the pairing vibrational quadrupole QRPA states with two- and three-phonon states. To disentangle the complex structure of the low-energy quadrupole states and separate their one-phonon character, two additional measurements of the gamma emission from the ^{124}Sn isotope excited by the isoscalar $(\alpha, \alpha'\gamma)$ and isovector (γ, γ') reactions were performed [111]. In both experiments, a concentration of 2^+ states in the energy region 2–5 MeV was observed. The results for the reaction $(\alpha, \alpha'\gamma)$ are shown in the upper frame of Fig. 50. These results have been used to deduce the B(E2) values, plotted in frame (b), by performing a coupled channel calculations using a standard collective form factor. They have been compared to the measured B(E2) values from (γ, γ') reaction plotted in frame (c) and other experimental measurements (for details see

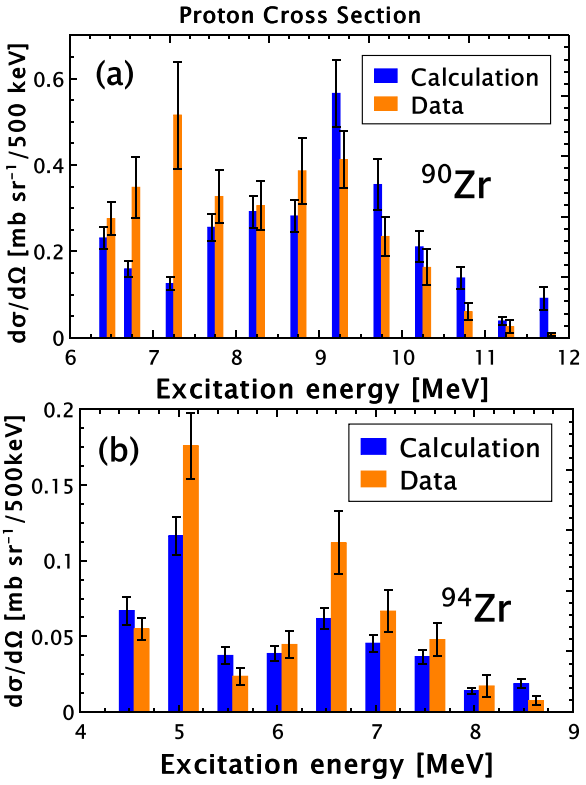

Fig. 48. The cross section measured with proton inelastic scattering at 80 MeV is shown with orange bars and the corresponding prediction is shown with blue bars. The calculation have been done using the strength determined by the $(\alpha, \alpha'\gamma)$ data. Panel (a) is for the ^{90}Zr nucleus and panel (b) for the ^{94}Zr nucleus.
Source: Taken from [63].

Ref. [111]), finding a good correspondence between the two data sets. The low-energy quadrupole states show a complex structure and only few of them present a one-phonon character. The experimental signature to distinguish between one- and multiphonon states was found to be to measure the ground state γ-decay branching ratio $b_0 = \Gamma_0/\Gamma$, with Γ_0 being the ground state width and Γ the total width. The states with a dominant ground-state decay (i.e. $b_0 > 0.5$) correspond to one-phonon type excitations. The measured γ-decay branching ratio $b_0 = \Gamma_0/\Gamma$ are plotted in frame (d) of Fig. 50. The states showed a large b_0 value implying a pure one-phonon quadrupole excitation.

Quasiparticle random-phase approximation and QPM calculations for the $B(E2)$ and b_0 show a good agreement with the experimental data. According to these calculations [111], the low-lying $E2$ strengths from the $E_x = 2$–5 MeV region in Sn isotopes mainly originate from a sequence of QRPA states with almost pure neutron structure related to excitations of weakly bound neutron two-quasiparticle states. It is also claimed that their degree of collectivity increase for states in the higher energy part of the 2–5 MeV region. A more detailed analysis of the composition of these quadrupole states is given in Ref. [113].

The corresponding transition densities can help to address the main character of these states. The analysis of the transition densities for many Sn isotopes have been done in Ref. [238] and the proton and neutron transition densities are separately shown in Fig. 5 of Ref. [238]. Only for the ^{134}Sn isotope and for the transition densities summed over the 0.8–3.7 MeV energy range, a clear contribution from the neutron at the nuclear surface can clearly be distinguished similar to what happens to the low-lying dipole states. The clustering of the quadrupole states at low energies together with the results on the transition densities, make the authors conclude that these low-lying states could belong to a new quadrupole mode related to a neutron surface vibration and they refer to Pygmy Quadrupole Resonance (PQR) in analogy to the dipole case.

It would be interesting to know whether these differences in the transition densities have a consequences on the inelastic cross sections. Two transition densities for the ^{124}Sn, calculated within the QPM framework, corresponding to the very low-lying collective 2^+ state at E = 1.2 MeV (2^+_1) and the ones lying between 2–5 MeV (2^+_2) which were freely extracted from Ref. [111] are shown in Fig. 51. In the top panels the proton (dashed black lines) and the neutron (solid red lines) transition densities are presented. The isoscalar (dashed blue lines) and isovector (solid magenta lines) transition densities are shown in the frames (b) and (d) where the pure isoscalar character of the very low-lying 2^+ state (panel (a)), in which the proton and neutron transition densities are in phase, can be appreciate. The other states do not show

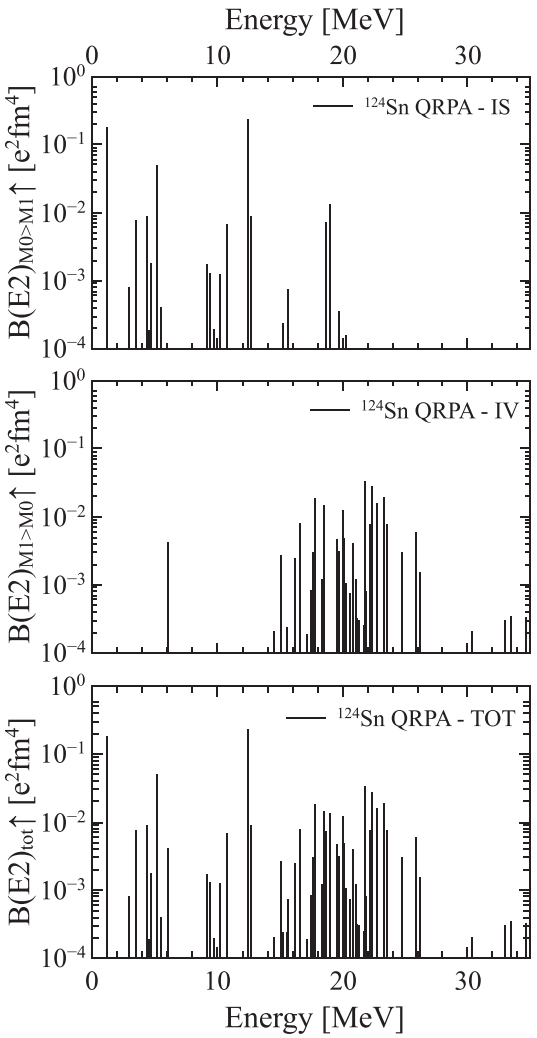

Fig. 49. Isoscalar (upper frame), isovector (middle frame) and total (lower frame) electric quadrupole strength B(E2) calculated within a QRPA based on HFB theory for the ^{124}Sn isotope.
Source: Taken from Ref. [65].

this preponderant isoscalar character because the neutron and proton transition densities are not in phase. However, at the nuclear surface region the isoscalar transition density (panel (d)) is stronger than the isovector one. Since the nuclear surface region is the only one explored in reaction with heavy ions, the two isoscalar transition densities in Fig. 51 should give the same answer when excited by an isoscalar probe like an α particle or a ^{17}O projectile. The only difference may lie in the different B(E2) values giving rise to a different magnitude of the response.

The radial form factors for the system $\alpha + {}^{124}$Sn constructed by a double-folding procedure, as described in Section 5.1, using the microscopic transition densities of the two quadrupole states in Fig. 51 and considering a M3Y nucleon–nucleon interaction are plotted in Fig. 52 [217]. The Coulomb (red dashed-dotted lines) and the nuclear (blue dashed lines) contribution are shown separately and together with the total form factor (black solid lines). They results to have very similar shape and the magnitude discrepancy can be simply ascribed to the different value of the B(E2) which can be deduced also from the value of the form factors at very large distances.

These form factor are employed in the cross section calculations whose results are shown in Fig. 53. The calculations have been performed within the semiclassical coupled channel model described in Section 5. An energy of 4.6 MeV for the 2_2^+ state was chosen. Due to the fact that the form factor for the 2_1^+ state is stronger than the one for the 2_2^+ state, the cross sections (solid red lines) from nuclear interaction is also found to be higher than the one for the 2_2^+ state (dashed blue lines) for all the incident energies considered as one can see in panel (a) of Fig. 53. The Coulomb contribution, see panel (b), is very small because of the isoscalar probe. At very low incident energies the cross section for the 2_1^+ state shows an increase due to the Q-value effect. The Coulomb cross section, although very small, contributes to the total cross section

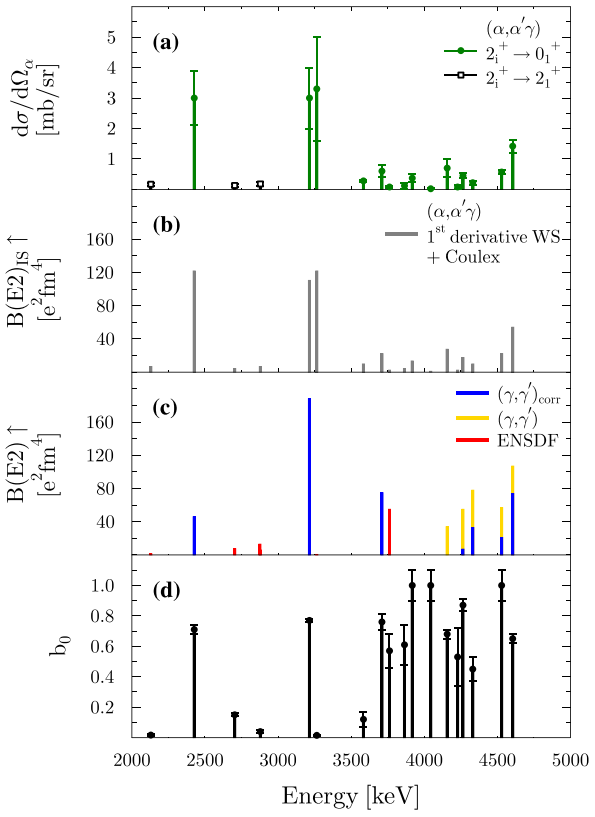

Fig. 50. Experimental result for the low energy quadrupole states for the ^{124}Sn isotope, from Ref. [111]. In frame (a) the cross section for the $(\alpha, \alpha'\gamma)$ reaction. In frame (b) the B(E2) values extracted from the α-scattering cross section. The B(E2) values measured with the (γ, γ') reaction are shown in frame (c) together to the results of other measurements (see Ref. [111]). The ground state γ-decay branching ratio $b_0 = \Gamma_0/\Gamma$ are plotted in frame (d).
Source: Taken from Ref. [111].

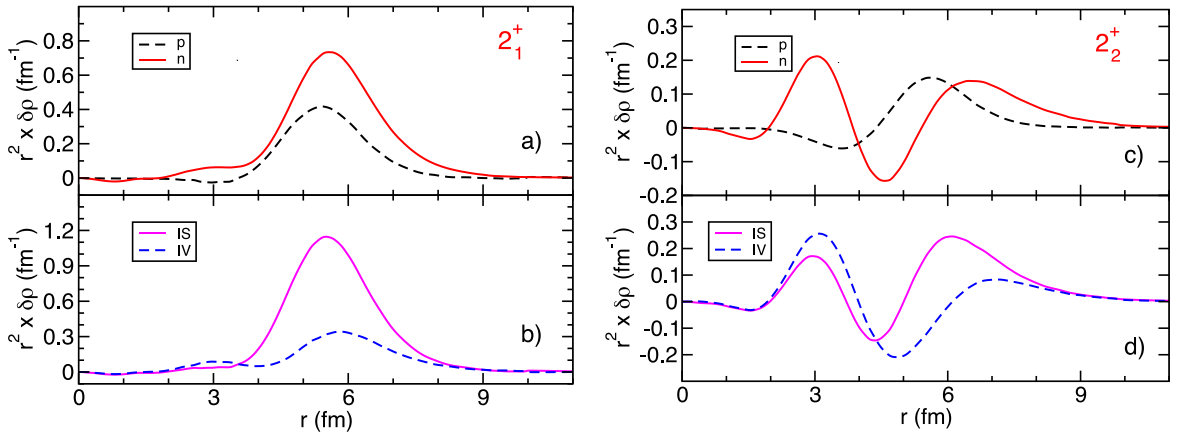

Fig. 51. Transition densities for two low-lying quadrupole states of ^{124}Sn. In the upper part there are plotted the proton (dashed black line) and neutron (solid red line) transition densities while in the lower frames the isovector (solid magenta line) and isoscalar (dashed blue line) ones are shown. The transition densities in frame (a) and (c) have been freely extracted from Ref. [111].
Source: Taken from Ref. [239].

with interference terms. In order to disentangle whether this difference was due to a Q-value effect, another calculation was done with the energy of the 2_1^+ state set to be equal to the higher one, namely 4.6 MeV. The results are shown in Fig. 53 with a black dashed lines and seems in agreement with the red lines which correspond to cross section for

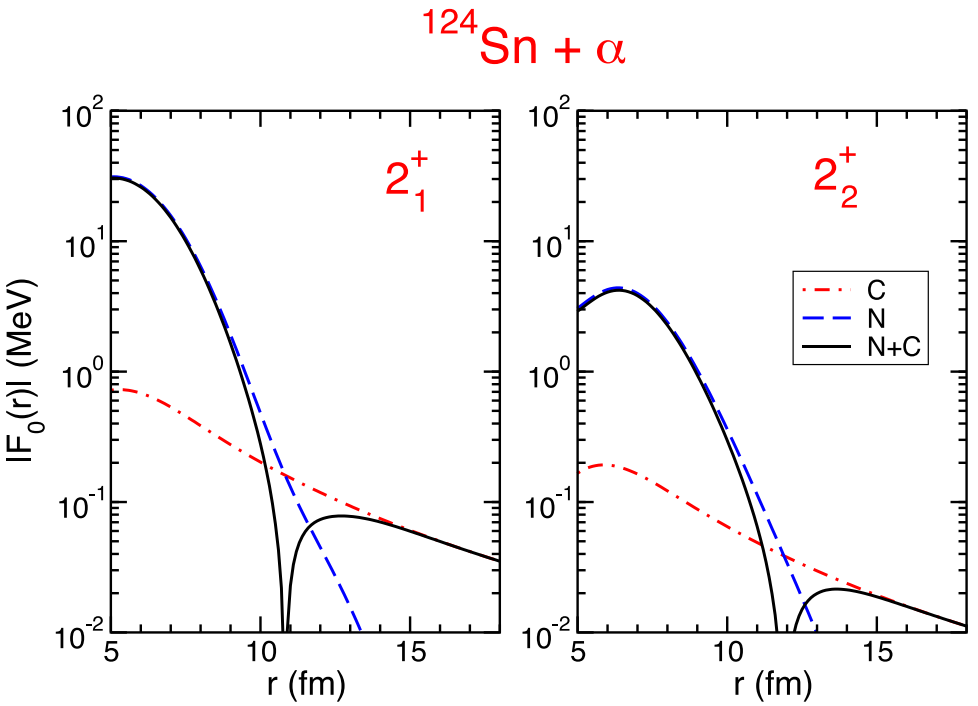

Fig. 52. Radial form factors for the low-lying quadrupole states for the system $\alpha + {}^{124}$Sn. In the left panel, the Coulomb (dot dashed red line), nuclear (dashed blue line) and total (solid black line) form factors are plotted for the very low-lying 2_1^+ state at E = 1.2 MeV. The right panel shows the form factors for the state 2_2^+ belonging to the group in the energy range 2–5 MeV of Ref. [111].
Source: Taken from Ref. [239].

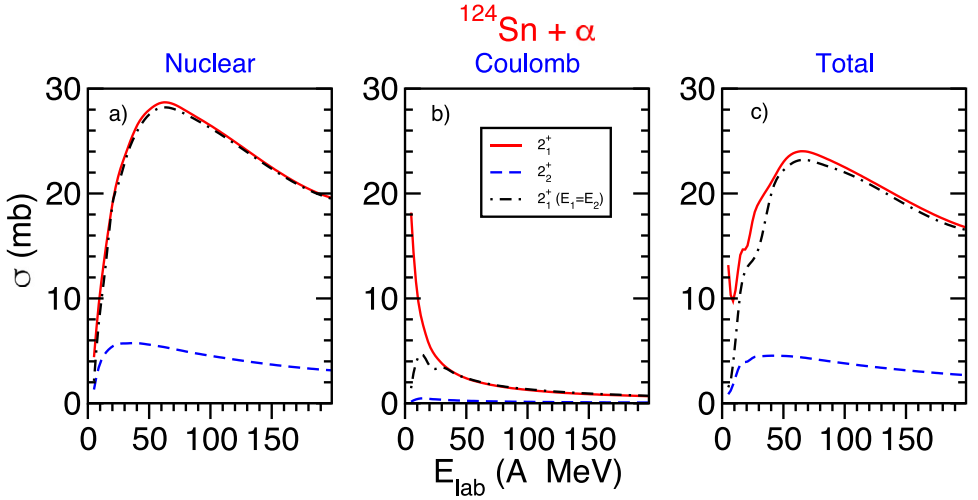

Fig. 53. Inelastic cross section for the two quadrupole states of Fig. 51 as function of the incident energy for the system $\alpha + {}^{124}$Sn. The cross sections obtained when only the nuclear, Coulomb or both interactions are active are shown in the panel (a), (b) and (c), respectively. The solid red line shows the results for the low-lying quadrupole state at 1.2 MeV excitation energy while the dashed blue lines refer to the cross section for the 2^+ state belonging to the group in the 2–5 MeV energy range. The calculation was done choosing an energy of 4.6 MeV for the 2_2^+ state. The dot dashed line corresponds to the results obtain when the energy of the first 2_1^+ state has been placed equal to the one of the state at higher energy 2_2^+, namely at 4.6 MeV.
Source: Taken from Ref. [239].

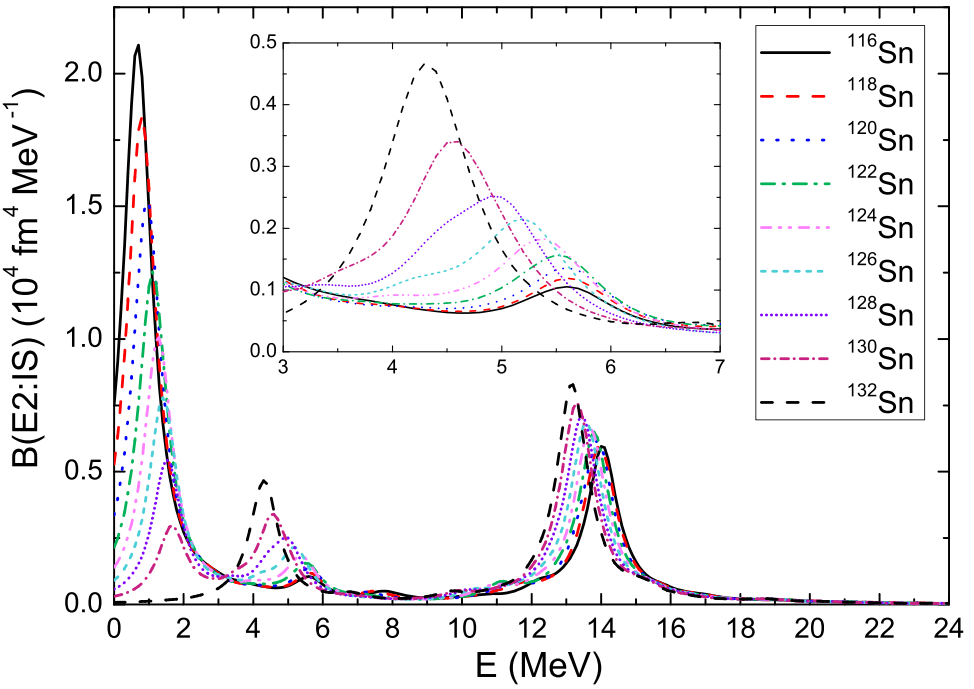

Fig. 54. QRPA isoscalar quadrupole strength for the thin isotope indicate in the legend. In the inset there are shown the low-energy B(E2) distributions. *Source:* Taken from Ref. [240].

the 2_1^+ state with its energy unchanged. This strong agreement implies that the two states have a predominant isoscalar character and only the different values of the B(E2) induce the variation in the cross section.

Different conclusions with respect to the one stated in Ref. [238] have been reached by QRPA calculations performed on top of Hartree–Fock BCS approach [240]. The calculations have been done for the Sn isotopes and with three Skyrme forces and it was found that the summed B(E2) for the low-energy quadrupole states between 3 and 6 MeV display, as function of the increasing neutron number, an opposite behaviour with respect to the one described in Ref. [238].

The results of these calculations for the B(E2) distribution are reported in Fig. 54 for the Sn isotopes shown in the legend. As the neutron number increases, the peak of the lowest isoscalar 2^+ state is depleting in favour of the 2^+ states lying in the 3–7 MeV range. By inspecting the inset of Fig. 54 one can envisage an increasing behaviour of the summed B(E2), over the energy interval between 3–7 MeV, as a function of the increasing neutron number. The analysis of the microscopic structure of these states shows that they are not collective and the effect can be related to the changing in shell structure. The calculations produce transition densities typical of isoscalar states and in particular they do not show strong neutron dominance at the nuclear surface region. Which is, on the contrary, a typical behaviour of the PDR. Furthermore, the transition densities for all the low-lying quadrupole states display a clear isoscalar structure without any sign of isospin mixing (see Fig. 6 of Ref. [240]). According to the authors of Ref. [240] the 2^+ of low-energy region does not present a quadrupole type skin core oscillation in nuclei.

Among the characteristic features that are described in the previous sections, the most qualifying property of the PDR is the mixing of the isoscalar and isovector character shown by these states both for theories and experiments. In fact, the isoscalar and isovector transition densities for these states exhibit at the nuclear surface the same shape and magnitude allowing both excitations. Theoretical and experimental findings suggest that the mixing properties can be the characterising feature of these low-lying dipole states which correspond to a new excitation mode.

On the other hand, for the low-lying quadrupole states the situation is not so clear and there are no strong evidence that these states are the manifestation of a different excitation mode. The two different theoretical approaches quoted above do not help to clarify the nature of these quadrupole states although both of them attribute the presence of the low-lying 2^+ states to neutrons of the outmost shells. The experimental data are also inconclusive to address the problem. However, since the studies of nuclei with neutron excess is an important source of information for nuclear structure and nuclear astrophysics, the investigation of the effect of the neutron excess on other multipole states should pursued further.

8. Summary and perspective

In this review we have discussed different aspects associated with the low-lying energy region of the dipole response, with particular focus on the theoretical studies. This dipole strength, found to be strongly correlated with the neutron

excess in both stable and unstable nuclei, is traditionally described in terms of a "new mode", named Pygmy Dipole Resonance (PDR). The existing research on the subject is extensive and a number of review papers have been published over the past years [6–10]. The majority of these works, however, focused their attention on the experimental results leaving the theoretical interpretation of this excitation mode less discussed. The scope of this work is to complement the previous reviews by giving a comprehensive overview and analysis on the theoretical models used to describe the PDR. At the same time, we found important to give a brief description of the experimental methods and new experimental findings to contextualise and guide the reader to interpret the theoretical results discussed. Therefore, this review starts with a brief overview of the different experimental techniques specifically used for the study of this mode (Section 2). The most relevant and recent experimental results have been divided in two groups (Section 3), above and below the neutron emission threshold. Recent results on some open problems are described in the following subsections. The attempt to find an effect of the neutron excess on other multipole states, other than the dipole ones, is also presented. Recent works on the presence of single particle states embedded in the PDR region, and the search of low-lying dipole states in deformed nuclei are reviewed since they present a challenge for both theoretical and experimental future investigations.

The different theoretical models developed for the PDR are illustrated in Section 4. The macroscopic models, in accordance with the ones used for the Giant Resonances, assume that the nucleus can be described as a liquid drop composed by neutrons' and protons' fluids. In the case of the PDR, the nucleus is conceived as a three fluids system, with the neutron excess considered as the third independent fluid. In this approximation the fluids are assumed to be incompressible and the modified version of the Steiwedel–Jensen model is applied. The picture of the PDR generated by the oscillation of an inert core against a neutron skin is the most common one. In this case, the excitation mode has to be treated within the Goldhaber–Teller model. The macroscopic features of the PDR can be deduced by both these approaches (Section 4.1).

A more details and satisfactory description of the PDR can be obtained by the microscopic self-consistent mean field models based on effective interactions. Most of them are reviewed in Section 4.2. The main characteristics of the low-lying dipole states – like isospin mixing, shown in the transition densities, or their non-collective feature – can be describe within the most basic microscopic approach, as can be considered the HF + RPA model. Selected examples have been chosen to illustrate these specific features and a detailed analysis of the transition densities was presented comparing the new PDR mode with the isoscalar and isovector Giant Dipole Resonances. The studies of open-shell nuclei is performed by using the Quasiparticle RPA (QRPA) where the pairing correlation is explicitly taken into account. Using this approach the investigation of the PDR could be extended to a huge number of nuclei, allowing studies of isotopic chains and comparison with the available experimental data. The examples selected to present this approach support the capability of the method to reproduce the evolution of the energy centroid with increasing neutron numbers, among others.

The Relativistic RPA (RRPA) is the small amplitude limit of the relativistic mean-field theory, where the interaction is due to the exchange of mesons and photons. The pairing correlation is included in the RQRPA, allowing the application of these methods to open-shell nuclei, obtaining a very good description of several nuclear structure phenomena. These two methods have been applied to the PDR studies with very similar results to the non-relativistic theories. It is interesting to note that also for this new excitation mode the relativistic approaches are able to describe the experimental data. However, the excellent description of the GR's and of the low energy excitations, given by both relativistic and non-relativistic theories, fails to reproduce the widths of their strength distributions. In fact, the main features – like centroid energies, EWSR and strengths – are generated by the superposition of 1p–1h configurations, while the width (the spreading width) raises from the coupling between the 1p–1h configurations with more complex ones, like 2p–2h, 3p–3h and more. This coupling is driven by the residual interaction. In the second RPA (SRPA) the coupling with 2p–2h configurations are explicitly introduced and the application of the model to the PDR gives a better description of the experimental data but with the unsatisfactory shift, by several MeV, of the GR energy centroids. This effect has been ascribed to the double counting of the correlation contained in the ground state. In fact, the inclusion of 2p–2h configuration generate correlations in the ground state which are already implicitly included by the use of the EDF to generate the effective interactions. The procedure of the so-called Subtraction SRPA (SSRPA) avoids this double counting and allows to have the right position of the GR energy centroids, maintaining at the same time the spreading of the PDR in many dipole states – below the neutron emission threshold – as observed in the experimental measurements. In Section 4.2.4, recent results are quoted to show how these methods are able to give some predictions on the low-lying dipole states also for nuclei far from the stability valley.

Increasing quality of the description of the PDR is obtained when higher order configurations – like two- and three-phonon states – are explicitly taken into account. In Section 4.2.5, the approach is illustrated by using the boson expansion of the fermion particle–hole operators whose lowest order is the RPA. The described way to introduce this coupling – due to the residual interaction – can be considered quite intuitive because one can identify the terms of the Hamiltonian that are taking part to the coupling process. This is not the only method to introduce the coupling to the multiphonon states and two additional methods are presented in Sections 4.2.6 and 4.2.7. Within these methods it is possible to estimate the contribution of other multipole states to the energy region of the PDR, whenever the experimental results do not allow to assign the multipolarity of the measured states. This was the case of the relativistic Coulomb excitation for few Sn isotopes measured at GSI. Calculations, done within the boson expansion approach, estimated the contribution of these multiphonon states up to about 20%, depending on the isotope and the effective Skyrme interaction used.

In the Quasiparticle Phonon Model (QPM), the starting blocks for the construction of the two- and three-phonon states are the solution of the QRPA approach. The Hamiltonian – containing the single particle contribution, the residual

interaction for pairing and for the coupling to more complex configurations – is diagonalised in this enlarged space. The main difference with the previous approach is the use of phenomenological Woods–Saxon potential instead of the Skyrme interaction. A good description of the experimental data is obtained notwithstanding the loss of full microscopic picture and self consistency. These two important properties are recovered in the Relativistic Quasiparticle Time Blocking Approximation (RQTBA). The self-consistent RQRPA is modified to include the coupling to two- and three-phonon states. Similar to the SRPA, the inclusion of more complex configurations implies that some correlations are double counted and the subtraction procedure has to be applied also to this approach. Despite of the differences, both approaches are able to accurately describe the experimental data of the PDR below the neutron emission threshold. From the selected examples, the effects of the coupling to configurations of increasing complexity clearly modifies the theoretical dipole strength distribution producing a fragmentation of the strength comparable to the one observed in the experimental data. The calculations of isoscalar and isovector reduced electric transition probability reproduce, even though not in a very detailed way, the so-called isospin splitting of the PDR.

Other models – discussed in Section 4.4 – have been proposed to study the low-lying dipole states. The Toroidal Dipole Resonance (TDR) (Section 4.4.1) was predicted by a nuclear fluid-dynamical model and it is generated by a transverse oscillation of the nucleons. Several stable and exotic nuclei have been studied within this approach where the evidence of this mode is present independently from the neutrons to protons ratio. Since the concentration of its strength lies in the same energy region of the PDR, it is suggested that the PDR could be a manifestation of the TDR, even though the pygmy states are specifically found in nuclei with neutron excess. The possible contribution of the TDR to the PDR has still to be clarified both in theoretical and experimental terms.

The extension of the Interacting Boson Model (IBM) to study the negative-parity states – achieved with the inclusion of p and f bosons (IBM-sdpf) – has allowed to investigate the energy region of the PDR (Section 4.4.2). A systematic study was performed for the $N = 82$ isotones and the results were compared with the available experimental data. The model is able to reproduce the shape of the B(E1) distributions as well as the slight shift of the energy centroids with isotope masses.

One of the most successful semiclassical approximation to the microscopic theories is the Vlasov equation. This equation can be considered as the semiclassical limit of the Time Dependent Hartree Fock (TDHF) theory. A collective motion is obtained by perturbing at the initial time the ground-state density and following the time evolution of the nuclear oscillation by the Vlasov equation. A satisfactory description of many collective excitations has been obtained within this approach. The electric dipole operator can be constructed as a function of time and the Fourier transform of its expectation value gives the strength function. By applying this method to a systematic study of the Sn isotopes (Section 4.4.3), an excess of strength appears at low energy for isotopes with N>Z. Although the corresponding transition densities can be extracted with further approximations, their shapes are similar to the ones derived with the methods listed above.

A section has been dedicated to the study of the PDR in deformed nuclei (Section 4.3). Microscopic theories give contradictory answers regarding the presence and characteristics of the PDR with respect to the spherical nuclei. Furthermore, there is the question of the possible splitting – due to the deformation – of the PDR peak with a mechanism similar to what observed in the case of the IVGDR. Until now, neither the theoretical studies nor the experimental measurements have been able to solve these problems. Further studies dedicated to enlighten these aspects should be pursued in the near future.

All models seem to reproduce the qualitative features of the energy distribution, as well as the mixed nature (isoscalar/isovector) of the mode. Indeed, all of them produce proton and neutron transition densities which are in phase inside the nuclear region while at the surface only the neutron contribution is surviving. As a consequence, at the nuclear surface a strong isospin mixing is present. This property might been taken as a theoretical definition of the PDR. However, in addition to the need of a more detailed quantitative description of the data, discrepancies on the models' results was found on certain aspects of this strength such as the energy splitting of the isoscalar and isovector components of low-lying dipole states or the collectivity (or not) of the mode.

The mixed nature of the mode is a common and well-established feature for all approaches described in Section 4. This opens the possibility, and the consequent need, to study the population of this state with different probes, both hadron (light or heavy, isoscalar or isovector) and electromagnetic. The study of the PDR with isoscalar probes – like in the $(\alpha, \alpha'\gamma)$, $(^{17}O, ^{17}O'\gamma)$ reactions – is done at incident energies and detection angles typical of peripheral direct reactions. The fundamental measured quantity is then the inelastic cross section which is compared to the other measured quantities obtained with different probes. Therefore, it is important to clarify different aspects of the reaction mechanisms to extract reliable structure informations and have a realistic comparison with experimental data. To this end in Section 5 it is recalled the basics of the coupled-channel formalism, the procedure to construct potentials and radial form factors from densities and transition densities, to investigate the interplay of nuclear and Coulomb contributions and its dependence on projectile's mass and charge, bombarding energy and impact parameter. The most precise way to calculate the inelastic cross section is via the Coupled Channel (CC) equations where the contribution of the included channels is taken to all orders. In some cases it is more appropriate and more practical to use the so-called Distorted Wave Born Approximation (DWBA) which is the first order approximation of the CC equations. A useful and convenient alternative way is the use of the semiclassical approximation of the CC equations which are applicable for the energies and masses involved in the cases treated here. The latter method has the advantage – when appropriately used – that the most important ingredient

of the scattering process can be identified and at the same time it allows to include much more channels in the numerical calculations. The semiclassical CC equations are described in Section 5.

Whatever is the method chosen to estimate the inelastic cross section, the basic and fundamental quantities for the description of the excitation process are the radial form factors. These quantities depend very much on the structure model chosen to describe the excited state. They can be derived within the macroscopic model or with a double-folding procedure using microscopic transition densities. Some of them are illustrated in Section 5.1 where a detailed and critical comparison is done on the form factors calculated with different approaches. From the comparison it is evident that the microscopic form factors, that include the essential feature of the PDR mode, the isospin mixing, are the most appropriate to describe the experimental data. They are derived with the double-folding procedure adopting the transition densities calculated with the microscopic mean-field models.

While dealing with heavy ion reactions, it is of paramount importance to be aware of the interplay between the nuclear and Coulomb excitations. This knowledge allows tuning the projectile mass, charge, bombarding energy and scattering angle, to optimise the conditions for the experimental measurements. Calculations performed within the semiclassical model, for several systems, and considering also others multipole states besides the dipole one, have been discussed at length in Section 5.2. An important results was obtained for the isospin splitting of the PDR, where cross section calculations confirmed the trend of the reduced electric probability when compared with the measured cross section. In addition, the theoretical results suggest that the investigation of the PDR with isoscalar probes can be better achieved at incident energy below or around 50 MeV/nucleon.

From our excursus we can conclude that a full understanding on the nature and properties of the PDR can only come from a combined and critical use of the information extracted with a variety of probes.

At the moment only the main characteristics and features of the mode are strongly supported by experiments and theoretical calculations while there are still few aspects, important and challenging, to be clarified. Some of them are reported in Section 6. This include the collectivity of the mode, the energy isospin splitting, and the role of deformation. The collectivity of the PDR (Section 6.1) is implicitly assumed when the macroscopic models are employed. For the microscopic models there are several ways to investigate that, however most of them reach the conclusion that the isovector response is not collective while the isoscalar one it is. As a consequence, the typical picture of the neutron skin oscillating out of phase against the inert core – even though very effective when used to explain this mode to neophytes – it does not adhere to reality. Recent experiments, using stripping or pick-up reactions, try to measure the extent of single particle nature present in the low energy region. On the other hand, the degree of isospin mixing is investigated within some microscopic theories (in Section 6.2). Assuming that the information on the isospin content obtained with an α reaction can be extended to the measurements done using protons, a general trend of the experimental results can be obtained. This kind of analysis may be improved to extract better informations on the isospin mixing of the PDR. To find the solution to these open problems are a challenge for future theoretical and experimental investigations.

The possible occurrence of "pygmy" modes with similar features in other multipolarities was also presented for the case of low-lying quadrupole states. Unfortunately, in this case there is no distinctive identifying characteristic – like the isospin mixing for the dipole case – that would allow a clear identification of the presence of a different mode of excitation in the quadrupole channel. However, studies of multipole excitations in nuclei with neutron excess should continue because of the important information on nuclear structure, around the neutron emission threshold, that can be extracted from these investigations.

For all the reasons presented and discussed in this review we consider that the field of the PDR is still one of the more active and promising line of research for the understanding of nuclear correlations and the occurrence of collective modes in the many-body nuclear environment.

Declaration of competing interest

The authors declare that they have no known competing financial interests or personal relationships that could have appeared to influence the work reported in this paper.

Acknowledgements

This work is part of the I + D + i projects with Ref. PID2020-114687GB-I00, funded by MCIN/AEI/ 10.13039 /501100011033. This work is also part of the grant Group FQM-160 and the project PAIDI 2020 with Ref. P20_01247, funded by the Consejería de Economía, Conocimiento, Empresas *y* Universidad, Junta de Andalucía (Spain). LP acknowledges support from the National Research Foundation of South Africa.

References

[1] N. Starfelt, Nuclear Phys. 53 (1964) 397.
[2] J. Brzosko, E. Gierlik, A. Soltan, Z. Wilhelmi, Can. J. Phys. 47 (1969) 2849.
[3] A.M. Lane, Ann. Physics 63 (1971) 171.
[4] A. Goswami, A. Khan, Nuclear Phys. 35 (1962) 544.
[5] M. Harvey, F.C. Khanna, Nuclear Phys. A 221 (1974) 77.

[6] N. Paar, D. Vretenar, E. Khan, G. Colò, Rep. Progr. Phys. 70 (2007) 691–793, http://dx.doi.org/10.1088/0034-4885/70/5/r02.
[7] D. Savran, T. Aumann, A. Zilges, Prog. Part. Nucl. Phys. 70 (2013) 210.
[8] A. Bracco, F. Crespi, E. Lanza, Eur Phys. J. A 51 (2015) 99.
[9] T. Aumann, Eur. Phys. J. A 55 (2019) 234, http://dx.doi.org/10.1140/epja/i2019-12862-7.
[10] A. Bracco, E.G. Lanza, A. Tamii, Prog. Part. Nucl. Phys. 106 (2019) 360.
[11] J. Piekarewicz, Phys. Rev. C 73 (2006) 044325, http://dx.doi.org/10.1103/PhysRevC.73.044325.
[12] A. Klimkiewicz, N. Paar, P. Adrich, M. Fallot, K. Boretzky, T. Aumann, D. Cortina-Gil, U.D. Pramanik, T.W. Elze, H. Emling, H. Geissel, M. Hellström, K.L. Jones, J.V. Kratz, R. Kulessa, C. Nociforo, R. Palit, H. Simon, G. Surówka, K. Sümmerer, D. Vretenar, W. Waluś, Phys. Rev. C 76 (2007) 051603, http://dx.doi.org/10.1103/PhysRevC.76.051603.
[13] A. Carbone, G. Colò, A. Bracco, L.-G. Cao, P.F. Bortignon, F. Camera, O. Wieland, Phys. Rev. C 81 (2010) 041301, http://dx.doi.org/10.1103/PhysRevC.81.041301.
[14] X. Roca-Maza, G. Pozzi, M. Brenna, K. Mizuyama, G. Coló, Phys. Rev. C 85 (2012) 024601.
[15] P. Papakonstantinou, H. Hergert, R. Roth, Phys. Rev. C 92 (2015) 034311.
[16] P.-G. Reinhard, W. Nazarewicz, Phys. Rev. C 81 (2010) 051303, http://dx.doi.org/10.1103/PhysRevC.81.051303.
[17] P. Klüpfel, P.-G. Reinhard, T.J. Bürvenich, J.A. Maruhn, Phys. Rev. C 79 (2009) 034310, http://dx.doi.org/10.1103/PhysRevC.79.034310.
[18] X. Roca-Maza, M. Brenna, B.K. Agrawal, P.F. Bortignon, G. Colò, L.-G. Cao, N. Paar, D. Vretenar, Phys. Rev. C 87 (2013) 034301, http://dx.doi.org/10.1103/PhysRevC.87.034301.
[19] W. Hauser, H. Feshbach, Phys. Rev. 87 (1952) 366–373, http://dx.doi.org/10.1103/PhysRev.87.366.
[20] S. Goriely, Phys. Lett. B 436 (1998) 10–18, http://dx.doi.org/10.1016/S0370-2693(98)00907-1.
[21] S. Goriely, E. Khan, Nuclear Phys. A 706 (2002) 217–232, http://dx.doi.org/10.1016/S0375-9474(02)00860-6.
[22] S. Goriely, E. Khan, M. Samyn, Nuclear Phys. A 739 (2004) 331–352, http://dx.doi.org/10.1016/j.nuclphysa.2004.04.105.
[23] E. Litvinova, H. Loens, K. Langanke, G. Martínez-Pinedo, T. Rauscher, P. Ring, F.-K. Thielemann, V. Tselyaev, Nuclear Phys. A 823 (2009) 26–37, http://dx.doi.org/10.1016/j.nuclphysa.2009.03.009.
[24] I. Daoutidis, S. Goriely, Phys. Rev. C 86 (2012) 034328, http://dx.doi.org/10.1103/PhysRevC.86.034328.
[25] N. Tsoneva, S. Goriely, H. Lenske, R. Schwengner, Phys. Rev. C 91 (2015) 044318, http://dx.doi.org/10.1103/PhysRevC.91.044318.
[26] A. Tonchev, N. Tsoneva, C. Bhatia, C. Arnold, S. Goriely, S. Hammond, J. Kelley, E. Kwan, H. Lenske, J. Piekarewicz, R. Raut, G. Rusev, T. Shizuma, W. Tornow, Phys. Lett. B 773 (2017) 20–25, http://dx.doi.org/10.1016/j.physletb.2017.07.062.
[27] A. Zilges, D. Balabanski, J. Isaak, N. Pietralla, Prog. Part. Nucl. Phys. (2021) 103903, http://dx.doi.org/10.1016/j.ppnp.2021.103903.
[28] N. Pietralla, J. Isaak, V. Werner, Eur. Phys. J. A 55 (2019) 237.
[29] R. Schwengner, et al., Phys. Rev. C 76 (2007) 034321.
[30] R. Schwengner, et al., Nucl. Instrum. Methods Phys. Res. A 555 (2005) 211.
[31] K. Sonnabend, et al., Nucl. Instrum. Methods Phys. Res. A 640 (2011) 6.
[32] H.R. Weller, et al., Prog. Part. Nucl. Phys. 62 (2009) 257.
[33] H.R. Weller, et al., Nucl. Phys. News 25 (2015) 19.
[34] B. Löher, et al., Nucl. Instrum. Methods Phys. Res. A 723 (2013) 136.
[35] M. Scheck, et al., Phys. Rev. C 87 (2013) 051304(R).
[36] J. Isaak, et al., Phys. Rev. C 103 (2021) 044317.
[37] O. Papst, et al., Phys. Rev. C 102 (2020) 034323.
[38] N. Zamfir, et al., Nucl. Phys. News 25 (2015) 34.
[39] F. Camera, et al., Rom. Rep. Phys. 68 (2016) S539.
[40] M. Krzysiek, et al., Nucl. Instrum. Methods Phys. Res. A 916 (2019) 257.
[41] P.-A. Söderström, et al., Rom. Rep. Phys. 71 (2019) 206.
[42] P.v. Neumann-Cosel, A. Tamii, Eur. Phys. J. A 55 (2019) 110.
[43] A. Tamii, et al., Phys. Rev. Lett. 107 (2011) 062502.
[44] A. Tamii, et al., Nucl. Instrum. Methods Phys. Res. A 605 (2009) 326.
[45] R. Neveling, et al., Nucl. Instrum. Methods Phys. Res. A 654 (2011) 29.
[46] C.A. Bertulani, G. Baur, Phys. Rep. 163 (1988) 299.
[47] D. Vretenar, N. Paar, P. Ring, G. Lalazissis, Nuclear Phys. A 692 (2001) 496–517, http://dx.doi.org/10.1016/S0375-9474(01)00653-4.
[48] E. Litvinova, P. Ring, V. Tselyaev, K. Langanke, Phys. Rev. C 79 (2009) 054312, http://dx.doi.org/10.1103/PhysRevC.79.054312.
[49] E.G. Lanza, F. Catara, D. Gambacurta, M.V. Andrés, P. Chomaz, Phys. Rev. C 79 (2009) 054615.
[50] D. Vretenar, Y.F. Niu, N. Paar, J. Meng, Phys. Rev. C 85 (2012) 044317, http://dx.doi.org/10.1103/PhysRevC.85.044317.
[51] D. Bianco, F. Knapp, N. Lo Iudice, F. Andreozzi, A. Porrino, P. Vesely, Phys. Rev. C 86 (2012) 044327.
[52] V. Baran, D.I. Palade, M. Colonna, M. Di Toro, A. Croitoru, A.I. Nicolin, Phys. Rev. C 91 (2015) 054303.
[53] N. Ryezayeva, et al., Phys. Rev. Lett. 89 (2002) 272502.
[54] P.C. Ries, et al., Phys. Rev. C 100 (2019) 021301.
[55] M. Spieker, et al., Phys. Rev. Lett. 125 (2020) 102503.
[56] E.G. Lanza, A. Vitturi, M.V. Andrés, F. Catara, D. Gambacurta, Phys. Rev. C 84 (2011) 064602.
[57] V. Derya, et al., Nuclear Phys. A 906 (2013) 94.
[58] J. Endres, et al., Phys. Rev. C 80 (2009) 034302.
[59] J. Endres, et al., Phys. Rev. C 85 (2012) 064331.
[60] H. Wörtche, et al., Nuclear Phys. A 788 (2007) 27.
[61] H. Wörtche, et al., Nuclear Phys. A 788 (2007) 165.
[62] D. Savran, V. Derya, S. Bagchi, J. Endres, M. Harakeh, J. Isaak, N. Kalantar-Nayestanaki, E. Lanza, B. Löher, A. Najafi, S. Pascu, S. Pickstone, N. Pietralla, V. Ponomarev, C. Rigollet, C. Romig, M. Spieker, A. Vitturi, A. Zilges, Phys. Lett. B 786 (2018) 16–20, http://dx.doi.org/10.1016/j.physletb.2018.09.025.
[63] F. Crespi, A. Bracco, E. Lanza, A. Tamii, N. Blasi, F. Camera, O. Wieland, et al., Phys. Lett. B 816 (2021) 136210, http://dx.doi.org/10.1016/j.physletb.2021.136210.
[64] L. Pellegri, et al., Phys. Lett. B 738 (2014) 519.
[65] L. Pellegri, et al., Phys. Rev. C 92 (2015) 014330.
[66] F.C.L. Crespi, et al., Phys. Rev. Lett. 113 (2014) 012501.
[67] F.C.L. Crespi, et al., Phys. Rev. C 91 (2015) 024323.
[68] M. Krzysiek, et al., Phys. Rev. C 93 (2016) 044330.
[69] S. Akkoyun, et al., Nucl. Instrum. Methods Phys. Res. A 688 (2012) 26.
[70] A. Gadea, et al., Nucl. Instrum. Methods Phys. Res. A 654 (2011) 88.
[71] E. Litvinova, P. Ring, V. Tselyaev, Phys. Rev. C 78 (2008) 014312, http://dx.doi.org/10.1103/PhysRevC.78.014312.

[72] N. Paar, Y.F. Niu, D. Vretenar, J. Meng, Phys. Rev. Lett. 103 (2009) 032502.
[73] S. Pickstone, et al., Nucl. Instrum. Methods Phys. Res. A 875 (2018) 104.
[74] M. Färber, et al., Eur. Phys. J. A 57 (2021) 191.
[75] M. Guttormsen, A. Bürger, T. Hansen, N. Lietaer, Nucl. Instrum. Methods Phys. Res. A 648 (2011) 168–173, http://dx.doi.org/10.1016/j.nima.2011.05.055.
[76] J. Rekstad, et al., Phys. Scr. T 5 (1983) 45.
[77] M. Guttormsen, et al., Nucl. Instrum. Methods Phys. Res. A 255 (1987) 518.
[78] M. Guttormsen, et al., Nucl. Instrum. Methods Phys. Res. A 374 (1996) 371.
[79] A. Schiller, et al., Nucl. Instrum. Methods Phys. Res. A 447 (2000) 498.
[80] M. Scheck, et al., Phys. Rev. Lett. 116 (2016) 132501.
[81] N. Nakatsuka, et al., Phys. Lett. B 768 (2017) 387.
[82] O. Wieland, et al., Phys. Rev. Lett. 102 (2009) 092502.
[83] O. Wieland, et al., Phys. Rev. C 98 (2018) 064313.
[84] E. Tryggestad, et al., Phys. Lett. B 541 (2002) 52.
[85] A. Leistenschneider, et al., Phys. Rev. Lett. 86 (2001) 5442.
[86] D. Rossi, et al., Phys. Rev. Lett. 111 (2013) 242503.
[87] J. Gibelin, et al., Phys. Rev. Lett. 101 (2008) 212503.
[88] P. Adrich, et al., Phys. Rev. Lett. 95 (2005) 132501.
[89] N. Martorana, et al., Phys. Lett. B 782 (2018) 112.
[90] Y. Togano, et al., Nucl. Instrum. Methods Phys. Res. B 463 (2020) 195.
[91] A. Bracco, et al., Eur. Phys. J. A 55 (2019) 233.
[92] S. Bassauer, et al., Phys. Rev. C 102 (2020) 034327.
[93] A. Krumbholz, et al., Phys. Lett. B 744 (2015) 7.
[94] D. Savran, M. Elvers, J. Endres, M. Fritzsche, B. Löher, N. Pietralla, V.Y. Ponomarev, C. Romig, L. Schnorrenberger, K. Sonnabend, A. Zilges, Phys. Rev. C 84 (2011) 024326, http://dx.doi.org/10.1103/PhysRevC.84.024326.
[95] M. Müscher, et al., Phys. Rev. C 102 (2020) 014317.
[96] J. Isaak, et al., Phys. Lett. B 727 (2013) 361.
[97] B. Löher, D. Savran, T. Aumann, J. Beller, M. Bhike, N. Cooper, V. Derya, M. Duchêne, J. Endres, A. Hennig, P. Humby, J. Isaak, J. Kelley, M. Knörzer, N. Pietralla, V. Ponomarev, C. Romig, M. Scheck, H. Scheit, J. Silva, A. Tonchev, W. Tornow, F. Wamers, H. Weller, V. Werner, A. Zilges, Phys. Lett. B 756 (2016) 72–76, http://dx.doi.org/10.1016/j.physletb.2016.02.042.
[98] C. Romig, et al., Phys. Rev. C 88 (2013) 044331.
[99] M. Tamkas, et al., Nuclear Phys. A 987 (2019) 79.
[100] A. Klimkiewicz, et al., Nuclear Phys. A 788 (2007) 145, http://dx.doi.org/10.1016/j.nuclphysa.2007.01.075.
[101] G. Dollinger, T. Faestermann, Nucl. Phys. News 28 (1) (2018) 5.
[102] A. Brown, Phys. Rev. Lett. 85 (2000) 5300.
[103] N. Tsoneva, H. Lenske, Phys. At. Nucl. 79 (2016) 885.
[104] M. Weinert, M. Spieker, G. Potel, N. Tsoneva, M. Müscher, J. Wilhelmy, A. Zilges, Phys. Rev. Lett. 127 (2021) 242501, http://dx.doi.org/10.1103/PhysRevLett.127.242501.
[105] T. Renstrøm, et al., Phys. Rev. C 98 (2018) 054310.
[106] C.T. Angell, et al., Phys. Rev. C 86 (2012) 051302(R).
[107] R. Massarczyk, et al., Phys. Rev. Lett. 112 (2014) 072501.
[108] P.M. Goddard, N. Cooper, V. Werner, G. Rusev, P.D. Stevenson, A. Rios, C. Bernards, A. Chakraborty, B.P. Crider, J. Glorius, R.S. Ilieva, J.H. Kelley, E. Kwan, E.E. Peters, N. Pietralla, R. Raut, C. Romig, D. Savran, L. Schnorrenberger, M.K. Smith, K. Sonnabend, A.P. Tonchev, W. Tornow, S.W. Yates, Phys. Rev. C 88 (2013) 064308, http://dx.doi.org/10.1103/PhysRevC.88.064308.
[109] K.S.E. Hammarén, P. Heikkinen, A. Faessler, Nuclear Phys. A 541 (1992) 226.
[110] N.Z.P. von Brentano, A. Zilges, Phys. Lett. B 278 (1992) 221.
[111] M. Spieke, et al., Phys. Lett. B 752 (2016) 102.
[112] J. Bryssinck, et al., Phys. Rev. C 61 (2000) 024309.
[113] N. Tsoneva, M. Spieker, H. Lenske, A. Zilges, Nuclear Phys. A 990 (2019) 183.
[114] M.N. Harakeh, A. van der Woude, Giant Resonances, Clarendon Press, Oxford, 2001.
[115] G. Satchler, Direct Nuclear Reactions, Oxford University Press, 1983.
[116] G. Baldwin, G. Klaiber, Phys. Rev. 71 (1947) 3.
[117] M. Goldhaber, E. Teller, Phys. Rev. 74 (1948) 1046.
[118] H. Steinwedel, J.H.D. Jensen, Z. Naturforsch. 5a (1950) 413.
[119] R. Mohan, M. Danos, L.C. Biedenharn, Phys. Rev. C 3 (1971) 1740.
[120] Y. Suzuki, K. Ikeda, H. Sato, Progr. Theoret. Phys. 83 (1990) 180.
[121] P.V. Isacker, M. Nagarajan, D. Warner, Phys. Rev. C 45 (1992) R13.
[122] S. Bastrukov, I. Molodtsova, D. Podgainy, Ş. Mişicu, H.-K. Chang, Phys. Lett. B 664 (2008) 258–264, http://dx.doi.org/10.1016/j.physletb.2008.05.036.
[123] P. Ring, P. Schuck, The Nuclear Many-Body Problem, Springer, 2004.
[124] T. Skyrme, Nuclear Phys. 9 (1958) 615.
[125] D. Vautherin, D.M. Brink, Phys. Rev. C 5 (1972) 626.
[126] J. Dechargé, D. Gogny, Phys. Rev. C 21 (1980) 1568–1593, http://dx.doi.org/10.1103/PhysRevC.21.1568.
[127] D.J. Rowe, Nuclear Collective Motion, World Scientific Publishing, 2010.
[128] I. Hamamoto, H. Sagawa, X.Z. Zhang, Phys. Rev. C 53 (1996) 765.
[129] I. Hamamoto, H. Sagawa, Phys. Rev. C 53 (1996) R1492.
[130] F. Catara, E.G. Lanza, M.A. Nagarajan, A. Vitturi, Nuclear Phys. A 614 (1997) 86.
[131] F. Catara, E.G. Lanza, M.A. Nagarajan, A. Vitturi, Nuclear Phys. A 624 (1997) 449.
[132] I. Hamamoto, H. Sagawa, X.Z. Zhang, Phys. Rev. C 57 (1998) R1064.
[133] N.V. Giai, H. Sagawa, Phys. Lett. B 106 (1981) 379.
[134] N.V. Giai, H. Sagawa, Nuclear Phys. A 371 (1981) 1.
[135] G. Coló, L. Cao, N. Van Giai, L. Capelli, Comput. Phys. Comm. 184 (2013) 142–161, http://dx.doi.org/10.1016/j.cpc.2012.07.016.
[136] E. Chabanat, P. Bonche, P. Haensel, J. Meyer, R. Schaeffer, Nuclear Phys. A 635 (1998) 231–256, http://dx.doi.org/10.1016/S0375-9474(98)00180-8.
[137] P.-G. Reinhard, H. Flocard, Nuclear Phys. A 584 (1995) 467–488, http://dx.doi.org/10.1016/0375-9474(94)00770-N.

[138] G. Có, V.D. Donno, C. Maieron, M. Anguiano, A.M. Lallena, Phys. Rev. C 80 (2009) 014308.
[139] J. Terasaki, J. Engel, Phys. Rev. C 74 (2006) 044301.
[140] P. Papakonstantinou, H. Hergert, V.Y. Ponomarev, R. Roth, Phys. Lett. B 709 (2012) 270.
[141] P. Papakonstantinou, H. Hergert, V.Y. Ponomarev, R. Roth, Phys. Rev. C 89 (2014) 034306.
[142] J. Berger, M. Girod, D. Gogny, Comput. Phys. Comm. 63 (1991) 365.
[143] A. Günther, R. Roth, H. Hergert, S. Reinhardt, Phys. Rev. C 82 (2010) 024319.
[144] E. Chabanat, E. Bonche, P. Haensel, J. Meyer, R. Schaeffer, Nuclear Phys. A 627 (1997) 710.
[145] J.D. Walecka, Ann. Physics 83 (1974) 491.
[146] D. Vretenar, H. Berghammer, P. Ring, Nuclear Phys. A 581 (1995) 679.
[147] N. Paar, P. Ring, T. Nikšić, D. Vretenar, Phys. Rev. C 67 (2003) 034312, http://dx.doi.org/10.1103/PhysRevC.67.034312.
[148] T. Nikŝić, D. Vretenar, P. Ring, Phys. Rev. C 66 (2002) 064302.
[149] J. Liang, L.-G. Cao, Z.-Y. Ma, Phys. Rev. C 75 (2007) 054320, http://dx.doi.org/10.1103/PhysRevC.75.054320.
[150] J. Piekarewicz, Phys. Rev. C 83 (2011) 034319, http://dx.doi.org/10.1103/PhysRevC.83.034319.
[151] H. Kucharek, P. Ring, Z. Phys. A 339 (1) (1991) 23–35, http://dx.doi.org/10.1007/BF01282930.
[152] G.A. Lalazissis, J. König, P. Ring, Phys. Rev. C 55 (1997) 540–543, http://dx.doi.org/10.1103/PhysRevC.55.540.
[153] C. Yannouleas, Phys. Rev. C 35 (1987) 1159–1161, http://dx.doi.org/10.1103/PhysRevC.35.1159.
[154] P. Papakonstantinou, R. Roth, Phys. Lett. B 671 (2009) 356–360, http://dx.doi.org/10.1016/j.physletb.2008.12.037.
[155] P. Papakonstantinou, R. Roth, Phys. Rev. C 81 (2010) 024317, http://dx.doi.org/10.1103/PhysRevC.81.024317.
[156] D. Gambacurta, M. Grasso, F. Catara, Phys. Rev. C 84 (2011) 034301, http://dx.doi.org/10.1103/PhysRevC.84.034301.
[157] M. Tohyama, T. Nakatsukasa, Phys. Rev. C 85 (2012) 031302, http://dx.doi.org/10.1103/PhysRevC.85.031302.
[158] M. Grasso, D. Gambacurta, Phys. Rev. C 101 (2020) 064314, http://dx.doi.org/10.1103/PhysRevC.101.064314.
[159] V.I. Tselyaev, Phys. Rev. C 75 (2007) 024306, http://dx.doi.org/10.1103/PhysRevC.75.024306.
[160] V.I. Tselyaev, Phys. Rev. C 88 (2013) 054301, http://dx.doi.org/10.1103/PhysRevC.88.054301.
[161] D. Gambacurta, M. Grasso, J. Engel, Phys. Rev. C 92 (2015) 034303, http://dx.doi.org/10.1103/PhysRevC.92.034303.
[162] D. Gambacurta, M. Grasso, O. Vasseur, Phys. Lett. B 777 (2018) 163–168, http://dx.doi.org/10.1016/j.physletb.2017.12.026.
[163] A. Bohr, B. Mottelson, Nuclear Structure, W.A. Benjamin, New York, 1975.
[164] E. Lanza, M. Andrés, F. Catara, P. Chomaz, C. Volpe, Nuclear Phys. A 613 (1997) 445–471, http://dx.doi.org/10.1016/S0375-9474(96)00444-7.
[165] M. Fallot, P. Chomaz, M. Andrés, F. Catara, E. Lanza, J. Scarpaci, Nuclear Phys. A 729 (2003) 699–712, http://dx.doi.org/10.1016/j.nuclphysa.2003.10.001.
[166] E.G. Lanza, F. Catara, M.V. Andrés, P. Chomaz, M. Fallot, J.A. Scarpaci, Phys. Rev. C 74 (2006) 064614, http://dx.doi.org/10.1103/PhysRevC.74.064614.
[167] M. Hage-Hassan, M. Lambert, Nuclear Phys. A 188 (1972) 545–565, http://dx.doi.org/10.1016/0375-9474(72)90219-9.
[168] V. Soloviev, Theory of Atomic Nucleus: Quasiparticles and Phonons, Institute of Physics, Bristol, 1992.
[169] C. Bertulani, V. Ponomarev, Phys. Rep. 321 (1999) 139.
[170] N. Tsoneva, H. Lenske, C. Stoyanov, Phys. Lett. B 586 (2004) 213–218, http://dx.doi.org/10.1016/j.physletb.2004.02.024.
[171] N. Tsoneva, H. Lenske, Phys. Rev. C 77 (2008) 024321, http://dx.doi.org/10.1103/PhysRevC.77.024321.
[172] E. Litvinova, P. Ring, V. Tselyaev, Phys. Rev. C 75 (2007) 064308, http://dx.doi.org/10.1103/PhysRevC.75.064308.
[173] E. Litvinova, P. Ring, V. Tselyaev, Phys. Rev. Lett. 105 (2010) 022502, http://dx.doi.org/10.1103/PhysRevLett.105.022502.
[174] E. Litvinova, P. Ring, V. Tselyaev, Phys. Rev. C 88 (2013) 044320, http://dx.doi.org/10.1103/PhysRevC.88.044320.
[175] E.N.R. Data, http://www-nds.iaea.or.at/exfor/exfor00.htm.
[176] F. Knapp, N. Lo Iudice, P. Veselý, F. Andreozzi, G. De Gregorio, A. Porrino, Phys. Rev. C 90 (2014) 014310, http://dx.doi.org/10.1103/PhysRevC.90.014310.
[177] G. De Gregorio, F. Knapp, N. Lo Iudice, P. Vesely, Phys. Rev. C 93 (2016) 044314, http://dx.doi.org/10.1103/PhysRevC.93.044314.
[178] K. Okamoto, Phys. Rev. 110 (1958) 143.
[179] M. Danos, Nuclear Phys. 5 (1958) 23.
[180] F. Iachello, A. Arima, The Interacting Boson Model, Cambridge University Press, 1987.
[181] F. Iachello, P.V. Isacker, The Interacting Boson-Fermion Model, Cambridge University Press, 1991.
[182] S. Péru, H. Goutte, J. Berger, Nuclear Phys. A 788 (2007) 44–49, http://dx.doi.org/10.1016/j.nuclphysa.2007.01.047.
[183] K. Yoshida, N.V. Giai, Phys. Rev. C 78 (2008) 064316, http://dx.doi.org/10.1103/PhysRevC.78.064316.
[184] J. Bartel, P. Quentin, M. Brack, C. Guet, H.-B. Håkansson, Nuclear Phys. A 386 (1982) 79–100, http://dx.doi.org/10.1016/0375-9474(82)90403-1.
[185] K. Yoshida, Phys. Rev. C 80 (2009) 044324, http://dx.doi.org/10.1103/PhysRevC.80.044324.
[186] S. Péru, H. Goutte, Phys. Rev. C 77 (2008) 044313, http://dx.doi.org/10.1103/PhysRevC.77.044313.
[187] M. Martini, S. Péru, M. Dupuis, Phys. Rev. C 83 (2011) 034309, http://dx.doi.org/10.1103/PhysRevC.83.034309.
[188] D. Peña Arteaga, P. Ring, Phys. Rev. C 77 (2008) 034317, http://dx.doi.org/10.1103/PhysRevC.77.034317.
[189] D. Peña Arteaga, E. Khan, P. Ring, Phys. Rev. C 79 (2009) 034311, http://dx.doi.org/10.1103/PhysRevC.79.034311.
[190] K. Yoshida, T. Nakatsukasa, Phys. Rev. C 83 (2011) 021304, http://dx.doi.org/10.1103/PhysRevC.83.021304.
[191] K. Yoshida, T. Nakatsukasa, Phys. Rev. C 88 (2013) 034309, http://dx.doi.org/10.1103/PhysRevC.88.034309.
[192] M. Yamagami, Y.R. Shimizu, T. Nakatsukasa, Phys. Rev. C 80 (2009) 064301, http://dx.doi.org/10.1103/PhysRevC.80.064301.
[193] D. Vretenar, N. Paar, P. Ring, T. Nikšić, Phys. Rev. C 65 (2002) 021301, http://dx.doi.org/10.1103/PhysRevC.65.021301.
[194] J. Kvasil, V.O. Nesterenko, W. Kleinig, P.-G. Reinhard, P. Vesely, Phys. Rev. C 84 (2011) 034303, http://dx.doi.org/10.1103/PhysRevC.84.034303.
[195] A. Repko, P.-G. Reinhard, V.O. Nesterenko, J. Kvasil, Phys. Rev. C 87 (2013) 024305, http://dx.doi.org/10.1103/PhysRevC.87.024305.
[196] V.O. Nesterenko, J. Kvasil, A. Repko, W. Kleinig, P.G. Reinhard, Phys. At. Nucl. 79 (2016) 842–850, http://dx.doi.org/10.1134/S106377881606020X.
[197] A. Repko, V.O. Nesterenko, J. Kvasil, P.G. Reinhard, Eur. Phys. J. A 55 (2019) 242, http://dx.doi.org/10.1140/epja/i2019-12770-x.
[198] S. Bastrukov, S. Misicu, A. Sushkov, Nuclear Phys. A 562 (1993) 191–204, http://dx.doi.org/10.1016/0375-9474(93)90195-4.
[199] S. Pascu, J. Endres, N.V. Zamfir, A. Zilges, Phys. Rev. C 85 (2012) 064315, http://dx.doi.org/10.1103/PhysRevC.85.064315.
[200] S. Volz, N. Tsoneva, M. Babilon, M. Elvers, J. Hasper, R.-D. Herzberg, H. Lenske, K. Lindenberg, D. Savran, A. Zilges, Nuclear Phys. A 779 (2006) 1–20, http://dx.doi.org/10.1016/j.nuclphysa.2006.08.012.
[201] M. Spieker, S. Pascu, A. Zilges, F. Iachello, Phys. Rev. Lett. 114 (2015) 192504, http://dx.doi.org/10.1103/PhysRevLett.114.192504.
[202] M. Spieker, S. Pascu, A. Zilges, J. Phys. Conf. Ser. 863 (2017) 012063, http://dx.doi.org/10.1088/1742-6596/863/1/012063.
[203] D. Brink, A. Dellafiore, M. Di Toro, Nuclear Phys. A 456 (1986) 205–234, http://dx.doi.org/10.1016/0375-9474(86)90390-8.
[204] G. Burgio, M. Di Toro, Nuclear Phys. A 476 (1988) 189–212, http://dx.doi.org/10.1016/0375-9474(88)90480-0.
[205] C. Grégoire, B. Remaud, F. Sébille, L. Vinet, Y. Raffray, Nuclear Phys. A 465 (1987) 317–338, http://dx.doi.org/10.1016/0375-9474(87)90437-4.
[206] M. Urban, Phys. Rev. C 85 (2012) 034322, http://dx.doi.org/10.1103/PhysRevC.85.034322.
[207] M. Baldo, P. Schuck, X. Viñas, Phys. Lett. B 663 (2008) 390–394, http://dx.doi.org/10.1016/j.physletb.2008.04.013.
[208] V. Baran, M. Colonna, M. Di Toro, A. Croitoru, D. Dumitru, Phys. Rev. C 88 (2013) 044610, http://dx.doi.org/10.1103/PhysRevC.88.044610.

[209] N. Paar, T. Nikšić, D. Vretenar, P. Ring, Phys. Lett. B 606 (2005) 288–294, http://dx.doi.org/10.1016/j.physletb.2004.12.011.
[210] X. Roca-Maza, G. Colò, H. Sagawa, Phys. Rev. C 86 (2012) 031306, http://dx.doi.org/10.1103/PhysRevC.86.031306.
[211] H. Zheng, S. Burrello, M. Colonna, V. Baran, Phys. Rev. C 94 (2016) 014313, http://dx.doi.org/10.1103/PhysRevC.94.014313.
[212] S. Burrello, M. Colonna, G. Colò, D. Lacroix, X. Roca-Maza, G. Scamps, H. Zheng, Phys. Rev. C 99 (2019) 054314, http://dx.doi.org/10.1103/PhysRevC.99.054314.
[213] G. Satchler, W. Love, Phys. Rep. 55 (1979) 183–254, http://dx.doi.org/10.1016/0370-1573(79)90081-4.
[214] R.A. Broglia, A. Winther, Heavy Ion Reactions: The Elementary Processes, Part I and II, CRC Press, 2004.
[215] S. Landowne, A. Vitturi, in: D.A. Bromley (Ed.), Treatise on Heavy-Ion Science, Vol. 1, Plenum, New York, 1984, p. 355.
[216] G. Bertsch, J. Borysowicz, H. McManus, W. Love, Nuclear Phys. A 284 (1977) 399–419, http://dx.doi.org/10.1016/0375-9474(77)90392-X.
[217] E.G. Lanza, A. Vitturi, M.V. Andrés, Phys. Rev. C 91 (2015) 054607.
[218] T.J. Deal, Nuclear Phys. A 217 (1973) 210–220, http://dx.doi.org/10.1016/0375-9474(73)90634-9.
[219] M.N. Harakeh, A.E.L. Dieperink, Phys. Rev. C 23 (1981) 2329–2334, http://dx.doi.org/10.1103/PhysRevC.23.2329.
[220] P. Kunz, DWUCK4 code for DWBA at https://people.nscl.msu.edu/brown/reaction-codes/.
[221] P. Kunz, E. Rost, Computational Nuclear Physics 2, Springer, New York, NY, 1993.
[222] E.G. Lanza, A. Vitturi, M.V. Andrés, J. Phys. Conf. Ser. 420 (2013) 012147, http://dx.doi.org/10.1088/1742-6596/420/1/012147.
[223] J. Endres, et al., Phys. Rev. Lett. 105 (2010) 212503.
[224] E.G. Lanza, A. Vitturi, E. Litvinova, D. Savran, Phys. Rev. C 89 (2014) 041601(R).
[225] D. Savran, et al., Phys. Rev. Lett. 97 (2006) 17502.
[226] C. Romig, D. Savran, J. Beller, J. Birkhan, A. Endres, M. Fritzsche, J. Glorius, J. Isaak, N. Pietralla, M. Scheck, L. Schnorrenberger, K. Sonnabend, M. Zweidinger, Phys. Lett. B 744 (2015) 369–374, http://dx.doi.org/10.1016/j.physletb.2015.04.013.
[227] J. Raynal, Program DWBA07 NEA Data Service NEA1209 /08.
[228] W.G. Love, M.A. Franey, Phys. Rev. C 24 (1981) 1073–1094, http://dx.doi.org/10.1103/PhysRevC.24.1073.
[229] M.A. Franey, W.G. Love, Phys. Rev. C 31 (1985) 488–498, http://dx.doi.org/10.1103/PhysRevC.31.488.
[230] T. Nikšić, D. Vretenar, P. Finelli, P. Ring, Phys. Rev. C 66 (2002) 024306, http://dx.doi.org/10.1103/PhysRevC.66.024306.
[231] G.A. Lalazissis, T. Nikšić, D. Vretenar, P. Ring, Phys. Rev. C 71 (2005) 024312, http://dx.doi.org/10.1103/PhysRevC.71.024312.
[232] P.-G. Reinhard, W. Nazarewicz, Phys. Rev. C 87 (2013) 014324, http://dx.doi.org/10.1103/PhysRevC.87.014324.
[233] G.E. Brown, M. Bolsterli, Phys. Rev. Lett. 3 (1959) 472–476, http://dx.doi.org/10.1103/PhysRevLett.3.472.
[234] G. Satchler, Nuclear Phys. A 472 (1987) 215–236, http://dx.doi.org/10.1016/0375-9474(87)90208-9.
[235] I. Hamamoto, H. Sagawa, Phys. Rev. C 96 (2017) 064312, http://dx.doi.org/10.1103/PhysRevC.96.064312.
[236] R. Schwengner, G. Rusev, N. Tsoneva, N. Benouaret, R. Beyer, M. Erhard, E. Grosse, A.R. Junghans, J. Klug, K. Kosev, H. Lenske, C. Nair, K.D. Schilling, A. Wagner, Phys. Rev. C 78 (2008) 064314, http://dx.doi.org/10.1103/PhysRevC.78.064314.
[237] M. Zweidinger, Nuclear Structure Studies on Medium-Heavy Mass Nuclei using the Method of Nuclear Resonance Fluorescence (Ph.D. thesis), Technische Universität Darmstadt, 2016.
[238] N. Tsoneva, H. Lenske, Phys. Lett. B 695 (2011) 174.
[239] E. Lanza, L. Pellegri, M. Andrés, F. Catara, A. Vitturi, Eur. Phys. J. A 55 (2019) 235.
[240] E. Yüksel, G. Coló, E. Khan, Y.F. Niu, Phys. Rev. C 97 (2018) 064308.